University of South-Eastern Norway

Faculty of Technology, Natural Sciences and Maritime Sciences

4317 – Master Thesis

Study programme: Environmental Science

Spring/Autumn 2020

Anastasiia Vasiakina

Modelling of the energy budgets at Imingfjell, Norway, using the Community Land Model (CLM4.5)

University of South-Eastern Norway
Faculty of Technology, Natural Sciences and Maritime Sciences
Department of Natural Sciences and Environmental Health
PO Box 235
NO-3603 Kongsberg, Norway

http://www.usn.no

This thesis is worth 60 study points

Abstract

Mountains are one of the most sensitive areas to climate change as they are biodiversity hotspots. One of the main problems in studying climate change for mountainous territories is the lack of meteorological data due to their inaccessibility. Currently, modelling is the most commonly used method for data scarcity, but it is still difficult to assess the effectiveness of models. Here, the Community Land Model 4.5 (CLM4.5) was used as a model for testing, with Mount Imingfjell in Southern Norway as the study object. The results of two experiments, the STANDARD and RCP4.5 experiments, were analysed to determine how the simulated results resemble the measured energy and radiation budgets at Imingfjell and to predict possible future changes in their components under the RCP4.5 scenario, respectively. In the STANDARD experiment, model inputs were compared with weather parameters from the two meteorological stations closest to Imingfjell for the period of 2002-2016, and model outputs were compared with measurements of the radiation and energy budgets for two types of vegetation (lichen and shrubs) from our research site at Imingfjell in summers 2018-2019. In the RCP4.5 experiment, the radiation and energy budgets components were compared between three different time periods from 1850 to 2100. Analysis of the input data in the STANDARD experiment indicated that CLM4.5 underestimated the Imingfjell altitude by 3 times and gave plausible results of all input parameters, but not for the actual height. As for the output data, the simulated data was in most cases closer to the data of shrubs than lichens. The RCP4.5 experiment showed that only half of the fluxes (Q_H, Q_E, K↑, L↓ and L*) have changed from pre-industrial times to the present day, but most of them, except Q_E, Q_G, and L*, will change by the end of 21st century.

Foreword

Firstly, I want to thank my supervisor Hans Renssen for his help and guidance.

A big thank you to Peter Aartsma for providing his field data of the radiation and energy budgets components at Imingfjell.

Additionally, I would like to thank Terje Berntsen and Jenny Bjordal from University of Oslo for their help with the Community Land Model 4.5.

Bø i Midt-Telemark / November 2020

Anastasiia Vasiakina

Contents

1 Introduction

Mountains cover a significant territory of the globe (Körner et al. 2011, Körner et al. 2017). Depending on the definition of mountainous areas, mountains occupy 21-24% of the Earth's terrestrial surface, based on the ruggedness criteria and elevation (>300 m above sea level) (Kapos et al. 2000, Meybeck et al. 2001, Tito et al. 2020), or around 12% of the land area outside Antarctica, based on the improved criteria with finer spatial resolution and local elevation range (Körner et al. 2011, Körner et al. 2017, Price et al. 2018, Tito et al. 2020). Therefore, mountain regions are important areas to study, especially regarding climate change (Körner et al. 2011; Körner et al. 2017; Tito et al. 2020). In this master's thesis, I will evaluate microclimatic conditions at a mountain site in Southern Norway by analysing the results of climate model and comparing them to local measurements.

1.1 Global climate change

1.1.1 Observed changes

The Earth's climate has always been changing due to natural external forcings such as solar, volcanic and orbital (Masson-Delmotte et al. 2013), but in recent decades a rapid warming is observed. Global temperature increased by 0.85°C (0.65 to 1.06°C) from 1880 to 2012 (Figure 1-1) (IPCC 2013).

Besides temperature, other indicators of the changing global climate are Northern Hemisphere spring snow cover, sea ice, upper ocean heat content (heat absorbed by the ocean) and sea level. Northern snow cover decreased over the 1967-2012 period by 1.6% per decade in March and April (Figure 1-2a). Arctic summer sea ice extent declined at a rate of 3.5-4.1% per decade from 1979 to 2012 (Figure 1-2b). Upper ocean heat content had an increase of 17 (15 to 19)x10^{22} J between 1971 and 2010 (Figure 1-2c). Sea level rose by 1.7 (1.5 to 1.9) mm per year from 1901 to 2010 and by 3.2 (2.8 to 3.6) mm per year from 1993 to 2010 (Figure 1-2d) (IPCC 2013).

Such rapid changes in the global climate are mainly caused by man-made radiative impact from emissions of well-mixed greenhouse gases (CO_2, CH_4, N_2O, and Halocarbons), as natural forcing only causes 0.05 (0.00 to 0.10) W m^{-2} of radiative forcing, and anthropogenic forcing has nearly doubled every 30 years since 1950 (Figure 1-3). The total anthropogenic emission from the mix of greenhouse gases (GHGs) is 3.00 (2.22 to 3.78) W m^{-2} from 1750 to 2011 (IPCC 2013). Although observed climate changes in the past were explained above, it is also important to know how the climate might change in the future.

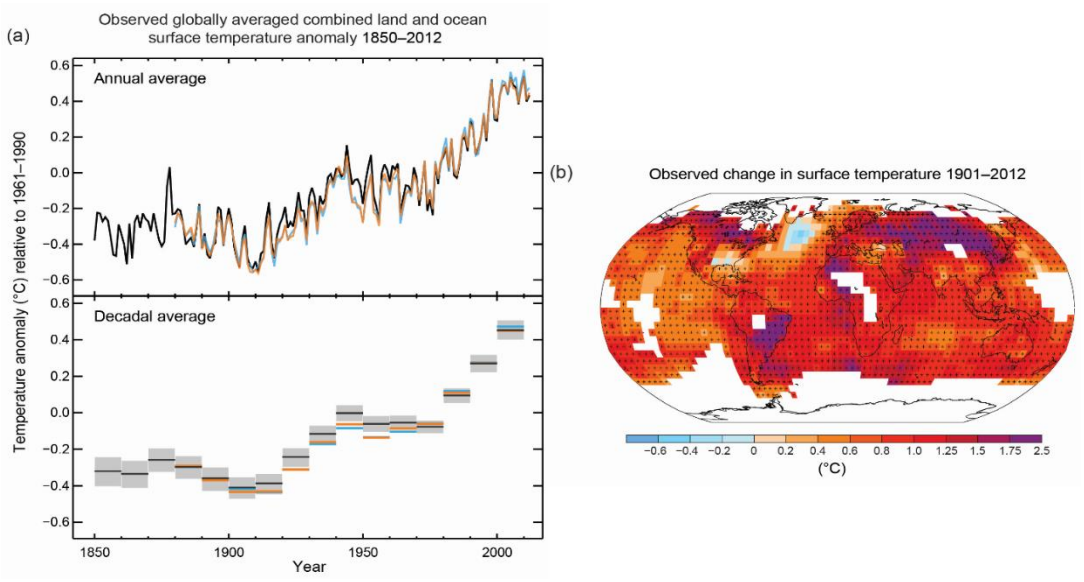

Figure 1-1 (a) Observed global average combined land and ocean surface temperature, 1850-2012. Top panel: annual averages from three different datasets. Bottom panel: decadal average temperature, including shaded areas for uncertainties; (b) Observed surface temperature change between 1901 and 2012, obtained from temperature trends determined by linear regression from the dataset represented by the orange line in the top panel (a). Trends were calculated where data availability allows a robust estimate. The rest of the areas are white. The '•' sign indicates where the trend is significant at the 10% level (IPCC 2013)

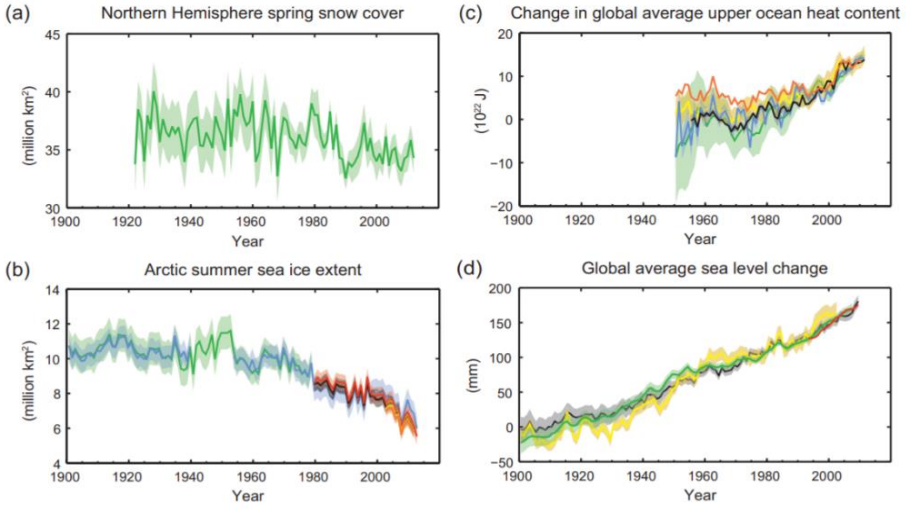

Figure 1-2 Observed indicators of global climate change: (a) average snow cover in the Northern Hemisphere, March-April (spring); (b) July-August-September (summer) average sea ice in the Arctic; (c) change in global average heat content in the upper ocean (0-700 m); (d) global mean sea level. All datasets present annual values with coloured shading to indicate uncertainty (IPCC 2013)

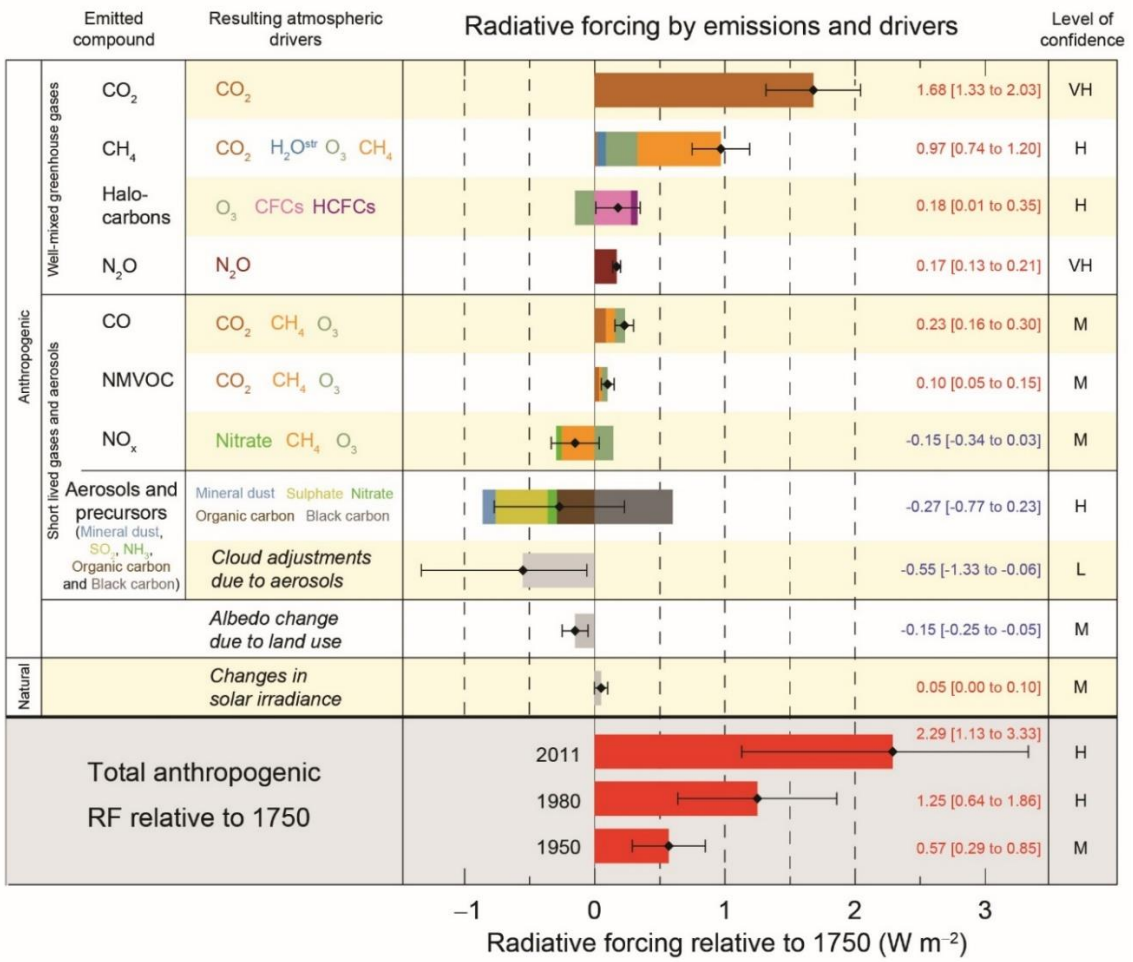

Figure 1-3 Estimates of radiative forcing in 2011 relative to 1750 with aggregated uncertainties for the main drivers of climate change. Net forcing confidence levels: VL – very low, L – low, M – medium, H – high, VH – very high. Due to the episodic nature of volcano eruptions, volcanic forcing was not included (IPCC 2013)

1.1.2 Projected future climate change

How climate will change in the future is predicted by models that use a set of anthropogenic forcing scenarios to simulate the changes. One type of scenario is the Representative Concentration Pathway (RCP), which depends on future trajectories of GHG concentrations. Four scenarios were introduced: RCP2.6 (low-emission scenario), RCP4.5, RCP6.0 (both medium-emission scenarios) and RCP8.5 (high-emission scenario). All scenarios, except RCP2.6, show that the global average surface temperature change will exceed 1.5°C by the end of the 21st century, and RCP6.0 and RCP8.5 will likely exceed 2°C (Figure 1-4) (IPCC 2013). Changes in the global climate have been observed in the past and projected into the future, but similar patterns of climate warming also occur on a regional scale.

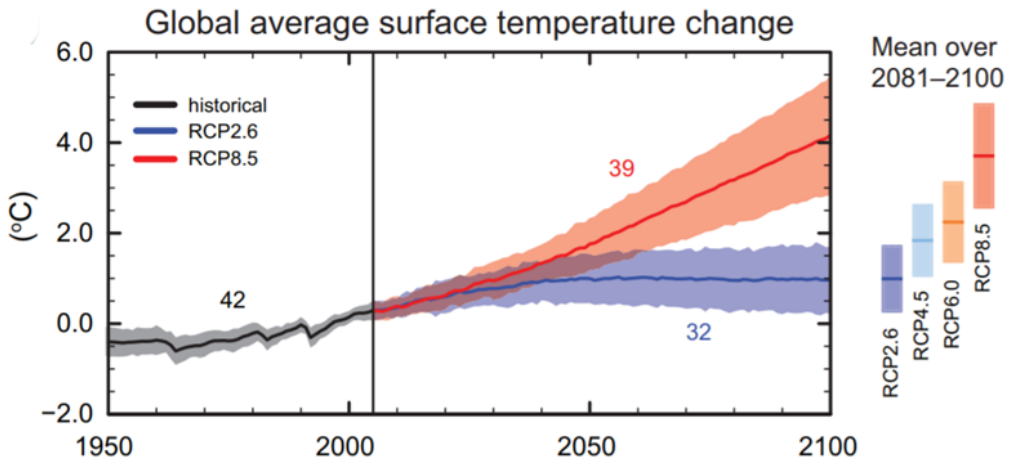

Figure 1-4 Change in global annual mean surface temperature relative to 1986-2005 for different RCPs, plotted from 1950 to 2100. Shaded areas used as a measure of uncertainty in the projections (IPCC 2013)

1.2 Regional climate change - Scandinavia

As for a regional climate change, we will focus on Scandinavia and its mountain areas (IPCC's Alpine North sector), since the study object of this thesis is Mount Imingfjell located in Southern Norway. Both observed and projected future climate changes in Scandinavia are discussed below.

1.2.1 Observed changes

Scandinavia experiences the strongest warming in Europe, especially in winter (Kovats et al. 2014). Annual mean temperature rose by 0.30-0.40°C per decade from 1960 to 2012 in Scandinavia (Füssel et al. 2012). Annual precipitation increased to 70 mm per decade in Northern Europe (Kovats et al. 2014).

1.2.2 Projected climate change

The greatest future warming in Europe is projected to continue over Scandinavia (Füssel et al. 2012). In 2071-2100 compared to 1971-2000, mean annual temperature for the Alpine North sector will increase by 3.0°C (1.9-3-9°C) for RCP4.5 and by 4.8°C (3.6-5.8°C) for RCP8.5. Due to this warming, the number of frost days per year will decrease by 42 (45 to 30) and by 75 (96 to 57) days per year for RCP4.5 and RCP8.5, respectively. Moreover, the length of the growing season will increase up to 35 (22 to 38) days per season for RCP4.5, and up to 64 (46 to 84) days for RCP8.5 (Jacob et al. 2014, Kovats et al. 2014).

Climate changes have been observed and are projected to continue on every spatial scale from regional to global. However, from an ecological perspective some regions, such as mountains, may be more vulnerable to climate change due to high biodiversity in their territories.

1.3 Mountains as biodiversity hotspots

Climatic and non-climatic parameters change rapidly over mountainous regions due to high altitudinal variability (Körner 2007, Rapp and Silman 2012). This variability causes a variety of living conditions, which makes mountains hotspots of biodiversity (Myers et al. 2000, Körner et al. 2011, Körner et al. 2017, Rahbek et al. 2019, Tito et al. 2020). Thus, mountains are sensitive regions to climate warming, largely due to possible shifts in the distribution and abundance of species (Braunisch et al. 2014, Shah et al. 2015, Ishaq et al. 2016), especially in the Arctic and Alpine areas (like the Scandinavian mountains) since they are the most climate-sensitive regions (Duarte et al. 2012, Kovats et al. 2014, Hock et al. 2019). For example, shrubs in response to climate warming are expanding into the Arctic and Alpine regions at the expense of lichens (Sturm et al. 2005, Elmendorf et al. 2012, Vowles and Björk 2019). Such " Shrubification" could potentially lead to a reduction of the alpine landscape albedo since most lichens have a higher albedo than shrubs (they are lighter in colour) (Aartsma et al. 2020), amplifying the warming of these areas (Sturm et al. 2005, Vowles and Björk 2019). In addressing these questions about the effects of climate change in mountainous areas, mountain climatology is used. However, it was difficult to scale it down for studies on small atmospheric scales (microscale).

1.4 Atmospheric scales for mountain studies

Processes in the Earth's atmosphere occur on a wide range of various temporal and spatial scales. The time scale is determined by the typical lifetime of the processes, while the space scale is determined by their typical size (Oke 1987). A visual explanation of atmospheric scales is presented in Figure 1-5. The following atmospheric scales have been adopted (Oke 1987):

Microscale 10^{-2} to 10^{3} meters

Local scale 10^{2} to 5×10^{4} meters

Mesoscale 10^{4} to 2×10^{5} meters

Macroscale 10^{5} to 10^{8} meters

Mountain climatology in the last century has mainly focused on the meso- (10^{4} to $2x10^{5}$ m) and macroscales (10^{5} to 10^{8} m) (Oke 1987, Saunders 1990, Saunders and Bailey 1994). However, in

connection with the technological development in recent years, more and more studies of mountain areas are carried out on the microclimate scale (10^{-2} to 10^{3} m) (Oke 1987, Hirata et al. 2020, Kopáček et al. 2020).

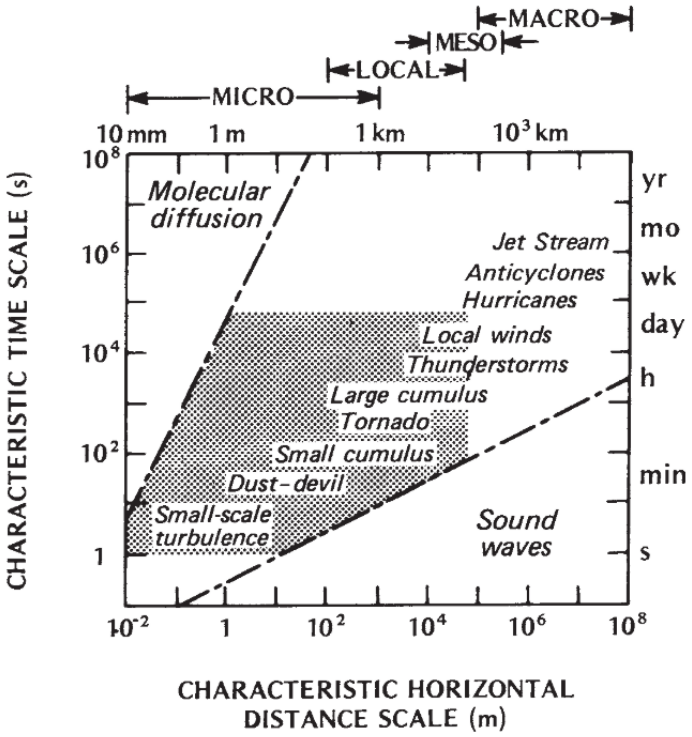

Figure 1-5 Atmospheric scales of phenomena, mainly associated with movement, in the grid of their possible spatial and temporal boundaries. The horizontal axis shows the space scale of processes or their size, while the vertical axis describes the time scale or lifetime of the phenomenon. Both time and space scales increase from the lower-left to the upper-right corner. The lower-left corner shows processes of small-scale turbulence, for example, tiny eddies with a life span of a few seconds. In the right-upper corner, jet streams are located, such as giant wind waves that encircle the entire Earth and continue to circulate for several months. The hatched region represents the characteristic region of the boundary layer elements (Smagorinsky 1974, Oke 1987)

1.5 Energy budget and radiation balance

Even though mountain climatology is actively developing on the microscale, studies of thr complete energy and radiation budgets for mountain areas are rarely conducted, and most of them date back to the end of the last century (Müller 1985, Saunders 1990, Saunders and Bailey 1994). Researches on the energy budget and radiation balance are valuable for understanding how climate change occurs, as changes in their components indicate what causes the surface to heat up or cool down (Oke 1987, Farmer and Cook 2013).

As Oke (1987) described in detail, radiation is a form of energy generated by rapid fluctuations of electromagnetic fields and is transferred by photons (bundles that have the properties of both waves and particles). All bodies with temperatures above absolute zero (0 K = -273.2°C) emit radiation (they can also transmit, reflect and/or absorb energy), the amount of which depends on the body surface temperature. Consequently, the Sun emits much more energy than the Earth-Atmosphere (E-A) system, but they also differ in wavelength composition. The Sun's peak wavelength is around 0.48 μm (visible part of the electromagnetic spectrum), and wavelengths range from 0.15 μm (ultra-violet) to 3.0 μm (near-infrared). The E-A system has a peak wavelength of 10 μm with wavelengths extending from 3.0 to 100 μm (infrared). Hence from this, it was decided to call the radiation observed in 0.15-3.0 μm - shortwave radiation (K), and the radiation in the 3.0 to 100 μm range - longwave radiation (L). Both net shortwave (K*) and net longwave (L*) represent the difference between the radiation emanating from the Sun and the E-A system, respectively, which is called incoming radiation (K↓ – shortwave; L↓ – longwave radiation), and the radiation going back into outer space – outgoing radiation (K↑ – shortwave; L↑ – longwave radiation).

Net shortwave radiation is (1-1) (Oke 1987)

$$K^* = K\downarrow - K\uparrow, \tag{1-1}$$

where K^* – net shortwave radiation, W m^{-2}; $K\downarrow$ – incoming shortwave radiation, W m^{-2}; $K\uparrow$ – outgoing shortwave radiation, W m^{-2}.

The energy that is coming from the Sun is considered constant (with small changes due to fluctuations in the solar cycle), so the pattern of incoming shortwave radiation (K↓) depends mainly on the azimuth (Ω) and zenith (Z) angles of the Sun relative to the horizon. In addition, atmospheric dust content and water vapour/clouds are important for K↓, as they cause reflection and scattering. Outgoing shortwave radiation (K↑) is influenced by the amount of incident radiation (K↓) and the reflective ability of the surface or albedo (α). Albedo is also defined as (1-2) (Oke 1987)

$$\alpha = \frac{K\uparrow}{K\downarrow}. \tag{1-2}$$

Albedo takes values from 0 to 1, with lighter surfaces having higher values (e.g., fresh snow – 0.95), and darker surfaces having lower ones (e.g., dark, wet soil – 0.05) (Oke 1987).

Net longwave radiation is equal to (1-3) (Oke 1987)

$$L^* = L\downarrow - L\uparrow, \tag{1-3}$$

where L^* – net longwave radiation, W m^{-2}; $L\downarrow$ – incoming longwave radiation, W m^{-2}; $L\uparrow$ – outgoing longwave radiation, W m^{-2}. Outgoing longwave radiation (L↑) is constantly emitted from the Earth's surface, but the heat loss into space is mostly blocked by the atmosphere. Atmospheric components, such as GHGs and clouds, can absorb outgoing longwave radiation and emit in all directions, including back to the surface (L↓). Effectively, GHGs thus "trap" radiative energy, causing the surface to heat up (Oke 1987).

The radiation balance (1-4) is the sum of net shortwave and net longwave radiation, calculated as (Oke 1987)

$$Q^* = K^* + L^* = K\downarrow - K\uparrow + L\downarrow - L\uparrow, \quad (1\text{-}4)$$

where Q^* is net all-wave radiation, W m^{-2}.

Besides the radiation from the Sun, Earth and the atmosphere, other contributors to the energy exchange are the heat fluxes towards or away from the surface, the so-called turbulent heat fluxes, i.e. the sensible and latent heat fluxes. The energy that resulted in the temperature change is called sensible heat (Q_H) and the energy, which is released or absorbed during the phase transitions of water, in practice at the surface mainly through evapotranspiration, is called latent heat (Q_E). At the local scale (Figure 1-5), another source of energy is the heat in or out of the ground/soil (Q_G). The sum of all heat fluxes makes up the energy budget equal to net all-wave radiation (Q*). The surface energy budget is shown in the formula (1-5) (Oke 1987).

$$Q^* = Q_H + Q_E + Q_G, \quad (1\text{-}5)$$

where Q_H – sensible heat flux, W m^{-2}; Q_E – latent heat flux, W m^{-2}; Q_G – soil heat flux, W m^{-2}.

The ratio between the sensible heat flux (Q_H) and the latent heat flux (Q_E) (1-6) is used to estimate the water available for evaporation and is called Bowen's ratio (β) (Oke 1987):

$$\beta = \frac{Q_H}{Q_E}. \quad (1\text{-}6)$$

On the one hand, if Q_H is greater than Q_E ($\beta > 1$), then the climate is probably warm and dry with limited moisture availability. On the other hand, if Q_E is greater than Q_H ($\beta < 1$), then the climate is likely to be cooler and more humid. Negative β values mean that fluxes move in different directions (Q_H – towards the surface, Q_E – away from the surface), which usually happens at night. Typically, Bowen ratio values of 0.1 are classified as tropical oceans; from 0.1 to 0.3 – tropical wet jungles; from 0.4 to 0.8 – temperate forests and grassland; 2.0-6.0 – semi-arid areas; and $\beta > 10.0$ as deserts.

A visual representation of the fluxes involved in the radiation and energy budgets for an 'ideal' site (horizontal, homogeneous and extensive) both during the day (a) and at night (b) is shown in Figure 1-6. The energy budget and radiation balance of mountains are important in studying mountain climatology, but data on mountains are insufficient.

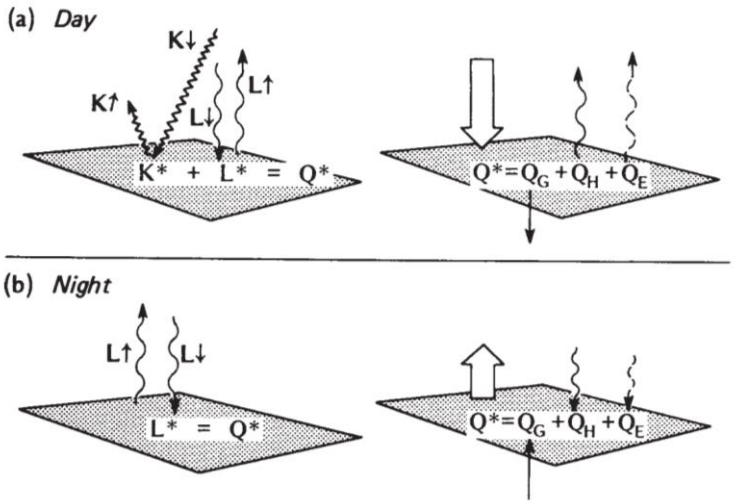

Figure 1-6 The fluxes involved in the radiation balance and energy budget for an 'ideal' site during the day (a) and at night (b) (Oke 1987)

1.6 Insufficient data for mountains

Mountains are hardly accessible regions to research (Khalatov and Abdul'myanov 2013). Thus, it became problematic to obtain sufficient measurements, such as weather parameters and components of the radiation and energy budgets due to the shortage of meteorological stations at high altitudes (Burlando et al. 2002, Lur'e and Panov 2011). One of the modern solutions to this problem is mathematical models, which are increasingly used to restore gaps in meteorological data and to obtain such information for mountainous areas (Lang and Lombargo 2011). However, due to the lack of initial data for mountains, it is difficult to assess how accurate models results are in order to use them for climate change projections or other studies. This issue can be addressed by comparing these results from climate models with local microclimatological measurements obtained at mountain sites. Here, this approach was applied to a site in Southern Norway (Imingfjell).

1.7 Aims of the thesis

The Community Land Model (CLM4.5), provided by the University of Oslo, was used in this research to verify the input and output precision and to assess the suitability of the model to study local climate conditions at Imingfjell. This model, in its previous versions, has been already tested for the accuracy of biogeophysical and biogeochemical parameters such as surface water and energy budgets (Kumar and Merwade 2011), plant photosynthesis (Wang et al. 2014), surface runoff and soil moisture (Du et al. 2016), leaf area index (Zhang et al. 2019), snow dynamics (Hu and Zhi-Peng 2019), but not for the energy fluxes for the Southern mountains in Norway.

The main aim of this study is to test how well the Community Land Model 4.5 simulates the radiation and energy budgets for the mountain region (Imingfjell) in Southern Norway. More specific research questions include:

1) To what extent is CLM4.5 capable of reproducing the energy and radiation budgets as well as weather parameters near Imingfjell, measured at nearby meteorological stations and at the USN study site? (daily timescale)
2) What future changes in the energy and radiation budgets does the CLM4.5 model project for Imingfjell based on the RCP4.5 scenario? (monthly timescale)

To answer these questions, the results of two experiments were used. Both performed with the CLM4.5 model and both provided results for the Imingfjell grid cell. The first experiment, hereafter referred to as the STANDARD experiment, was run at USN with daily output and covers the period from 1901 to 2016. From this STANDARD experiment, only the results from 1993-2016 were used to answer the 1st question. The second experiment, hereafter called the RCP4.5 experiment, was conducted by others within the Climate Model Intercomparison Project phase 5 (CMIP5) to obtain monthly output and covers the period 1850-2100. The RCP4.5 experiment was used to answer the 2nd question.

We did not use only the RCP4.5 experiment data for all analyses, even though it also includes the same years as in the STANDARD experiment, as we wanted to distinguish between the weather timescale (daily data from the STANDARD experiment) and the climate timescale (monthly data for decadal (20-year) periods from the RCP4.5 experiment) to see how the CLM4.5 model performs at different timescales. In addition, no daily output was available for the RCP4.5 experiment, otherwise, we could have used it, and the STANDARD experiment does not include a future scenario forcing to be used for the global warming analysis.

2 Methods

2.1 Study site

The University of South-Eastern Norway uses a 2.5 x 0.2 km site on Mount Imingfjell (60°11’11.7"N 8°34’45.2"E) at an altitude of 1191 meters in Southern Norway (Figure 2-1) to measure the microclimate of lichen and shrub vegetation in order to understand the differences between them. These measurements are part of the Peter Aartsma’s Ph.D. project and have been running since 2018 (Aartsma et al. 2020).

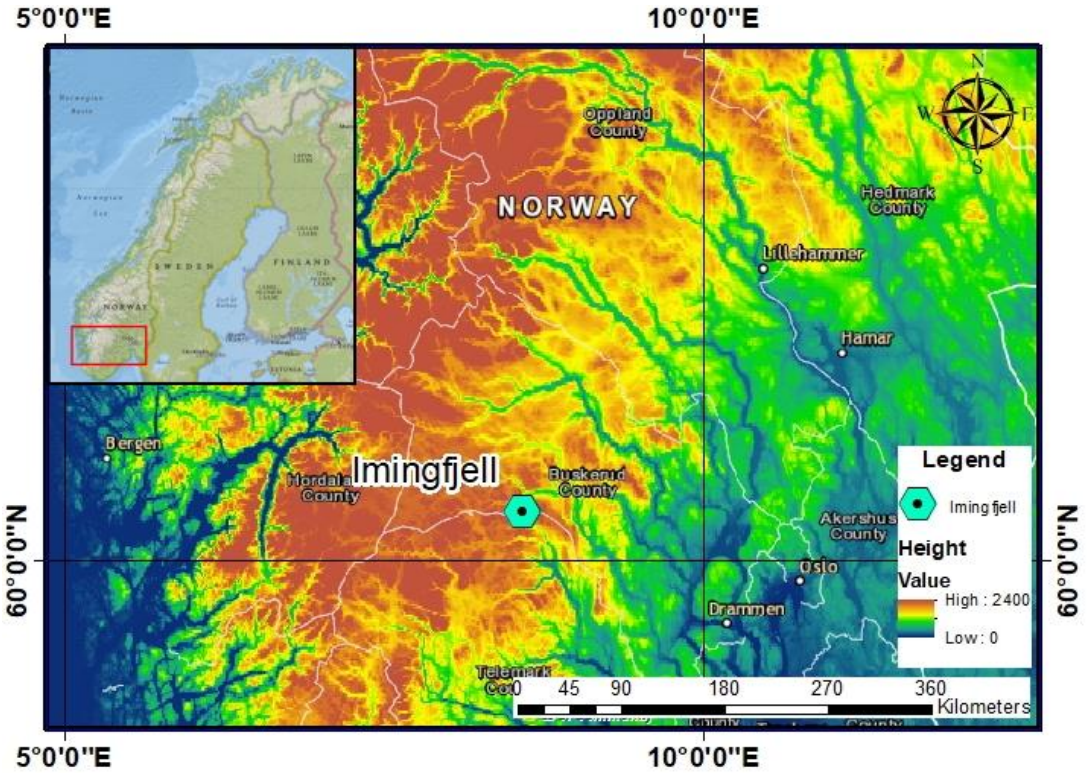

Figure 2-1 Location map showing Southern Norway with marked Mount Imingfjell modified from Vasiakina et al. (2020). The map was made in ArcMap using DEM from USGS (2020). The smaller map of Norway was made from the base map “National Geographic World Map” in ArcMap

The main problems at the Imingfjell site are that measurements of radiation fluxes cannot be continuous and cannot be performed for all energy fluxes (i.e. the sensible heat and latent heat fluxes were not measured). Thus, the application of the CLM4.5 model in our case can verify the physical consistency of the measurements and can help to compare microclimatological responses between lichen- and shrub-dominated surfaces. On the other hand, measured datasets for radiation fluxes and the soil heat flux can also be used to check the accuracy of the model results.

2.2 The Community Land Model (CLM4.5) brief description

The Community Land Model (CLM4.5) is a one-dimensional model that is the default land component for the Community Earth System Model version 1.2 (CESM1.2) (Oleson et al. 2013). A special feature of the CLM4.5 model is that it uses several weather parameters as input (see Section 2.3.1) to calculate local processes for a selected area. It can be used for the entire Earth's surface or for a specific area of different scales, like for individual mountains or mountain ranges. A new version of the Community Land Model (CLM5) was released in 2018 with major updates mainly related to snow density, soil and plant hydrology, carbon and nitrogen cycling and coupling, river modelling and crop modelling (Lawrence et al. 2019). CLM4.5 can either be run in offline mode, receiving its input from an existing dataset (observed or modelled), or in coupled mode, interacting constantly with the Community Atmospheric Model (CAM, the atmospheric component in CESM) (Oleson et al. 2013).

The CLM4.5 model can simulate various biogeochemical and biogeophysical (such as hydrological cycle and surface energy fluxes) processes (Figure 2-2). The model calculates these processes based on the balances of surface energy, water, and carbon. All formulas used in the model are detailed in its technical description by Oleson et al. (2013).

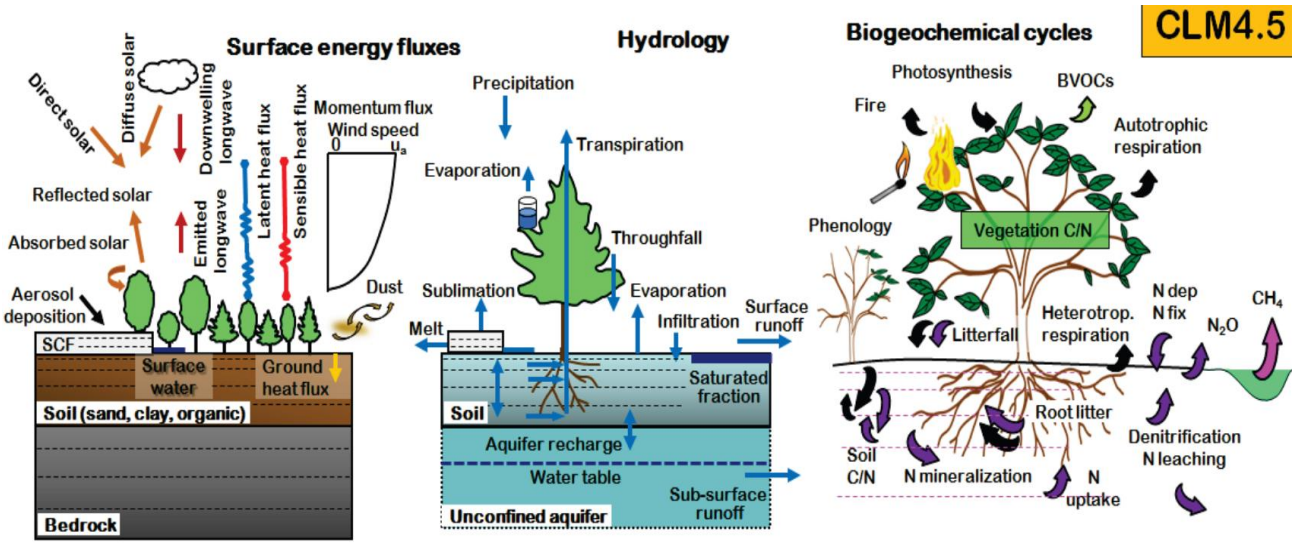

Figure 2-2 Schematic representation of biogeochemical and biogeophysical processes simulated by the CLM4.5 model (Oleson et al. 2013)

In the model, the Earth's surface is divided into grid cells, which can consist of up to three subgrid levels (Figure 2-3). The single grid cell size is 1x1 degree latitude-longitude (Oleson et al. 2013).

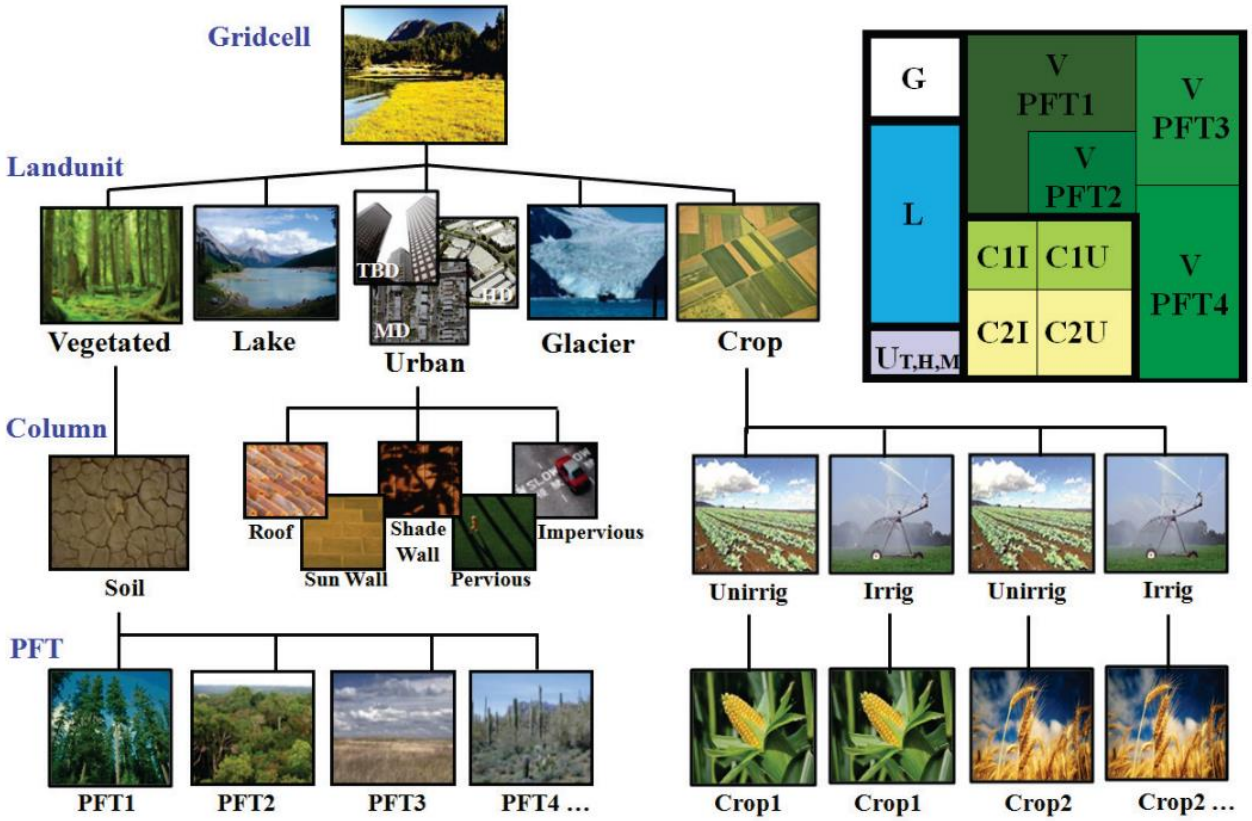

Figure 2-3 CLM4.5 subgrid hierarchy diagram (Oleson et al. 2013)

The first subgrid level is called the land unit and is designed to reflect the spatial diversity of subgrid heterogeneity. The land unit can be represented as a crop, glacier, lake, vegetated and/or urban (Oleson et al. 2013).

Then, the first subgrid unit can be further divided into soil/snow columns, which is the second subgrid level. It was designed to identify potential variability in different soil and snow states. The column can have up to fifteen layers of soil and a maximum of five layers of snow. The crop land unit can be divided into irrigated and non-irrigated columns; the urban land unit – into five columns such as pervious and impervious canyon floor, sunlit walls and shaded walls, and roof. Lake, glacier, and vegetated land units are each represented as a single column (Oleson et al. 2013).

The third and final subgrid level is the plant functional types (PFT) level, including bare ground. The PFT level is designed to capture biogeochemical and biogeophysical differences between broad categories of plants. For the vegetated land unit, a single column can have up to 16 possible PFTs (Table 2-1), depending on structure and physiology. For the crop land unit, each column can have several different crop types. All incoming and outgoing fluxes are defined at this level (Oleson et al. 2013).

Table 2-1 Plant functional types in CLM4.5 (Oleson et al. 2013)

№	Plant functional type	Acronym
1	Needleleaf evergreen tree – temperate	NET Temperate
2	Needleleaf evergreen tree – boreal	NET Boreal
3	Needleleaf deciduous tree – boreal	NDT Boreal
4	Broadleaf evergreen tree – tropical	BET Tropical
5	Broadleaf evergreen tree – temperate	BET Temperate
6	Broadleaf deciduous tree – tropical	BDT Tropical
7	Broadleaf deciduous tree – temperate	BDT Temperate
8	Broadleaf deciduous tree – boreal	BDT Boreal
9	Broadleaf evergreen shrub – temperate	BES Temperate
10	Broadleaf deciduous shrub – temperate	BDS Temperate
11	Broadleaf deciduous shrub – boreal	BDS Boreal
12	C_3 arctic grass	–
13	C_3 grass	–
14	C_4 grass	–
15	[1]C_3 Unmanaged Rainfed Crop	Crop R
16	C_3 Unmanaged Irrigated Crop	Crop I

[1] Only used if irrigation is active

For a complete and more detailed description of the CLM4.5 model and its components, see its technical description by Oleson et al. (2013).

2.3 STANDARD experiment vs observed data (daily data)

In our research, we focus on the block simulating biogeophysical processes (Figure 2-2), or, more precisely, surface energy fluxes since we are interested in the radiation and energy budgets components.

A single grid cell containing the Imingfjell area was used for the STANDARD experiment. The grid cell had the first subgrid level as the vegetated land unit with the following PFTs in the third subgrid level: needleleaf deciduous tree – boreal (30% of the Imingfjell grid cell), broadleaf evergreen shrub – temperate (1%), C3 arctic grass (34%) and C3 grass (35%). In reality, the vegetation of the Imingfjell research site is represented by lichen, shrubs, and some grasses, but without trees (Sundstøl and

Odland, 2017). The STANDARD experiment was run in offline mode where the PFTs were fixed, so the actual vegetation differed from the percentages plugged into the model. In the STANDARD experiment, the model was run for the grid cell representing Imingfjell for the entire 20th century and beyond, until 2016, and used simulated input data to produce output data.

2.3.1 Input data for the STANDARD experiment

As the input, CLM4.5 uses weather parameters such as temperature, K (abbreviation in the model – TBOT); specific humidity, kg kg^{-1} (SHUM); wind speed, m s^{-1} (WIND); surface pressure, Pa (PSRF); total precipitation, mm H_20 sec^{-1} (PRECTmms); and total incident radiation, W m^{-2} (FSDS). The model can derive these parameters either from the CAM atmospheric model in coupled mode or through an existing dataset in offline mode (Oleson et al. 2013). For the STANDARD experiment, CLM4.5 was run for the grid cell of Imingfjell with daily output in offline mode, using the input from the CAM model that was part of the CESM simulation, which was done by others. The STANDARD experiment had 4 values each day as the input from 1901-2016, but our analysis only used data from 2002 to 2016.

A comparison was made with field data to test how well the model determines weather parameters for its input data (as a part of the 1st research question). The data from the two meteorological stations closest to Imingfjell with the longest available observation periods were taken as field data. Weather data (to be used for comparison) was taken from the Norwegian Meteorological Institute database called eKlima (2019). The first station, located 26 km from Imingfjell at an altitude of 798 meters, was 'Dagali Lufthavn'. The second station (870 meters), located 32 km from our study site, was 'Tunhovd'. The description of meteorological stations is presented in Table 2-2.

Tale 2-2 Description of the 'Dagali Lufthavn' and 'Tunhovd' stations from eKlima (2019)

Stnr	Name	Operates from	Operates until	Altitude, m	Latitude, °N	Longitude, °E	Municipality	County
29600	Tunhovd	Jul 1895	TD[1]	870	60.4629	8.7511	Nore Og Uvdal	Viken
29720	Dagali Lufthavn	Nov 2001	TD[1]	798	60.4188	8.5263	Hol	Viken

[1]TD – to date

Despite that the 'Tunhovd' station has been running since 1895, of all the parameters we need, it has only precipitation observations. 'Dagali Lufthavn' began its observations at the end of 2001 and

has data on temperature (°C), surface air pressure (hPa), wind speed (m s^{-1}) and specific humidity (g kg^{-1}). The period of 15 years (from 2002 to 2016) was chosen for the input data comparison since this was the longest joint period between stations and the model. Mean monthly values were calculated over the selected period for the model inputs and station data. For some months, the station datasets had gaps or no data, therefore, mean monthly values were calculated for a different number of years (from 9 to 15 years). Annexes 1 – 5 show tables with monthly averages and the number of available years used to calculate them.

No data on total incident radiation (W m^{-2}) was available from the stations. However, we used an alternative such as solar radiation at the top of the atmosphere for the comparison instead. This radiation is considered approximately constant from year to year for the same territory, so only one year of data is required for the comparison. The solar flux for Imingfjell for each day of the year was calculated using the formula 2-1 (Rose 2019):

$$Q = S_0 \left(\frac{\overline{d}}{d}\right)^2 \cos\theta_s \,, \tag{2-1}$$

where S_0 is the solar constant (1366 W m^{-2}); $\overline{d}$ is the mean Earth-Sun distance equal to 1.0, in astronomical units; d is the Earth-Sun distance for Day of the Year expressed in astronomical units (values taken from USGS, 2019); θ_S is the zenith angle equal to (2-2):

$$\theta_s = 90^o - Sun\ Position^o, \tag{2-2}$$

where $Sun\ Position^o$ obtained from SunEarthTools (2019) for the Imingfjell area.

The earliest available year (2010) from SunEarthTools for Imingfjell was chosen to calculate the solar flux and compare it with the simulated total incident radiation. 2016 was also calculated using formula 2-2 to check if the solar flux is constant throughout the years for Imingfjell.

The grid cell height was not readily provided by CLM4.5, so we used the barometric formula (2-3) to calculate it as the elevation above sea level (Svirin 2019):

$$P = P_o \exp\left(-\frac{Mg}{RT}h\right), \tag{2-3}$$

where P is the air pressure in kPa; P_0 is the average sea level pressure (101.325 kPa); M is the molar mass of Earth's air equal to 0.02896 kg mol^{-1}; g is the gravitational acceleration equal to 9.807 m s^{-2}; h is the altitude above sea level in meters; R is the universal gas constant (8.3143 N m mol^{-1} K^{-1}); and T is the standard temperature (288.15 K).

2.3.2 Output data for the STANDARD experiment

The model produces a huge number of different parameters as the output data (in the STANDARD experiment there were 428 daily and 38 two-days values). Nevertheless, this thesis focuses on energy and radiation fluxes. Net shortwave and net all-wave radiation were not presented in the model output, so these fluxes were derived from the radiation budget. The modelled incoming (abbreviation in the model – FSDS) and outgoing shortwave radiation (FSR) were used to calculate net shortwave radiation using formula (1-1) from Section 1.5. Net longwave radiation was present in the model output (FIRA). However, it was also verified by the same method (Equation 1-2) as net shortwave radiation, using modelled incoming (FLDS) and outgoing (FIRE) longwave radiation. Energy budget components such as the sensible heat flux (FSH), the latent heat flux (EFLX_LH_TOT), and the soil heat flux (FGR) were also extracted from the model. Net all-wave radiation was both calculated from the radiation budget (Equation 1-3) and the energy balance (Equation 1-4) to check whether these values coincide as they should. The daily output data from the model was available from 1901 to 2014, but only the modern period (1990-2014) was used in the STANDARD experiment.

The accuracy of the output data was analysed by the comparison with field data obtained by Ph.D. student Peter Aartsma at the Imingfjell site (under the 1st research question). Measurements were made for two types of vegetation (lichen and shrub) to capture their theorized differences in energy fluxes. All components of the radiation balance, the soil heat flux and some other weather parameters were measured, except for the sensible heat flux and the latent heat flux. The data was collected over several days during two summers – 2018 and 2019. In total, there were 44 days with field data (Vasiakina et al. 2020).

Summer temperatures from the 'Dagali Lufthavn' station were taken to analyse temperature trends over the observed period. Summers of 2018 (summer mean temperature was 12.5°C) and 2019 (summer mean temperature was 11.5°C) were abnormally warm, as their average summer temperature was 1-2°C higher than the average long-term summer temperature (10.7°C). Nevertheless, the mean daily temperature varied greatly during these two summers: from 5.1°C to 18.2°C for 2018, and from 9.4°C to 18.7 °C for 2019.

On the observation side, field data from Imingfjell consists of only 44 days over two years – 2018 and 2019. While from the modelling side, we have CLM4.5 values for many years, but not including 2018 and 2019. Also, the CLM4.5 input in the STANDARD experiment was received from CAM in offline mode, so the weather in the model was fixed and cannot be expected to be similar to reality. Therefore, we created datasets using 44 observation days, which represent "average" conditions that

can be meaningfully compared with the model. Three different "average" conditions were chosen: "cold", "normal" and "extremely warm", based on temperatures. 44 observation days were classified in one of these three groups, creating three so-called composites. Next, three summers were selected from the model output that represents these three different temperature regimes.

The limits of temperature regimes were chosen arbitrarily, but so that each one had at least 10 days of data. Observation days with daily temperatures of more than 16°C, were united into an "extremely warm" regime. 13 out of 44 days were categorized as "extremely warm". The second regime with daily summer temperatures between 12-16°C was called the "normal". The "normal" regime consisted of 19 days. The last one was called the "cold" regime for temperatures below 12°C. Of the total 44 days, 12 days were used for the "cold" regime. The temperature regimes were redefined since Vasiakina et al. (2020).

The modelled modern 25-year period (1990-2014) was analysed to find years with similar summer temperature conditions for each period ("cold", "normal", "extremely warm"). 2006 was chosen for the comparison with the "extremely warm" regime, as it was the warmest year available in the model with an average summer temperature of 14.99°C. The modelled long-term average summer temperature for the modern period was 12.92°C, so 2011 was chosen with the closest summer average (12.93 °C) for the "normal" regime analysis. The coldest year in the model (1993) with a summer temperature of 10.48°C, was used for the "cold" regime (Vasiakina et al. 2020). As a result, the modelled dataset consisted of data from three different simulated years that differ in temperature regimes. In some cases, observations were made on the same dates every year, so the modelled dataset consisted of fewer days (37 days) than the observed one (44 days).

Means, standard deviation and coefficient of variance for the fluxes from the energy and radiation budgets were calculated for each temperature period for the modelled dataset and for the two observed datasets – lichens and shrubs.

2.4 RCP4.5 experiment (monthly data)

For the analysis of past and future climate changes for Imingfjell (i.e. 2nd research question), the data from one of the Climate Model Intercomparison Project phase 5 (CMIP5) experiments were used (Taylor et al. 2012). CMIP5 consists of long-term (century time scale) and near-term (10-30 years) climate model experiments carried out by the World Climate Research Programme's (WCRP) Working Group on Coupled Modelling (WGCM), Integration and Modelling of the Earth System (AIMES) project and the International Geosphere-Biosphere Programme's (IGBP) Analysis (Taylor et al. 2012).

The RCP4.5 experiment was selected from CMIP5 for our climate change study at Imingfjell. Given the current trend in GHG concentrations, RCP4.5 can be considered the most likely future climate scenario (see Section 1.1.2), in which radiative forcing is simulated to reach 4.5 W m^{-2} in 2100 compared to pre-industrial conditions. The RCP4.5 experiment consists of two periods based on the changes in forcing over the time series from 1850 to 2100 (Figure 2-4): the so-called Historical experiment and the Non-historical experiment. The Historical experiment (1850-2005) is an evaluation of the past climate with forcing changes partly based on what actually happened. Meanwhile, the Non-historical experiment (2006-2100) is based on the future RCP4.5 scenario rather than on observed data (Taylor et al. 2011).

Compared to the STANDARD experiment, the same CLM4.5 version, the same spatial resolution (1x1 latitude-longitude), and the same grid cell were chosen for the RCP4.5 experiment. The RCP4.5 experiment was run with CESM in fully coupled mode, so CLM4.5 received its updated input from the CAM model. For the output data, fluxes from the radiation balance and energy budget were selected as in Section 2.3.2. Mean monthly summer temperature (TSA) and precipitation (PRECT) were also taken from the RCP4.5 experiment to compare the dependence of these fluxes on changes in temperature and precipitation.

Since in the STANDARD experiment the analysis was carried out only for the summer period, it was decided to use the same time frame for this experiment (i.e. summer).

For a more accurate study of climate change (the 2nd research question), the period from 1850 to 2100 was divided into three time periods (the “past”, the “present”, and the “future”) of 20 years. The “past” period from 1850 to 1869 was taken from the Historical experiment as the pre-industrial control climate for our region. The “present” and the “future” periods were taken from the RCP4.5 Non-historical experiment. For the “present” period, data from 2006-2025 were selected for the analysis, as this was the earliest possible 20-year period in the Non-Historical experiment. The 2081-2100 period was chosen as the “future” period since it was the latest available period and the radiative forcing is projected to reach 4.5 W m^{-2} by the end of it (2100).

Means, standard deviation, coefficient of variation and Bowen’s ratio were calculated for each 20-year period. Comparisons of the “past” with the “present” and the “present” with the “future” were made to see how energy and radiation fluxes changed over time and what could be the reasons for his – natural and/or anthropogenic forcings.

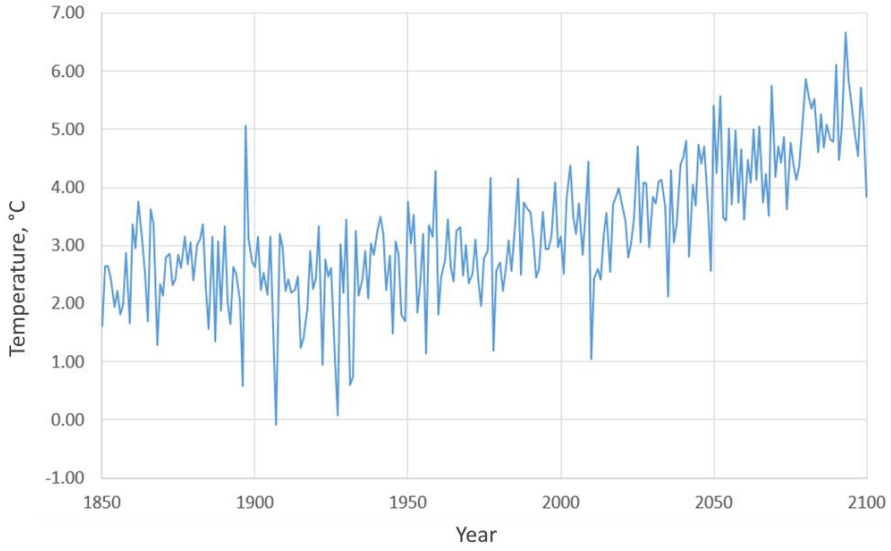

Figure 2-4 Annual mean temperature (°C) as a time series from 1850 to 2100 for the Imingfjell grid cell from the RCP4.5 experiment (Taylor et al. 2011, 2012)

2.5 T-test

Statistical tests of the data from the STANDARD experiment and the RCP4.5 experiment, such as two sample t-tests, were performed to see if there were any significant differences between the datasets in each experiment. For the STANDARD experiment, we compared the modelled results with fluxes from both lichens and shrubs. For the RCP4.5 experiment, the "past" with the "present" and the "present" with the "future" were tested. Two sample t-test compares the means and variance/distributions of each energy and radiation flux between two datasets by comparing a t-value from the Student's t-distribution with a t-value calculated by (2-4) (Schluter and Whitlock 2015):

$$t = \frac{\overline{Y_1} - \overline{Y_2}}{SE_{\overline{Y_1} - \overline{Y_2}}}, \tag{2-4}$$

where $\bar{Y}_1$ and $\bar{Y}_2$ are mean values of the first and second datasets, respectively. $SE_{\bar{Y}_1 - \bar{Y}_2}$ is the standard error of difference in means, calculated through (2-5) (Schluter and Whitlock 2015):

$$SE_{\overline{Y_1} - \overline{Y_2}} = \sqrt{\frac{s_p^2}{n_1} + \frac{s_p^2}{n_2}}, \tag{2-5}$$

where n_1 is a sample size of the first dataset; n_2 is a sample size of the second dataset; s^2_p is a pooled variance, calculated by (2-6) (Schluter and Whitlock 2015):

$$s_p^2 = \frac{df_1 s_1^2 + df_2 s_2^2}{df_1 + df_2}, \quad (2\text{-}6)$$

where df_1 and df_2 are degrees of freedom (2-7) for the first and second datasets, respectively, calculated as (Schluter and Whitlock 2015)

$$df_1 = n_1 - 1;\ df_2 = n_2 - 1. \quad (2\text{-}7)$$

For the STANDARD experiment, we compared the observed and modelled fluxes between different temperature regimes, so the sample size (*n*) for the "extremely warm" period was 13 days, for the "normal" – 19 days and for the "cold"– 12 days. All RCP4.5 datasets have the same sample size of 20 years.

In order to find out which tabular t-value from the Student's t-distribution (Schluter and Whitlock 2015) is necessary for a comparison with the calculated t-value (2-4), the formula (2-8) was used, depending on degrees of freedom:

$$df = df_1 + df_2 = n_1 + n_2 - 2. \quad (2\text{-}8)$$

Using the obtained *df*-values from (2-8), the tabulated t-value for the "extremely warm" period was 2.06 with *df*=24, for the "normal" period – 2.03 (*df*=36) and for the "cold" period – 2.03 (*df*=22). The tabulated t-value for the RCP4.5 experiment was 2.02 with *df*=38.

Our null (2-9) and alternative (2-10) hypotheses were:

$$H_0: \text{No difference between datasets}, \quad (2\text{-}9)$$

$$H_A: \text{Datasets differ from each other}. \quad (2\text{-}10)$$

A 95%-significance level was used for all t-values from the Student's t-distribution. If the calculated t-value (2-4) is less than the t-value from Student's t-distribution (Schluter and Whitlock 2015), then we do not reject the null hypothesis (2-9). Therefore, these data are insufficient to speak of a statistically significant difference between the datasets. In this case, we consider that CLM4.5 managed to successfully model similar datasets. However, if a calculated t-value (2-4) is greater than a t-value from the Student's t-distribution (Schluter and Whitlock 2015), then we reject the null hypothesis (2-9), which means that the selected datasets differ from each other. Hence, in this case, we consider that the model was unable to accurately simulate the data.

3 Results

3.1 Comparison of input data from the STANDARD experiment with observations

We compared the CLM4.5 input data, produced by the atmospheric model CAM in offline mode, with observations to contribute to the answer of the 1st research question about how well the CLM4.5 resembles measurements near Imingfjell. To understand the output of CLM4.5, it is important to first analyse the received input. The compared results consist of combined modelled input and observed datasets for temperature (°C), specific humidity (g kg^{-1}), wind speed (m s^{-1}), air pressure (hPa), total precipitation (mm) and solar radiation (W m^{-2}).

3.1.1 Temperature

A comparison of the modelled mean monthly temperature with observations from 'Dagali Lufthavn' revealed that the CAM model simulated warmer conditions in all months (Figure 3-1). The largest difference between modelled and observed values was registered in December, when the model was 3.62°C warmer. On the other hand, in mid-summer the difference was much smaller: in July, the model was warmer by 1.65°C (see Annex 1). All modelled temperature values fell within the range possible at 'Dagali Lufthavn'.

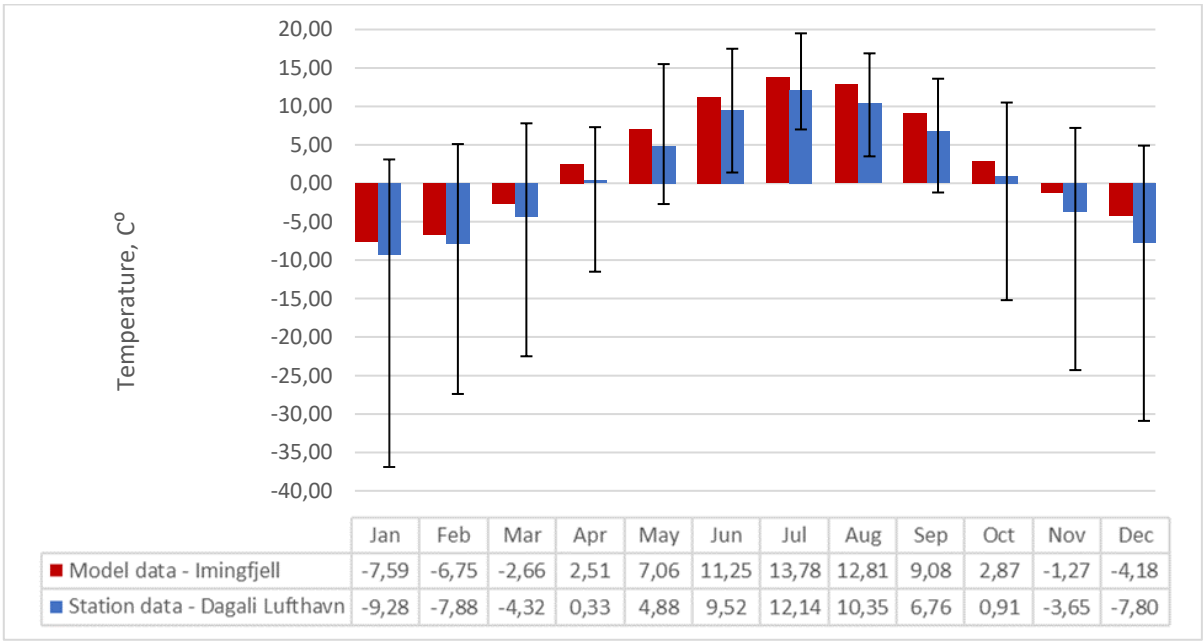

	Jan	Feb	Mar	Apr	May	Jun	Jul	Aug	Sep	Oct	Nov	Dec
Model data - Imingfjell	-7,59	-6,75	-2,66	2,51	7,06	11,25	13,78	12,81	9,08	2,87	-1,27	-4,18
Station data - Dagali Lufthavn	-9,28	-7,88	-4,32	0,33	4,88	9,52	12,14	10,35	6,76	0,91	-3,65	-7,80

Figure 3-1 Observed data from the 'Dagali Lufthavn' station (in blue) with its range of values (from minimum to maximum) and modelled data from the STANDARD experiment (in red) for mean monthly temperatures calculated over 2002-2016 period

Generally, both datasets showed the standard response for the Northern Hemisphere temperature trend throughout the year – with the lowest temperatures during the colder months (November-March) and peak temperatures in mid-summer (Herman et al. 2010).

3.1.2 Specific humidity

When comparing the simulated and observed specific humidity (Figure 3-2), there was no general pattern in differences between the datasets. The model results for specific humidity appeared to be slightly higher than those observed for most of the year (April till August, November, December), with the largest difference in August of 0.36 g kg^{-1}. In the remaining months, specific humidity at Imingfjell was lower than at 'Dagali Lufthavn' with the maximum difference between datasets of 0.16 g kg^{-1} (Annex 2). The modelled specific humidity fell within the observed range.

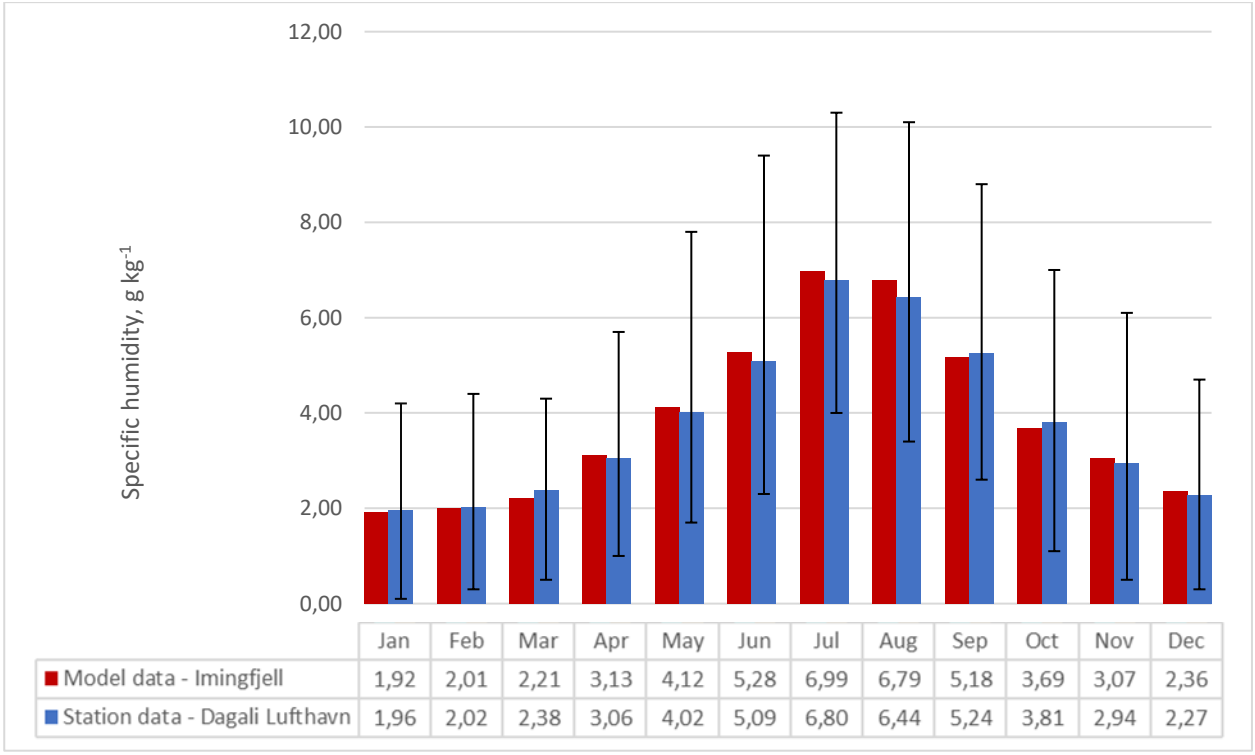

	Jan	Feb	Mar	Apr	May	Jun	Jul	Aug	Sep	Oct	Nov	Dec
Model data - Imingfjell	1,92	2,01	2,21	3,13	4,12	5,28	6,99	6,79	5,18	3,69	3,07	2,36
Station data - Dagali Lufthavn	1,96	2,02	2,38	3,06	4,02	5,09	6,80	6,44	5,24	3,81	2,94	2,27

Figure 3-2 Observed data from the 'Dagali Lufthavn' station (in blue) with its range of values (from minimum to maximum) and modelled data from the STANDARD experiment (in red) for mean monthly specific humidity calculated over 2002-2016 period

Both datasets showed a similar trend throughout the year: a maximum specific humidity in the summer months with minimal values in winter.

3.1.3 Wind speed

As shown in Figure 3-3, the simulated wind speed values were higher than those observed for all months. The largest difference in values between datasets occurred in the winter months - up to 3.42 m s^{-1}. In the summer months, the difference decreased to around 1 m s^{-1} (see Annex 3). Despite the overestimation of the simulated average wind speeds, they did not exceed maximal possible observed values of the meteorological station.

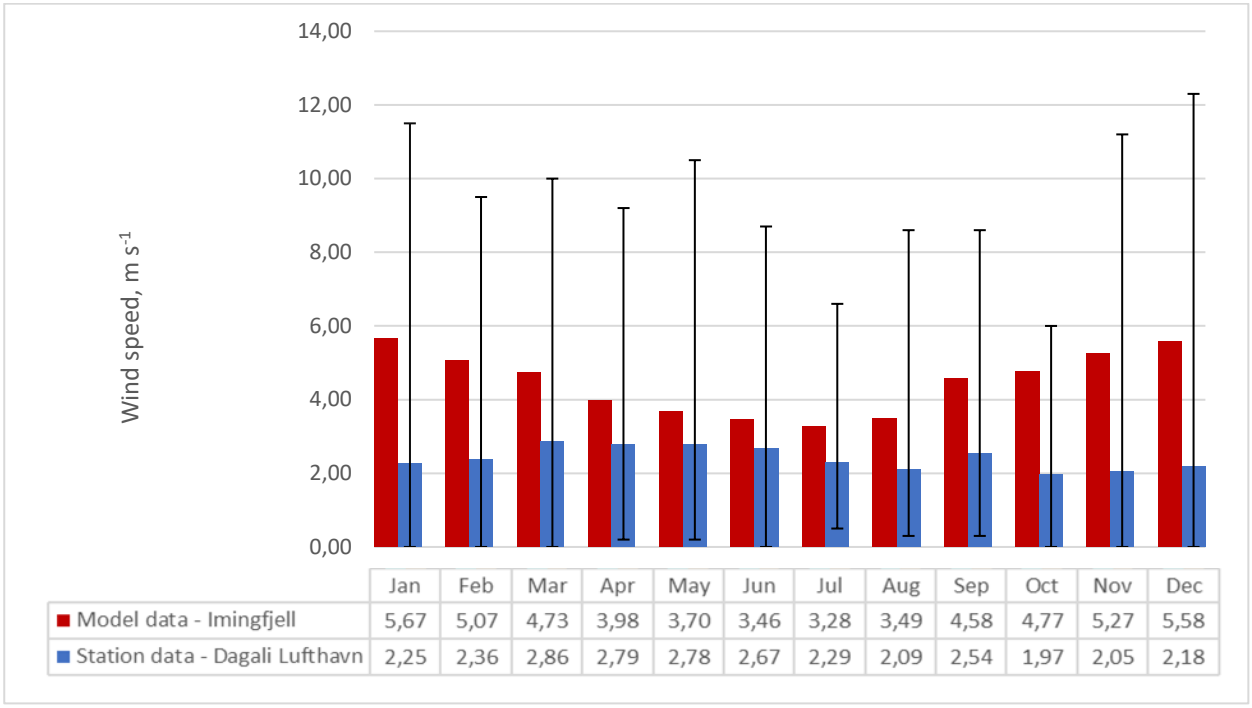

	Jan	Feb	Mar	Apr	May	Jun	Jul	Aug	Sep	Oct	Nov	Dec
Model data - Imingfjell	5,67	5,07	4,73	3,98	3,70	3,46	3,28	3,49	4,58	4,77	5,27	5,58
Station data - Dagali Lufthavn	2,25	2,36	2,86	2,79	2,78	2,67	2,29	2,09	2,54	1,97	2,05	2,18

Figure 3-3 Observed data from the 'Dagali Lufthavn' station (in blue) with its range of values (from minimum to maximum) and modelled data from the STANDARD experiment (in red) for mean monthly wind speed calculated over 2002-2016 period

The observed monthly mean wind speed did not change much during the year, remaining at about 2 m s^{-1}. The modelled wind values had a noticeable pattern throughout the year: the wind speed decreased from January to a minimum in July, after which it began to increase.

3.1.4 Air pressure

Based on Figure 3-4, the simulated air pressure values were always higher than the observed. The largest difference between the datasets was observed in January and April – 46 hPa, while the smallest in July and August – 45 hPa. In all other months, the difference between datasets was approximately the same – around 44 hPa (see Annex 4). The simulated air pressure values never fell within the range of possible values from the 'Dagali Lufthavn' station and always exceeded them.

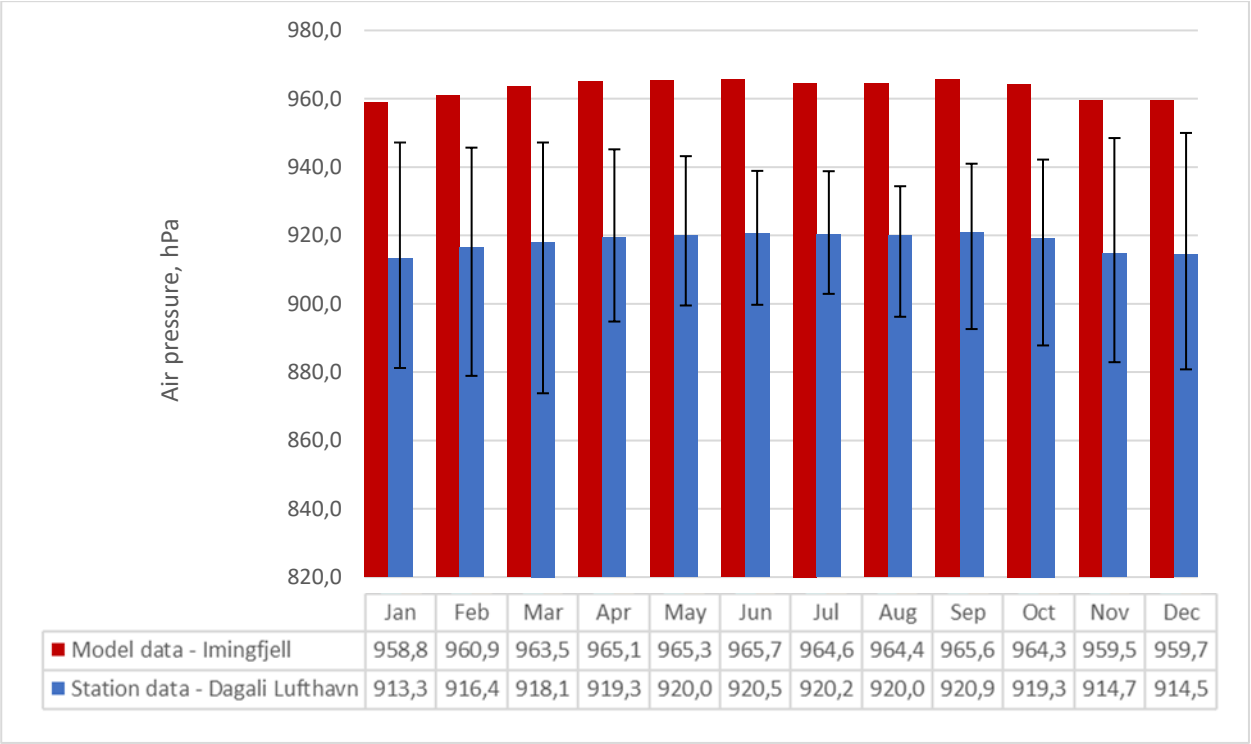

	Jan	Feb	Mar	Apr	May	Jun	Jul	Aug	Sep	Oct	Nov	Dec
Model data - Imingfjell	958,8	960,9	963,5	965,1	965,3	965,7	964,6	964,4	965,6	964,3	959,5	959,7
Station data - Dagali Lufthavn	913,3	916,4	918,1	919,3	920,0	920,5	920,2	920,0	920,9	919,3	914,7	914,5

Figure 3-4 Observed data from the 'Dagali Lufthavn' station (in blue) with its range of values (from minimum to maximum) and modelled data from the STANDARD experiment (in red) for mean monthly air pressure calculated over 2002-2016 period

For both datasets, air pressure remained virtually unchanged between months. Although, a slight increase in air pressure for both datasets was observed in the warmer months from April to September.

3.1.5 Total precipitation

The modelled mean monthly total precipitation was lower than the observed values at the 'Tunhovd' station throughout the year, except for October (Figure 3-5). The largest difference between precipitation datasets occurred in the summer months – the 'Tunhovd' values were about 30 mm higher than the CAM ones. The smallest difference of 2 mm was observed in October (Annex 5). The simulated precipitation fell within the range of possible values for 'Tunhovd'.

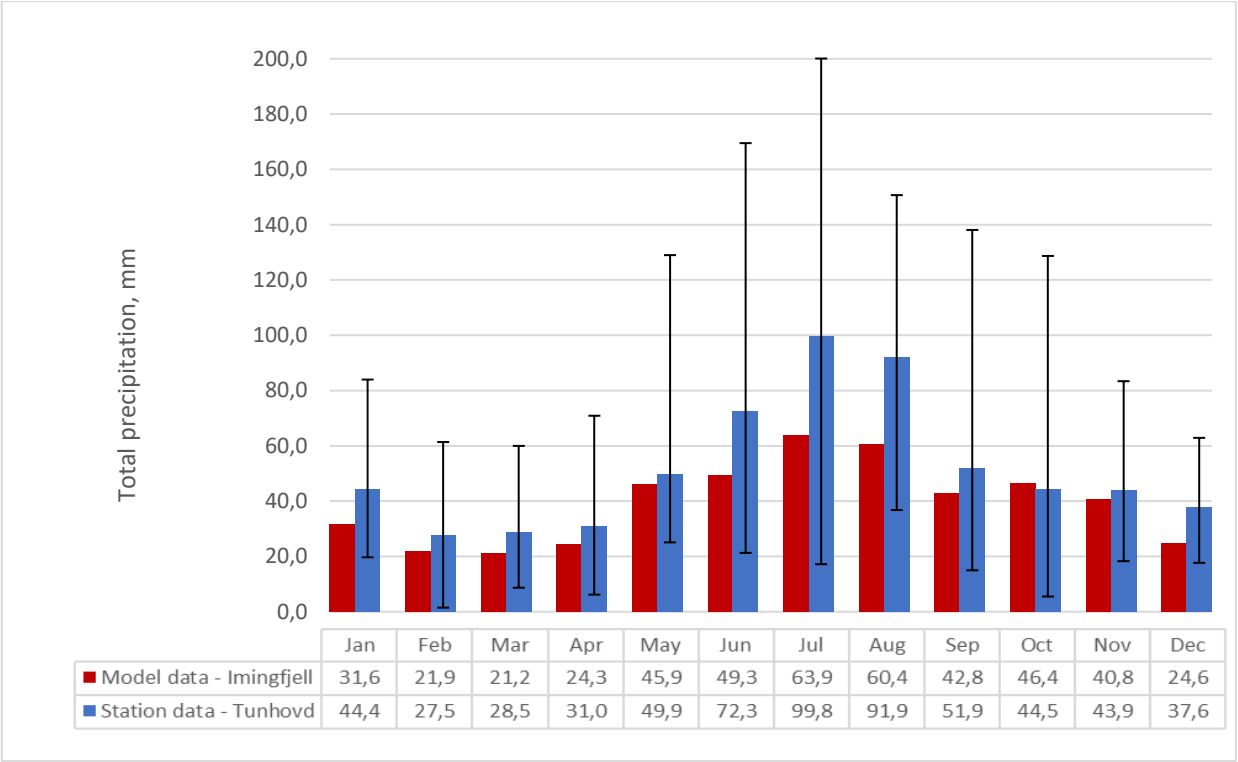

	Jan	Feb	Mar	Apr	May	Jun	Jul	Aug	Sep	Oct	Nov	Dec
Model data - Imingfjell	31,6	21,9	21,2	24,3	45,9	49,3	63,9	60,4	42,8	46,4	40,8	24,6
Station data - Tunhovd	44,4	27,5	28,5	31,0	49,9	72,3	99,8	91,9	51,9	44,5	43,9	37,6

Figure 3-5 Observed data from the 'Tunhovd' station (in blue) with its range of values (from minimum to maximum) and modelled data from the STANDARD experiment (in red) for mean monthly total precipitation calculated over 2002-2016 period. Values for modelled data in June and December were calculated over 14 years.

Both datasets followed the similar trend – more precipitation in the summer months, less precipitation in February-April.

3.1.6 Solar radiation

The measured incident solar radiation was not available, so the input radiation was compared to the potential radiation. Figure 3-6 shows the modelled total incident solar radiation and potential radiation in the Imingfjell area. Maximal daily values of the Sun position were used in formulas 2-1 – 2-2 (see 2.3.1 Section) to plot the potential radiation.

As expected, the total incident radiation from the model was always far below the potential radiation since maximum values were used for its calculation. Due to the sharp fluctuations in the simulated radiation, the distinctions between the datasets were not constant throughout the year. The greatest differences were observed during warm season and reached up to 700 W m^{-2} in May, while the smallest difference was around 110 W m^{-2} in December (cold season).

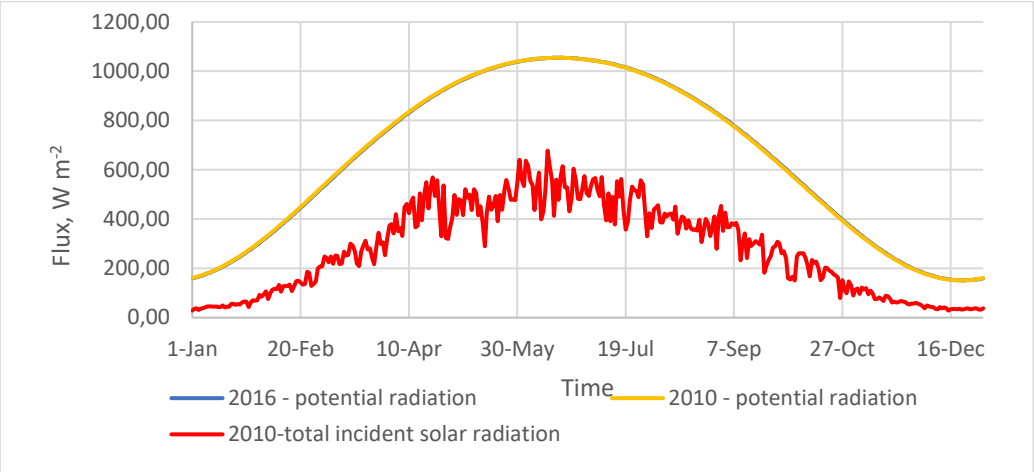

Figure 3-6 Potential radiation for Imingfjell (in yellow and blue) and modelled radiation from the STANDARD experiment (in red). Potential radiation does not change much from year to year, so the lines of the graphs for 2010 and 2016 coincide, making it difficult to see the data for 2016

The potential radiation for the studied area has been constant throughout the years (the lines of the radiation graphs for 2010 and 2016 coincide). The graph of the potential radiation was smooth, while the graph of the modelled radiation had significant fluctuations.

3.2 Comparison of output data from the STANDARD experiment with observations

In the STANDARD experiment, the model output and the 2018-2019 observations from Imingfjell of incoming shortwave (K↓), outgoing shortwave (K↑), shortwave net (K*), incoming longwave (L↓), outgoing longwave (L↑), longwave net (L*), and net all-wave (Q*) radiation were used to plot the radiation budget. Outgoing radiation values (K↑ and L↑) were plotted as negative to show the direction of fluxes relative to the surface (axis '0' in the graphs). The radiation budgets from the STANDARD experiment, as well as lichen and shrub observations for three temperature regimes are presented in Figure 3-7 – Figure 3-15.

Mean values and their range from minimum and maximum for each component of the radiation and energy balances for all datasets, except the latent and sensible heat fluxes were plotted only for modelled data, are presented in Annexes 6 – 25.

All three datasets showed a similar pattern for the radiation fluxes in relation to temperature (interdependent changes): lower temperatures ("cold" regime) coincided with lower values of the radiation budget components, and higher temperatures ("extremely warm" regime) – with higher values.

Since no observed data for the sensible and latent heat fluxes were available, it was impossible to conduct a comparative analysis between the energy balance components from the model and lichen/shrub datasets. Only simulated energy balances are shown in Annexes 26 – 28.

3.2.1 "Extremely warm" regime

The radiation budget and its components for the model, lichens, and shrubs during the "extremely warm" regime are presented in Figures 3-7 – 3-9, respectively.

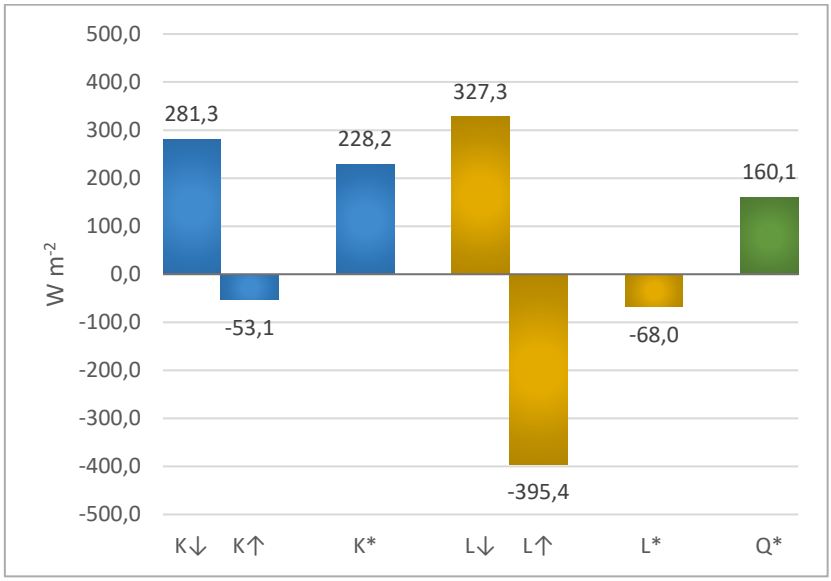

Figure 3-7 Mean values for the modelled radiation budget (the STANDARD experiment data) over the "extremely warm" period with an albedo value of 0.19

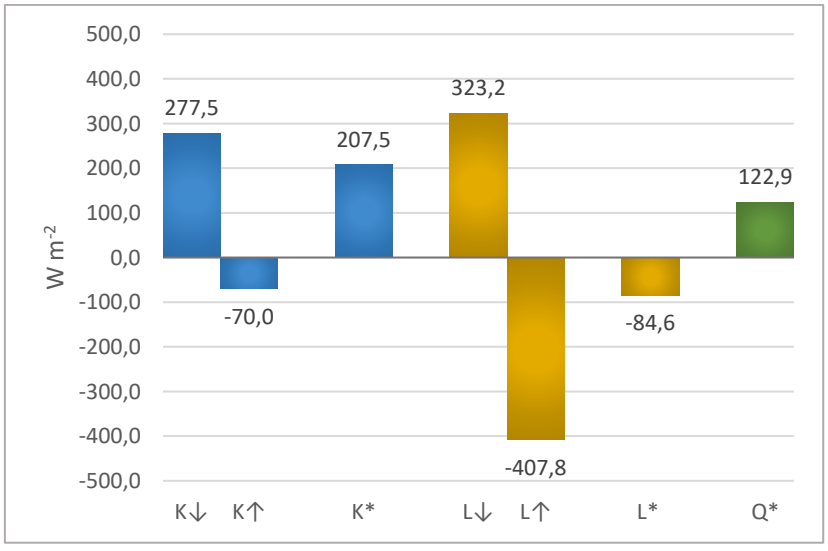

Figure 3-8 Mean values for the observed radiation budget (Lichen data) over the "extremely warm" period with an albedo value of 0.25

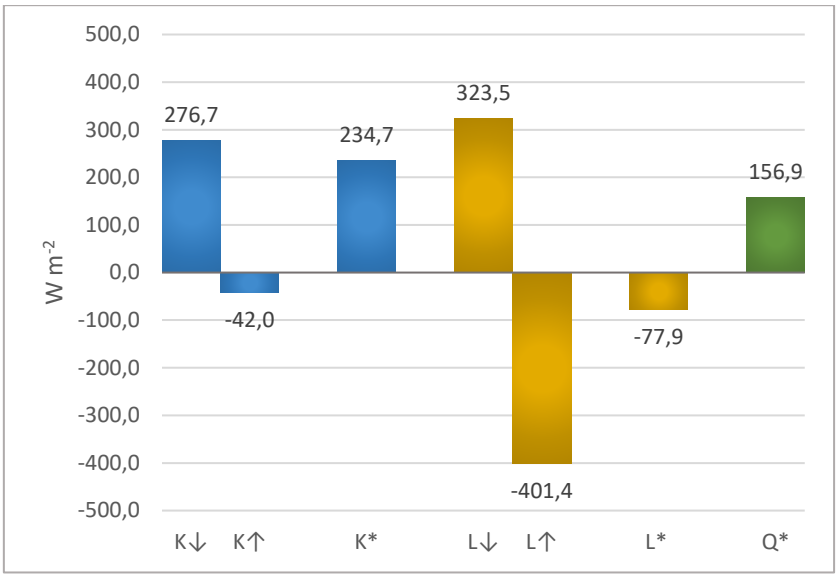

Figure 3-9 Mean values for the observed radiation budget (Shrub data) over the "extremely warm" period with an albedo value of 0.15

From the plots above, the closest resemble in the "extremely warm" regime was between the model and shrub datasets. The differences in the mean values of K↑, K*, L↓, L↑, L* and Q* between the model/shrub were up to 10 times smaller than between the model/lichen. Only for K↓, the difference in means was smaller between the model/lichen data (see Annex 29).

The values of standard deviation varied greatly between datasets and fluxes. However, the standard deviation for the modelled data was lower (with the exception of L↑) than for the observed data for K↑, K↓, K*, L* and Q*. For L↓, the standard deviation was almost the same for all datasets (around 16.7). The coefficients of variation for the observed datasets (lichen and shrubs) differed little from each other. Therefore, the difference between the coefficients of variation for the modelled dataset was the same for lichens and shrubs. The modelled dataset had lower coefficients of variation for K↓, K↑, K*, L*, Q*, and slightly different coefficients of variation for L↓ and L↑ compared with the observed datasets.

3.2.2 "Normal" regime

The radiation budgets during the "normal" regime for the modelled and observed data are presented in Figures 3-10 – 3-12.

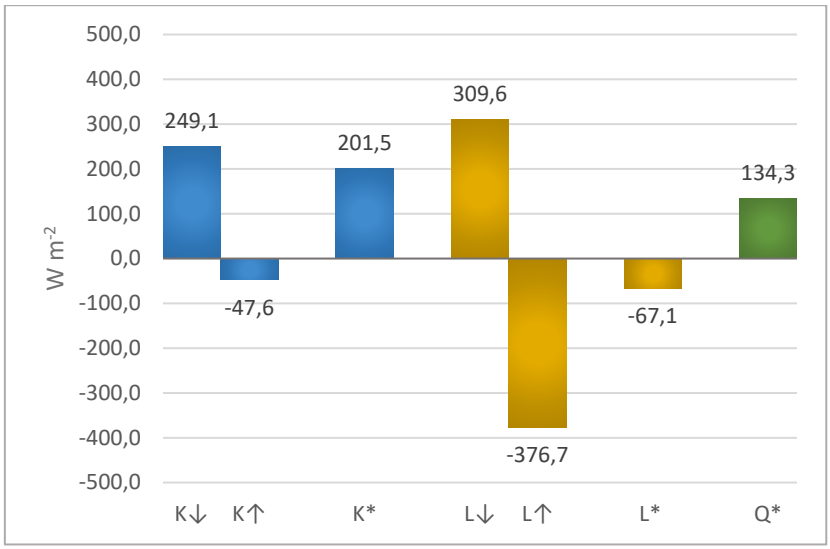

Figure 3-10 Mean values for the modelled radiation budget (the STANDARD experiment data) over the "normal" period with an albedo value of 0.19

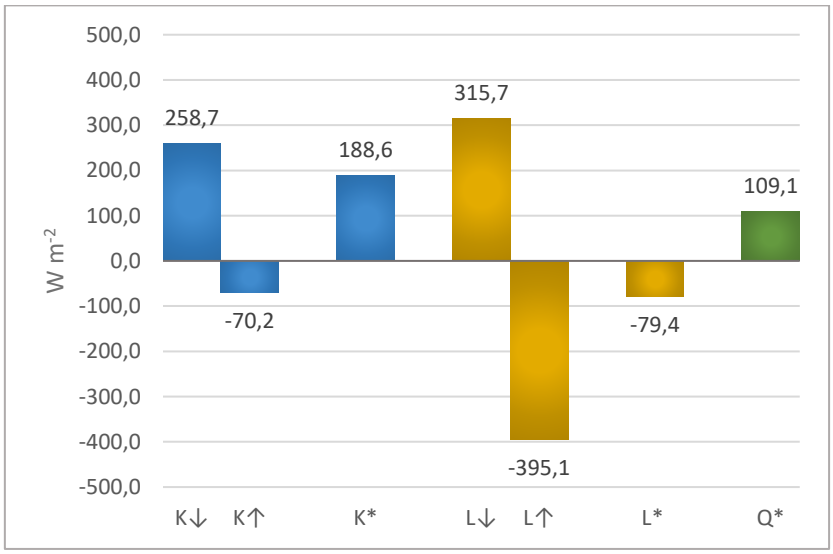

Figure 3-11 Mean values for the observed radiation budget (Lichen data) over the "normal" period with an albedo value of 0.27

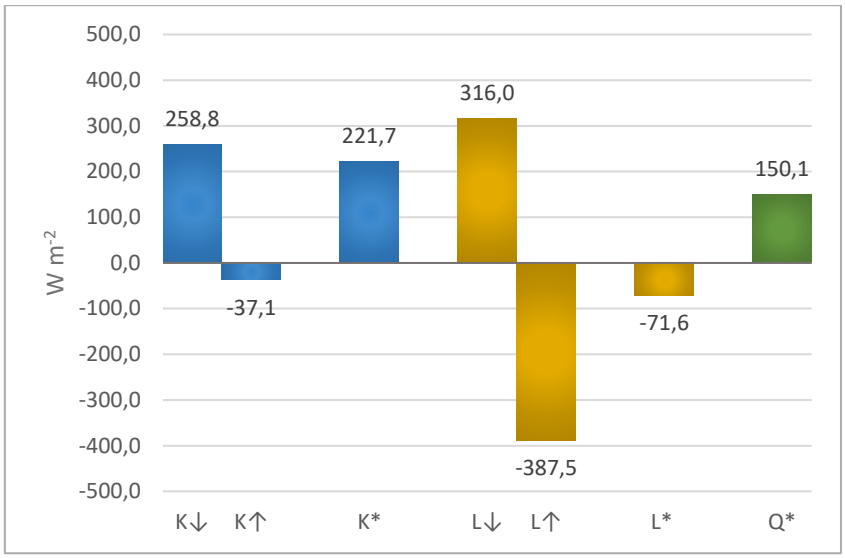

Figure 3-12 Mean values for the observed radiation budget (Shrub data) over the "normal" period with an albedo value of 0.14

Modelled dataset averages were still closer to shrubs than lichens, but not for all fluxes (only for K↑, L↑, L* and Q*). The modelled K* and L↓ closely resembled lichen data in the "normal" temperature regime. For K↓, the differences between the model and the two types of observations were the same (see Annex 30).

The standard deviations for the simulated dataset were significantly less than for both observed datasets for each component of the radiation balance. The coefficients of variation for modelled data were twice or much lower than those of lichens and shrubs for all the radiation budget components, except for L↑.

3.2.3 "Cold" regime

The radiation budgets calculated over "cold" regimes for datasets from the model and observations (lichens and shrubs) are presented in Figures 3-13 – 3-15.

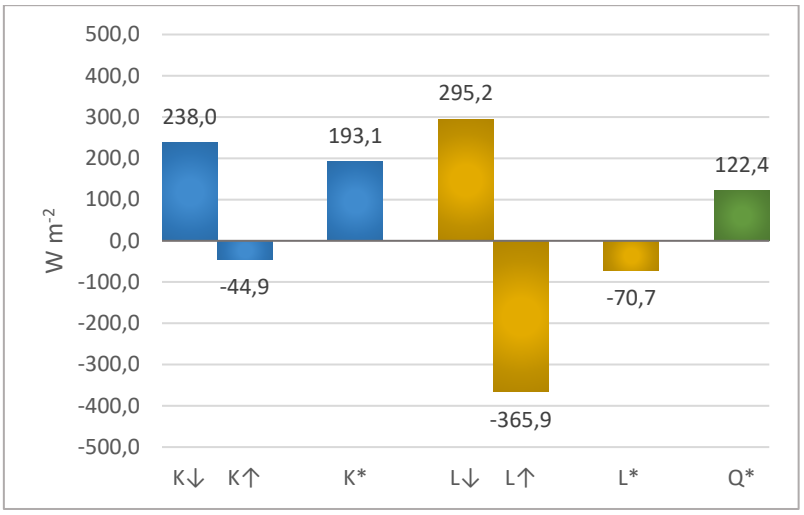

Figure 3-13 Mean values for the modelled radiation budget (the STANDARD experiment data) over the "cold" period with an albedo value of 0.19

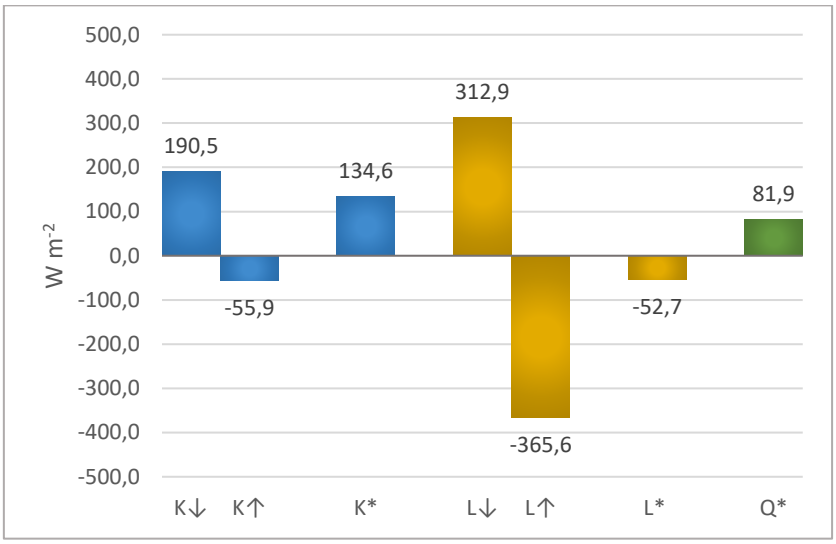

Figure 3-14 Mean values for the observed radiation budget (Lichen data) over the "cold" period with an albedo value of 0.29

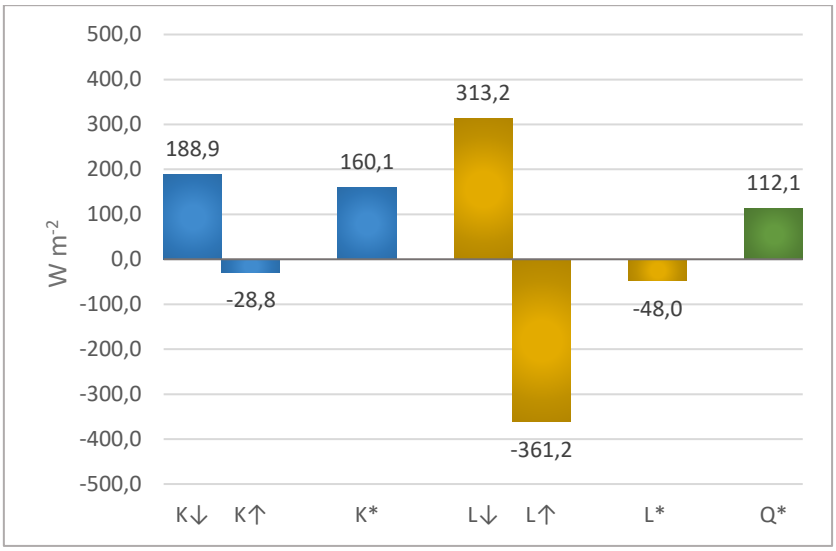

Figure 3-15 Mean values for the observed radiation budget (Shrub data) over the "cold" period with an albedo value of 0.15

In the "cold" regime, the model began to resemble fluxes from the lichen dataset more than from the shrub one (in contrast to other temperature regimes where the model data were closer to the shrub data). However, the modelled net shortwave and net all-wave radiation were still closer to the shrub dataset (Annex 31).

The standard deviations for the model remained the same as in the "normal" regime: smaller in observed ones for all components of the radiation balance. The coefficients of variation for L↑ were the same for all datasets. For all other fluxes, the coefficients of variation for the modelled data were much lower than for the observed data (as in the "normal" regime).

3.2.4 T-test

Comparing statistical characteristics can help us understand in general what data the model provides. But beyond that, a number of t-tests were conducted to more accurately evaluate CLM4.5 and to determine for which component of the radiation balance, temperature regime, and vegetation type the model gives the closest results.

Table 3-1 provides t-values for all components of the radiation budget and the soil heat flux between the model and observed lichen and shrub datasets calculated for each temperature regime. None of the t-values were calculated for the latent and sensible heat fluxes, since there is no observed data available for testing.

If a table cell is blue, it means a calculated t-value is less than a t-value from the Student's distribution, and the null hypothesis is not rejected (i.e., there is no statistically significant difference

between the datasets at the 95% level). If a table cell is red, then a t-calculated is greater than a t-tabulated, and the null hypothesis is rejected (i.e., the datasets are statistically significantly different).

Table 3-1 Calculated t-values for t-tests between the model (m), lichen (l) and shrub (s) datasets (blue cells mean that the null hypothesis is not rejected and red cells – the null hypothesis is rejected)

Temperature regime/$t_{tabular}$	Datasets	Q_G	K↓	K↑	K*[1]	L↓	L↑	L*[1]	Q*[1]
warm/2,06	m/l[2]	1,98	0,24	3,78	1,65	0,63	2,99	2,53	4,37
	m/s[3]	1,75	0,28	4,11	0,48	0,60	1,50	1,53	0,37
normal/2,03	m/l	0,10	0,42	4,18	0,88	1,21	4,92	1,58	2,78
	m/s	1,33	0,42	3,26	1,09	1,28	3,48	0,60	1,32
cold/2,07	m/l	0,48	1,90	1,52	3,23	2,28	0,09	2,09	3,54
	m/s	0,77	1,95	3,91	1,56	2,22	1,65	2,82	0,69

[1]t-values were obtained for the calculated data sets, not observed
[2]m/l – t-value between modelled and lichen datasets
[3]m/s – t-value between modelled and shrub datasets

3.3 RCP4.5 experiment

We analysed the RCP4.5 experiment results to answer the 2nd research question, namely how the energy and radiation budgets for Imingfjell will change in the future if we follow the RCP4.5 scenario. Thus, similarly to the graphs from Sections 3.2.1 – 3.2.3 and from Annexes 26 – 28, the radiation and energy balances for the whole summer were plotted for the RCP4.5 experiment (Annex 32) over the "past", the "present" and the "future" periods (see Section 2.4).

3.3.1 Radiation budget

The radiation budget during the "past", the "present" and the "future" periods are presented in Figures 3-16, 3-17, and 3-18, respectively.

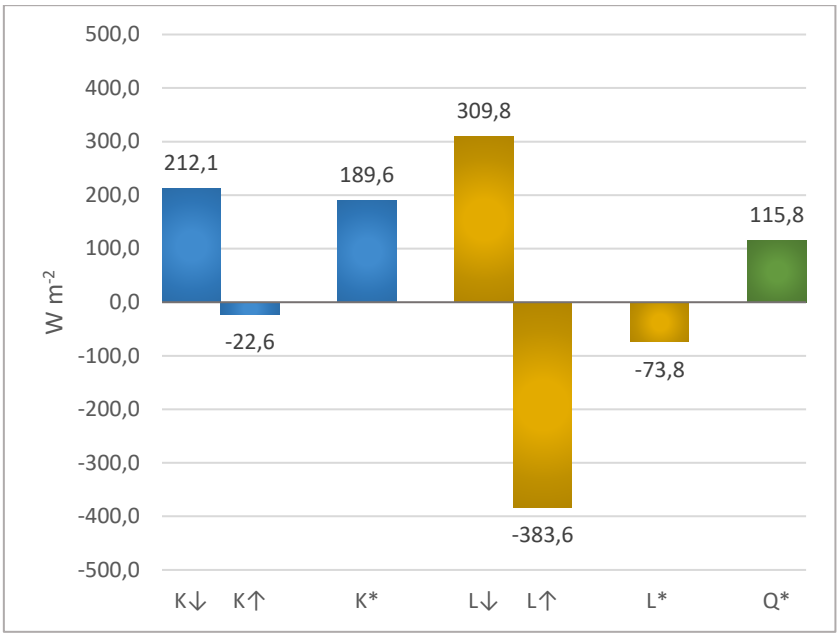

Figure 3-16 Mean values for the modelled radiation budget (the RCP4.5 experiment data) over the "past" period (1850-1869) calculated for the whole summer with an albedo value of 0.11

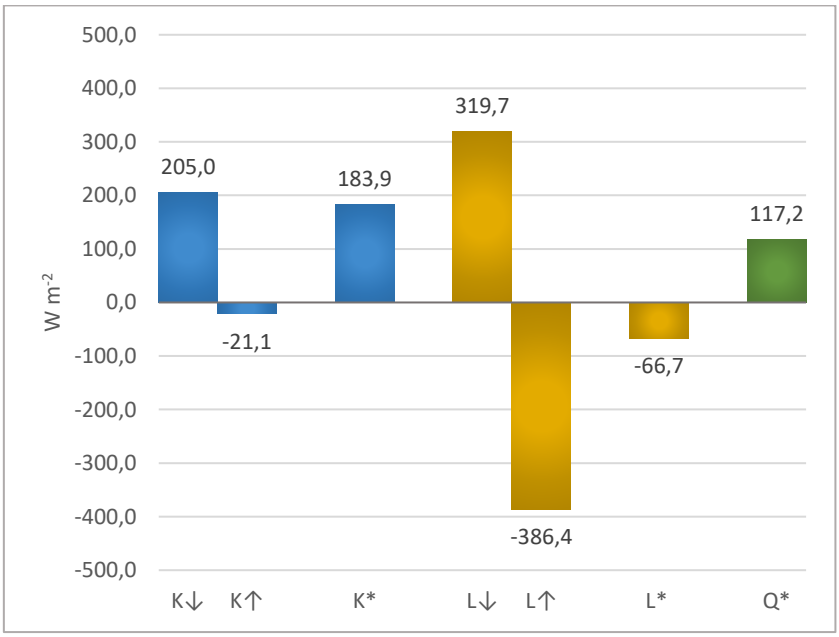

Figure 3-17 Mean values for the modelled radiation budget (the RCP4.5 experiment data) over the "present" period (2006-2025) calculated for the whole summer with an albedo value of 0.10

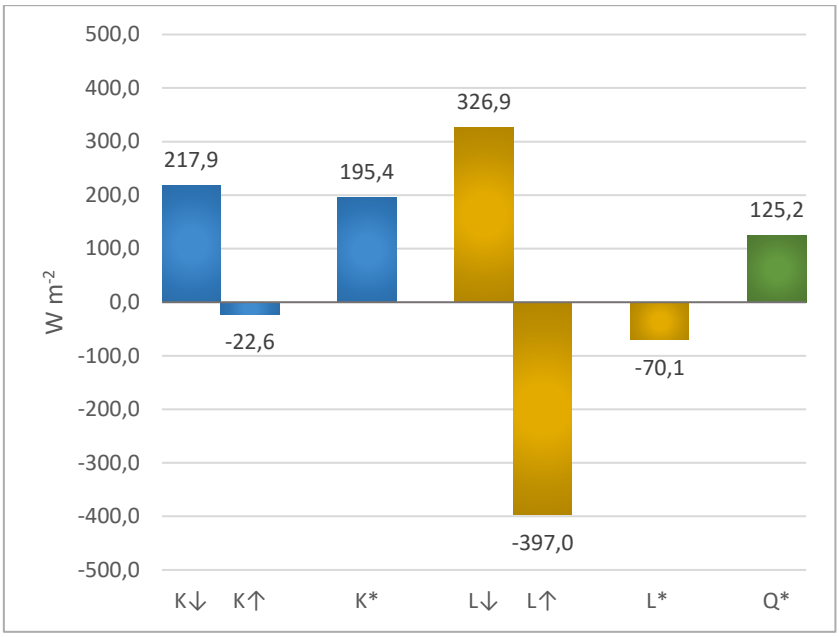

Figure 3-18 Mean values for the modelled radiation budget (the RCP4.5 experiment data) over the "future" period (2081-2100) calculated for the whole summer with an albedo value of 0.10

Comparing the "past" period with the "present" (Annex 32), K↓, K↑, and K* all decreased over time by 7.2 W m^{-2}, 1.5 W m^{-2} and 5.7 W m^{-2}, respectively. The "past" longwave radiation was lower than the "present" radiation by around 10 W m^{-2} for incoming and around 3 W m^{-2} for outgoing fluxes. However, net longwave radiation was higher in the "past", possibly due to the larger differences between the longwave fluxes. Despite the fact that the radiation budget components changed differently over time, net all-wave radiation increased in the "present" for the whole summer.

From the "present" to the "future" (Annex 32), the shortwave radiation was projected to increase: for K↓ by 13.0 W m^{-2}; for K↑ by 1.5 W m^{-2}; and for K* by 11.5 W m^{-2}. Likewise, the longwave radiation also increased by 7.2-10.6 W m^{-2} for L↓ and L↑, and 3.4 W m^{-2} for the longwave net radiation. Net all-wave radiation continued to increase into the "future", but at a much greater magnitude than between the "past" and "present" periods.

3.3.2 Energy balance

The energy balance charts for each time period were plotted and presented in Figures 3-19 – 3-21.

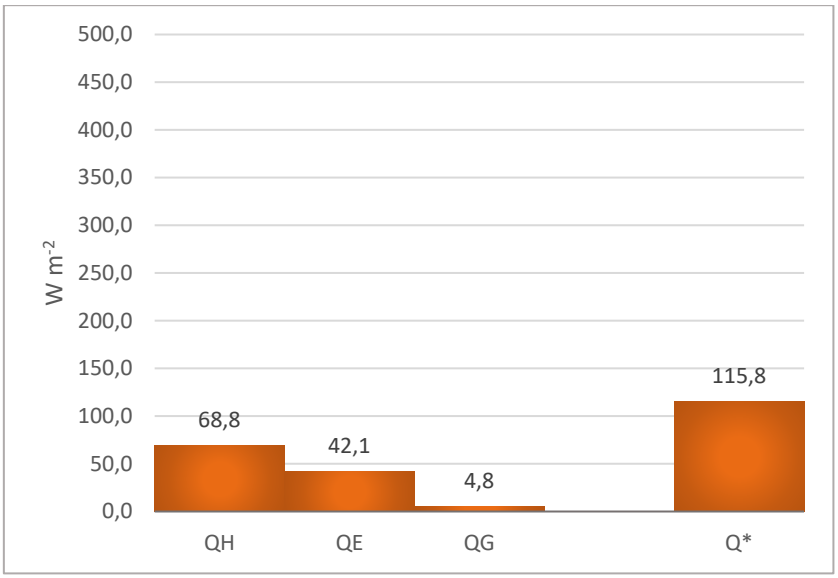

Figure 3-19 Mean values for the modelled energy balance (the RCP4.5 experiment data) over the "past" period (1850-1869) calculated for the whole summer with an albedo value of 0.11

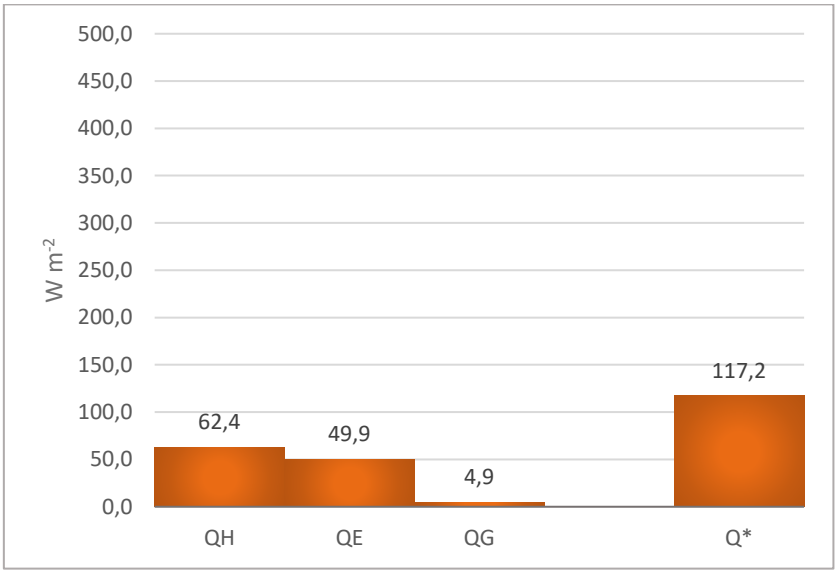

Figure 3-20 Mean values for the modelled energy balance (the RCP4.5 experiment data) over the "present" period (2006-2025) calculated for the whole summer with an albedo value of 0.10

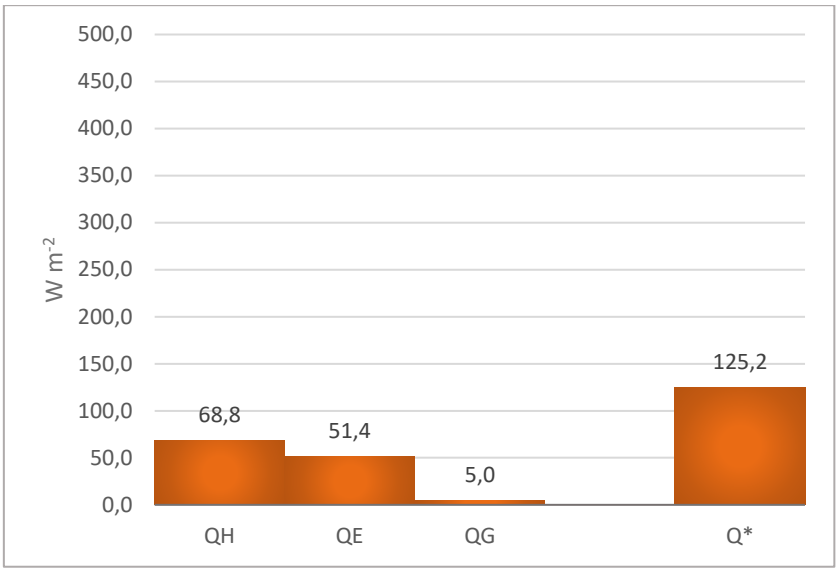

Figure 3-21 Mean values for the modelled energy balance (the RCP4.5 experiment data) over the "future" period (2081-2100) calculated for the whole summer with an albedo value of 0.10

The sensible heat flux (Q_H) decreased from the "past" to the "present" by 6.4 W m^{-2} (Annex 32), while the latent heat flux (Q_E), on the contrary, increased over time by 7.7 W m^{-2}. No clear trends were identified in the soil heat flux (Q_G) between the "past" and the "present" periods. Bowen's ratio has declined since the "past" period.

The comparison between the "present" and the "future" (Annex 32) showed that the sensible heat flux (Q_H) increased over time by 6.5 W m^{-2}. The latent heat flux (Q_E) continued to increase, but only slightly. As before, no significant changes in the soil heat flux were observed. An almost imperceptible increase from the "present" to the "future" was found in Bowen's ratio.

The Q* in the energy balance (Figures 3-19 – 3-21) was the same as the Q* in the radiation budget (Figure 3-16 – 3-18), so its tendency remained the same: it was still increasing over time, only much faster between the "present" and the "future" periods.

3.3.3 T-test

The t-test, as in the STANDARD experiment data analysis, was again used to check whether the differences in the radiation and energy balances components between the specified periods ("past", "present" and "future") were in fact significant enough to draw legitimate conclusions (Table 3-2).

T-values were calculated for the two pairs of datasets: the "past" with the "present" and the "present" with the "future". For this experiment, t-tests were conducted for each component of the radiation and energy budgets (with Q_H and Q_E, unlike in the STANDARD experiment in Section 3.2.4) since we had all the necessary data.

Table 3-2 Calculated t-values for T-tests between the "past" and the "present" (ps/pr) summers, as well between the "present" and the "future" (pr/ft) from the RCP4.5 experiment (blue cells mean that the null hypothesis is not rejected and red cells – the null hypothesis is rejected)

Datasets	$t_{tabular}$	Q_H	Q_E	Q_G	K↓	K↑	K*[1]	L↓	L↑	L*[1]	Q*[1]
ps/pr[2]	2,02	2,48	7,58	0,71	1,35	2,28	1,22	7,35	1,45	3,62	0,50
pr/ft[3]		2,62	1,50	0,32	2,37	2,39	2,36	4,72	4,60	1,72	2,74

[1]t-values were obtained for the calculated data sets, not observed
[2]ps/pr – t-value between the "past" and the "present" periods
[3]pr/ft – t-value between the "present" and the "future" periods

4 Discussion

4.1 Input data from the STANDARD experiment

Before analysing the input results of the STANDARD experiment and the observed data, we determined the altitude that the model assumes for our site. Mount Imingfjell (1191 metres) is located above the consulted weather stations: 'Dagali Lufthavn', at 798 meters, which was used for the input data analysis of temperature, surface air pressure, wind speed, and specific humidity; and 'Tunhovd' with an altitude of 870 m, which was used for precipitation. Therefore, some trends in weather parameters can be explained in relation to the height. The model did not openly provide the elevation of the chosen grid cell, so the barometric formula (Equation 2-3 in Section 2.3.1) was used to determine the altitude of the Imingfjell grid cell in the CAM and CLM4.5 models. The calculated value turned out to be approximately 423 metres, which is almost 3 times lower than the actual height of Imingfjell (1191 m), and about half the height of weather stations. This created discrepancies in the model data in the following parameters.

4.1.1 Temperature

Temperatures drop with altitude by approximately 6°C per km (or by 0.6°C per 100 m) in the troposphere (Baum 1949), therefore average temperatures at Imingfjell, with the actual altitude of 1191 m, should be lower than those at the 'Dagali Lufthavn' station, located at the altitude of 798 m. However, the modelled temperature showed other outcomes.

The model gave much higher values then expected: on the average by 2.08°C higher than the observed temperature (Annex 1). Although, the overestimated values may be the result of the modelled elevation for Imingfjell, as it was below the actual value by 768 m and below the 'Dagali Lufthavn' station by 375 m.

The CLM4.5 model may have simulated reasonable temperature values according to the modelled elevation of Imingfjell (423 m). We calculated what temperatures would be at the 'Dagali Lufthavn' elevation (798 m) as in the model. For this case, the temperature gradient was used to estimate whether the modelled values correspond to observed. The modelled elevation was 375 m lower than the 'Dagali Lufthavn' elevation, which translates to temperatures being 2.25°C warmer than those observed using 0.6°C per 100 m (mean lapse rate). According to Annex 1, the model was on average 2.08°C warmer, so CLM4.5 values closely match observations (i.e. within 0.2°C).

4.1.2 Specific humidity

Specific humidity is independent of altitude, but positively correlates with temperature. In the STANDARD experiment, the modelled and observed values of specific humidity did not have regular differences between themselves (Annex 2). The simulated specific humidity for most months (April, May, June, July, August, November, December) was higher by an average of 0.16 g kg^{-1} than at the 'Dagali Lufthavn' station. However, in January, March, September and October, the model data, on the contrary, were less by 0.08 g kg^{-1}. Simulated values for specific humidity did not go beyond the possible values for 'Dagali Lufthavn'. Therefore, the modelled specific humidity can be considered plausible. Nevertheless, it should be borne in mind that specific humidity still depends on temperature, which in the STANDARD experiment was overestimated.

4.1.3 Wind speed

Wind speed increases normally with height (Oke 1987). Here, the model displayed higher wind speeds than in the station observations by approximately 2 m s^{-1} (Annex 3). However, the simulated altitude (423 meters) was underestimated and was lower than of 'Dagali Lufthavn' (798 m), and, consequently, the CLM4.5 values for wind speed should have been lower than the observed. Additionally, the modelled wind speed had pronounced seasonal fluctuations, as opposed to the observed one, which did not project the same trend: slight changes throughout the year.

From all this, it is difficult to confirm if wind speeds were over- or underestimated due to the lowered modelled altitude. Still, modelled wind speed values fell within the 'Dagali Lufthavn' possible limits. Therefore, it can be assumed that the model likely gave plausible results for wind speeds.

4.1.4 Air pressure

According to the barometric formula (2-3) in Section 2.3.1, air pressure, similar to temperature, declines with altitude. Thus, air pressure values at Imingfjell (1191 m) should be lower than at the 'Dagali Lufthavn' station (798 m). However, the model did not show the expected results. The simulated pressure values were higher than the observed ones by 44-46 hPa (Annex 4) and were never within the possible station limits. So, It is difficult to verify the modelled air pressure accuracy.

Most likely, these irregularities in the model are connected with the highly understated modelled elevation of our site (423 m), as in the case with temperature (Section 4.1.1), and the simulated values for air pressure are realistic in relation to 423 m, but not to the actual altitude of Imingfjell (1191 m).

4.1.5 Total precipitation

Both precipitation datasets followed the same trend throughout the year. The total precipitation from the station exceeded modelled precipitation in all months, except October. A maximum difference between the datasets of 36 mm was found in July, and a minimum of around 2 mm was in October (Annex 5). However, the simulated precipitation was always within the possible precipitation range for the 'Tunhovd' station.

Based on the data comparison results, the model plausibly simulates precipitation in colder months or when there is less precipitation and underestimates precipitation values in warmer months when there is more. Since the simulated precipitation was at 423 meters, which is half the height of 'Tunhovd' station (870 m), underestimated precipitation values from CLM4.5 for Imingfjell were possible. Therefore, just like for temperature (see Section 4.1.1) and air pressure (see Section 4.1.4), the modelled values of precipitation were correctly calculated based on the altitude specified in the model, but not for the real Imingfjell height.

4.1.6 Solar radiation

The modelled radiation was lower than observed and had a lot of fluctuations. Nonetheless, the observed data become more similar to the modelled, when the simulated radiation compared with the radiation calculated not at a maximum Sun position, but at an average daily Sun position (Figure 4-1).

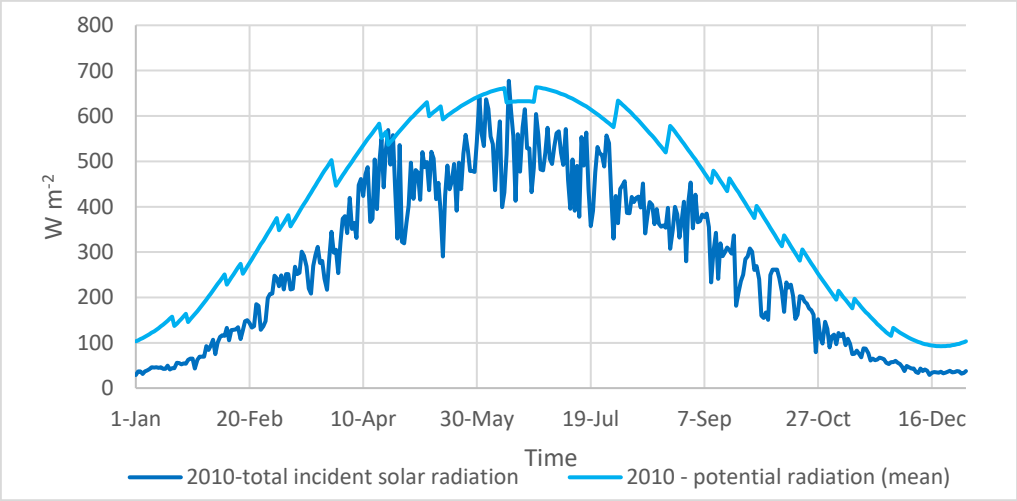

Figure 4-1 Modelled total incident solar radiation with potential radiation calculated from the average daily Sun position for the same year – 2010

The modelled radiation was 50-300 W m^{-2} less than the potential radiation calculated with the average daily Sun position. However, the values of modelled radiation might be reduced by dust and clouds in the atmosphere, which were not taken into account for the potential radiation. In addition, only 4 values per day were simulated in the STANDARD experiment, while the potential radiation had values for each hour of the year, so the plot for potential values has less scatter. Hence, the simulated radiation appears to be reliable for our site.

4.2 Output data from the STANDARD experiment

4.2.1 Modelled data versus Lichen data

Analysing the t-test results between the output and the observed data for lichens (m/l in Table 3-1), the null hypothesis was rejected for almost half of the values (46 %). Consequently, the model results validity for lichens is highly dependent on which component of the radiation or energy budgets has been modelled. However, CLM4.5 lacks the PFT lichen type and assumes a forest cover of 30% for the grid cell of Imingfjell (see Section 2.3). Therefore, modelling of the lichen radiation and energy balances initially may be unrepresentative, because the model cannot specify the type of simulated vegetation as lichens. The importance of adding lichens as a new PFT has already been proven in the thesis by Bjordal (2018). The 30% forest cover implies a lower albedo than with a full lichen cover, which is confirmed by the Figures in Section 3.2, showing an albedo of 0.19 for the model, compared to 0.25 to 0.29 for lichens.

When comparing the temperature regimes, much of the similarity between the datasets was found for the “normal” period: out of 8 modelled fluxes, only 3 were different from observed. For both the “extremely warm” and the “normal” regimes, half of the lichen fluxes were proven to differentiate from the model results.

The null hypothesis was not rejected for the soil heat flux (Q_G) and incoming shortwave radiation (K↓) in all temperature regimes between the simulated and observed datasets. Hence, the CLM4.5 model accurately predicts the soil heat flux and incoming shortwave radiation for lichens.

The opposite is true for outgoing shortwave radiation (K↑): for almost every t-value, with the exception of the “cold” period, the null hypothesis was rejected, which means that the modelled outgoing shortwave radiation differed too much from the lichen values. In addition to K↓, K↑ also depends on the surface albedo (Equation 1-2 in Section 1.5), and, therefore, the differences between the observed and simulated data can be associated with distinctions in albedo values: 0.19 (same in every temperature regime) for the model and 0.27 (on average between temperature regimes) for

lichens. However, the modelled vegetation from the STANDARD experiment consisted mainly of trees and grass, so the simulated albedo was not representative of the lichen albedo. The only case with the modelled K↑ appeared to be similar to the lichen K↑ (with the highest observed albedo of 0.29) is insufficient to conclude that the model better simulates outgoing shortwave radiation at higher albedos or for whiter vegetation, and this relationship may be coincidental.

It was proved that the values of incoming longwave radiation (L↓) are similar (the null hypothesis was not rejected) between the model and lichens for all temperature regimes expect for the "cold" one. Thus, CLM4.5 is not robust enough to model values for lichen L↓ at lower temperatures.

In contrast to L↓, the t-test showed that for outgoing longwave radiation (L↑) the simulated and observed data were considered similar only in the "cold" period. Hence, the model better simulates L↑ for lichens in colder conditions.

Net shortwave (K*), net longwave (L*) and net all-wave (Q*) radiation data from the model were calculated using other modelled parameters (see Section 2.3.2), therefore, the t-values for these fluxes may not display the correct picture between the simulated data and lichens.

All t-values for net shortwave radiation (K*), with the exception of the "cold" period, were less than the tabular values, which means that the simulated data were largely similar to the lichen data. However, K* was calculated through K↓ and K↑, and the "cold" regime was the only one in which both K↓ and K↑ were found to be similar between the observed and modelled datasets. Accordingly, the t-test values for K* seem to be influenced by the t-values for K↓ and K↑: the null hypothesis is rejected (datasets are too different) for K* if the null hypothesises for both K↓ and K↑ were not rejected (datasets are similar); and the null hypothesis is not rejected for K* if only K↑ rejected the null hypothesis.

Net longwave radiation (L*) had the rejected null hypothesis (the modelled dataset differentiated from the lichen one) in the "extremely warm" and the "cold" regimes. Unlike net shortwave radiation, L* had no obvious dependence on the t-test results for incoming and outgoing radiation. Therefore, it is difficult to draw clear conclusions about the quality of the modelled net longwave radiation.

Net radiation (Q*) t-tests rejected the null hypothesis for each temperature regime. While this may mean that the CLM4.5 data, regardless of the temperature regime, differ too much from the lichen data, Q * was not taken directly from the model and cannot be used as a t-test comparison with the same precision as the simulated data.

4.2.2 Modelled data versus Shrub data

The t-test results between the model and shrub datasets (m/s in Table 3-1) showed that the null hypothesis was rejected in a quarter of cases (25%), which is noticeably lower than for lichens (46%). Hence, the simulated data was more similar to shrubs than to lichens. This is most likely due to the fact that the vegetation prescribed in the model was closer to shrubs than to lichen. In the STANDARD experiment, the modelled vegetation consisted mostly of needleleaf trees (PFT3 - 30%) and grass (PFT12 – 34%, PFT13 – 35%) with only 1% of the Imingfjell grid cell for shrubs. Therefore, the modelled data could resemble shrub data even more if the vegetation in the STANDARD experiment was made out of shrub PFTs.

During the “extremely warm” period, all simulated fluxes were similar to observed ones, except for K↑. In the “normal” regime, 2 out of 8 modelled fluxes differed from those observed for shrubs, and in the “cold” regime – 3 out of 8 fluxes.

Just like for lichens, t-tests for each temperature regime confirmed that all simulated values of the soil heat flux (Q_G) and incoming shortwave radiation (K↓) are identical to those observed for shrubs. Again, CLM4.5 provides robust modelled values of the soil heat flux and incoming shortwave radiation.

However, for outgoing shortwave radiation (K↑), the t-test results showed a completely opposite picture between shrubs and the model: the observed K↑ values in all temperature regimes were too different from the simulated ones. Since K↑ depends on the albedo (α), data mismatch can be explained by differences in its values. However, the shrub albedo (0.15 on average between temperature regimes) was close enough to the modelled albedo (0.19), so the model seems to have a problem with simulating K↑ according to the albedo.

For shrubs, as well as for lichens, the simulated values of incoming longwave radiation (L↓) were close to the observed values (the null hypothesis was not rejected) in all temperature conditions, except for the “cold” regime. Once again, the t-test confirmed that the model does not give reliable results for L↓ at lower temperatures.

The null hypothesis for outgoing longwave radiation (L↑) from shrubs was not rejected during the “extremely warm” and “cold” periods, which means that the observed and simulated datasets were similar. However, it is unclear why the model did not perform well during the “normal” temperature period. Still, the model appears to simulate more accurate L↑ values for shrubs than lichens.

As noted above (see Section 2.3.2), the values for all modelled net radiation (K*, L* and Q*) have been calculated from the modelled fluxes, so this could affect the t-test and its results may not be entirely reliable when compared with the data from shrubs.

The modelled net shortwave radiation (K*) for all temperature regimes was shown to be similar to the shrub data (the null hypothesis was not rejected). Still, the t-test results for K* followed the same principle as in the lichen analysis (Section 4.2.1), where they depended on the K↓ and K↑ results.

The t-test between the model and shrubs showed that the null hypothesis for net longwave radiation (L*) was rejected only in the "cold" period, i.e. the datasets were different. Again, it is difficult to confirm whether these results are reliable or not due to their possible dependence on the L↓ and L↑.

In contrast to the t-test results of net radiation (Q*) between the model and lichens, the null hypothesis was not rejected under any temperature regimes for shrubs, and, therefore, the modulated data can be considered similar to shrubs. However, again, these test results may be inadequate as Q* was not modelled, but rather calculated through the modelled components of the radiation balance.

4.3 RCP4.5 experiment

4.3.1 The "past" versus the "present"

The null hypothesis between the "past" and the "present" was rejected in half of the cases, which means that changes occurred over time, but not for all fluxes (Table 3-2 and Annex 32). In addition to the radiation and energy budgets, temperature and precipitation also increased into the "present" (Figure 4-2). From 1850-1869 (the "past") to 2006-2025 (the "present"), the temperature rose by around 1°C for each summer month (Figure 4-2a). The amount of precipitation generally increased by 0.5-1.0 mm in the "present "summer, except for a slight decline of 0.2 mm in August (Figure 4-2b).

The decrease in K↓, K↑, K* from the "past" to the "present" may be related to averages calculated for periods with a mismatching solar cycle since shortwave radiation depends on the Sun (see Section 1.5). Nevertheless, the t-test results for shortwave radiation, except for outgoing shortwave radiation, showed that no significant differences were found between the "past" and the "present".

Both incoming and outgoing longwave radiation increased in the “present”, but only for incoming longwave radiation the differences were proven significant by the t-test. The decline in net longwave radiation between the “past” and the “present” was also confirmed.

The t-test showed that the sensible heat flux (Q_H) decrease from the “past” to the “present” can be considered plausible (the null hypothesis was rejected). This reduction means that the observed higher temperatures (Figure 4-2a) in the “present” were not enough to increase Q_H. Therefore, the Q_H decline could be caused by an increase in the latent heat flux due to the sufficient amount of available moisture.

The latent heat flux was proven to raise over time. Higher values of the latent heat flux indicate greater evapotranspiration due to more water available. The data on precipitation (Figure 4-2b) was used to check if this was true. In the “present”, the amount of precipitation has indeed increased on average over the entire summer, which explains the observed changes in the latent heat flux. In addition, the “past” Bowen’s ration of 1.63 was closer to semi-arid areas, then changed in the “present” (1.25) to temperate forests and grassland (see Section 1.5), which also indicates that climate becomes more humid.

The soil heat flux has hardly changed since the “past”, and the t-test confirmed it. No changes were expected in Q_G, since it does not depend on the surface temperature, but on the soil temperature.

Net all-wave radiation has increased in the “present”, which could be the indicator that climate is warming. Nonetheless, the t-test showed that net all-wave radiation is still too similar to the “past” values to validate it.

However, the $L\downarrow$ rise meant that radiation was trapped near the surface and caused warming, as can be seen on the temperature graph (Figure 4-2a). Additionally, the increase in the latent heat flux and the change in Bowen’s ratio indicated that more water was available for evaporation, as evidenced by the precipitation graph (Figure 4-2b). Therefore, the climate in the “present” became a little hotter and more humid compared to the “past” period, which is well reflected in the energy and radiation balances.

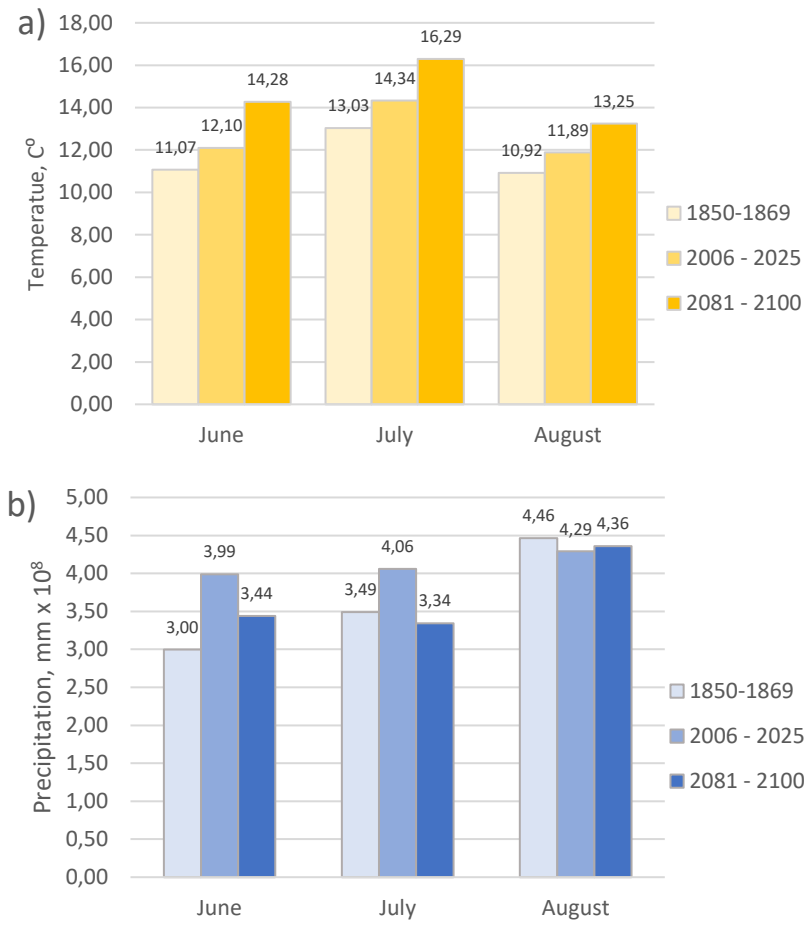

Figure 4-2 Mean air temperature (a) and mean precipitation (b) from the RCP4.5 experiment calculated over 20-years periods for each summer month

4.3.2 The "present" versus the "future"

Between the "present" and the "future", the null hypothesis was rejected for 7 out of 10 fluxes, which means that more changes occurred compared to the "past"/the "present".

Net, incoming, and outgoing shortwave radiation has increased since the "present". T-tests confirmed that these changes were valid for all shortwave fluxes. However, the rise in shortwave radiation was likely caused by an possible increase in the amount of aerosols, leading to more scattering/reflection.

For longwave fluxes, the increase in both incoming and outgoing radiation from the "present" to the "future" was confirmed by t-tests. Thus, more radiation is captured near the surface by greenhouse gases that cause climate warming (Figure 4-2a). However, the t-test showed that the differences in net longwave radiation between time periods were not significant. The similarities in net longwave radiation could be due to the same rate of change in incoming and outgoing longwave radiation.

Temperatures rose sharply by almost 2°C from the "present" to the "future" (Figure 4-2a). The t-test confirmed that the sensible heat flux has increased since the “present” period, which means more energy comes from temperature changes.

The latent heat flux seemed to increase in the “future”, but the t-test showed that those changes were negligible. The similar latent heat fluxes in the “present” and the “future” mean that no significant change in water availability has happened, although the amount of precipitation seemly has decreased over time (Figure 4-2b).

Still, no confirmed changes in the soil heat flux occurred from the “present” to the “future”, since it is considered as a constant supply of energy from the soil.

Bowen’s ratio slightly increased from the “present” (1.25) to the “future” (1.34), but the climate of study area is still considered closer to temperate forests and grassland.

It has been proven that in the "future" net all-wave radiation will increase, which means heating of the surface is taking place. This has also been confirmed by early stated trends in shortwave, longwave radiation, and the sensible heat flux. However, no concrete evidence has been found that the “future” climate will become wetter or drier. Therefore, the climate in the “future” will become much hotter, but remains unchanged in water availability. Additionally, more changes were found in the radiation and energy budgets from the “present” to the “future” than from the “past” to the “present”, which could indicate acceleration of warming and climate change in the future.

4.4 Comparison with other studies

The aims of comparisons with other modelling and observational studies were, firstly, to ensure that the energy and radiation budgets simulations were performed correctly, and secondly, to see if our data were consistent and plausible for the alpine climate.

4.4.1 Comparison with Kumar and Merwade (2011)

Kumar and Merwade (2011) compared the results of a couple different models results, including the Community Land Model (version 3.5), with the energy flux observations from 16 AmeriFlux sites in the United States Mississippi Basin.

The Mississippi River Basin has a total area of 3.2 million km^2 and covers around 40% of the continental United States. As a result, the area of the CLM3.5 grid cell for the Mississippi Basin was 280 x 280 km. CLM3.5 simulated monthly data of the energy balance components such as incoming shortwave radiation (K↓), the latent heat flux (Q_E) and the sensible heat flux (Q_H) from 1980 to 2004

(25 years). Data from the AmeriFlux sites were available at earliest from 1995 until 2007, with an average observation period of 5.8 years. Since the temporal and spatial coverage of the AmeriFlux stations did not match the CLM3.5 grid, the observations were compared with the modelled data from the closest grid cell over the available time period (equal sample size principle). Consequently, no CLM output data was available for 4 AmeriFlux sites, and only 12 out of 16 total stations were used for the comparison (Kumar and Merwade 2011).

Statistical measures such as mean, standard deviation, Pearson's correlation coefficient, square of correlation coefficient (R^2) were calculated by Kumar and Merwade (2011) to compare modelled and observed datasets. Since no observations of Q_E and Q_H were made in the STANDARD experiment, only data on K↓ were used for the comparison with Kumar and Merwade (2011). Table 4-1 shows the combined data of Kumar and Merwade (2011) and our results.

For all sites from Kumar and Merwade (2011), the R^2 was greater than 0.80, which means that the modelled values of K↓ explained most (at least 80%) of the variation in the observed K↓ from the AmeriFlux sites. In the STANDARD experiment, the R^2 for both lichens and shrubs was around 0.25 and much lower than in Kumar and Merwade (2011). Therefore, K↓ from the STANDARD experiment predicted a moderate percentage of the variation in incoming shortwave radiation from both lichen and shrub datasets.

Such high R^2 in the results of Kumar and Merwade (2011) can be explained by the long observation period used in the calculation: on average more than five years for each site compared to our two summers. Additionally, CLM3.5 in Kumar and Merwade (2011) mainly simulated believable heights with a maximum difference between the actual and modelled elevations of about 500 m (Site 16) and a minimum of 0 m (Site 4). In the STANDARD experiment, the simulated altitude of Imingfjell was 3 times lower than the real one. Kumar and Merwade (2011) work was also much larger than ours and covered almost half of the US territory with at least 12 stations, while we only explored one site on Mount Imingfjell. As a result, they used a huge grid for modelling, but we only had a single grid cell in CLM4.5. However, their research is a bit dated as they used an older model version than we did – CLM3.5 versus CLM4.5.

Table 4-1 Mean values for given periods of incoming shortwave radiation in W m^{-2}, and performance evaluation of the Community Land Model from Kumar and Merwade (2011) and the STANDARD experiment

Data	Site	Location	Time period	Site elevation, m	CLM elevation, m	K↓	R^2
Kumar and Merwade (2011)	3	OK, USA 36.61°N -97.49°E	2003-2004	414	503	180,1	0,91
	4	MS, USA 34.25°N -89.97°E	2002-2004	87	87	181,3	0,86
	5	IN, USA 39.32°N -86.41°E	1999-2004	275	214	167,0	0,94
	7	TN, USA 35.96°N -84.29°E	1995-1999	343	412	172,2	0,94
	9	IL, USA 40.01°N -88.29°E	1997-1999; 2001-2004	219	214	167,5	0,94
	10	NE, USA 41.17°N -96.48°E	2002-2004	361	351	177,3	0,96
	11	NE, USA 41.16°N -96.47°E	2002-2004	362	351	180,9	0,96
	12	NE, USA 41.18°N -96.44°E	2002-2004	363	351	176,8	0,96
	13	WI, USA 45.81°N -90.08°E	1999-2004	515	363	145,9	0,96
	14	WI, USA 46.08°N -89.98°E	2001-2004	480	363	159,3	0,92
	15	MT, USA 48.31°N -105.10°E	2000-2004	634	670	159	0,96
	16	CO, USA 40.03°N -105.55°E	1999-2004	3050	2531	182,7	0,81
STANDART experiment (2020)	Lichen	Imingfjell, Norway 60°11’11.7"N 8°34’45.2"E	Summers of 2018-2019	1191	423	245,6	0,25
	Shrub					245,0	0,26

4.4.2 Comparison with Müller (1985)

In a review article by Müller (1985), the radiation balance components were analysed from several observational studies for the Alps (mainly the Swiss Alps) with an altitude of more than 1500 m, which is at least 300 m higher than Imingfjell.

Data on incoming shortwave radiation were available in a number of publications. Outgoing shortwave radiation was described only as a product of incoming shortwave radiation and albedo, so the main focus for Müller was on the albedo results. Since most researches did not have clear results on outgoing shortwave radiation, only K↓ was used for the comparison.

As in the case with K↑, no pronounced observations of L↓ and L↑ were mentioned in most studies, since longwave radiation values were not reliable enough due to systematic errors in measurements at the time. Incoming longwave radiation was mainly calculated through humidity and temperature. Outgoing longwave radiation was determined through formula 4-1:

$$L\uparrow = \varepsilon\sigma T^4 + (1-\varepsilon)L\downarrow, \quad (4\text{-}1)$$

where ε and T are emissivity and temperature in K, respectively; σ is the Stefan-Boltzmann constant equal to 5.67 x 10^{-8} W m^{-2} K^{-4}.

Since in almost all publications most of the components were not available to complete radiation balance, only a comparison with Sauberer and Dirmhirn (1958) was made, which had data on K↓, L↓, L↑ and Q*. Müller investigated the radiation balance for the canton of Valais located in South-western Switzerland at altitudes from 2000 to 3500 m in summer under different sky conditions based on Sauberer and Dirmhirn (1958). The combined results of STANDARD experiment data and the studies by Müller (1985) and Sauberer and Dirmhirn (1958) are presented in Table 4-2.

Table 4-2 Components of the radiation budgets in W m^{-2} based on data from Sauberer and Dirmhirn (1958) and the STANDARD experiment calculated for summer months. Adapted from Müller (1985)

Study	Location	Site	Height, m	K↓			L↓			L↑			Q*		
				Jun	Jul	Aug	Jun	Jul	Aug	Jun	Jul	Aug	Jun	Jul	Aug
STANDARD experiment (2020)	Imingfjell, Norway 60°11'11.7"N 8°34'45.2"E	Lichen	1191	262	272	172	305	317	324	378	402	372	109	118	75
		Shrub		263	272	170	305	318	324	372	394	367	154	155	102
Müller (1985); Sauberer and Dirmhirn (1958)	Canton of Valais, Switzerland 46°4'N 7°36'E	Glacier	2000	270	258	220	299	312	306	319	319	319	182	186	152
			2500	283	268	226	282	294	290	310	316	315	127	180	145
			3000	297	278	235	265	276	274	301	311	310	82	90	69
			3500	311	287	242	243	259	257	287	296	295	66	77	46

Our data on lichens and shrubs for incoming shortwave radiation were closest to the Müller's data in June at an altitude of 2000 m with a difference of 7-8 W m^{-2}. For July at the same altitude, the STANDARD experiment data was higher by 14 W m^{-2}, while in August, on the contrary, it was lower by around 50 W m^{-2}. Such variations between datasets by months may be due to differences in surface types, seasonal fluctuations of K↓ or/and cloudiness.

One of the advantages of Müller's work, which was not carried out in the STANDARD experiment, is that the measurements were done at different heights, which makes it possible to analyse the dependence of the radiation fluxes trends on altitude. Under clear-sky conditions, incoming shortwave radiation (K↓) increases with altitude due to a decrease in atmospheric turbidity (Körner 2007). On average, according to Müller (1985), K↓ increased by 10 W m^{-2} every 500 meters. Apart from being dependent on altitude, K↓ also varies with latitude. The K↓ maxima can be found over sub-tropical areas: between 10 and 35° of latitude. In summer (in June and July for Northern Hemisphere), high values of K↓ also occur in polar regions (Hatzianastassiou et al. 2005). Our K↓ values were not much lower than the Müller's values, but the increased differences in August can be explained by the fact that the site in Valais was closer to the subtropical regions, where maximal values are usually observed.

In Müller's work, incoming longwave radiation steadily declined with height. The summer means of L↓ for both lichens and shrubs were around 315 W m^{-2} at 1191 m, while for Valais, they were 306 W m^{-2} at 2000 m. The lowest observed values for both datasets were in June, but the highest ones for the STANDARD experiment were in August, and for Müller's data – in July for all heights.

The STANDARD experiment values of outgoing longwave radiation were much higher, at least by 50 W m^{-2}. According to Müller's data, the differences in L↑ between altitudes were not so large, with an average decrease of 10 W m^{-2} per 500 m. Such a gap in values between our data and Müller's can once again be explained by different types of surfaces: glacier versus vegetated area.

Net radiation also varied greatly between datasets, though the STANDARD experiment Q* values for shrub data appeared to be closer to Müller's data at 2000 m than Q* for lichens. Net radiation for lichens has a difference of at least 65 W m^{-2} for all summer months, while net radiation for shrubs has a maximum difference of around 50 W m^{-2} in August. However, as can be seen from Table 4-2, the indicated components of the radiation balance, with the exception of Q*, were approximately equal between lichens and shrubs with a maximum difference of 6 W m^{-2}. Consequently, the radiation balance component, not directly indicated in Müller's work, namely, outgoing shortwave radiation, was apparently closer in values to shrubs than to lichens. Since K↑ depends on the albedo, it can also

be assumed that the albedo of the glacier surface in Valais was closer to the albedo of shrubs, i.e. more darkened surface.

In conclusion, the results of the STANDARD experiment and Müller's are comparable and significant differences in the radiation fluxes can be explained by different elevations of sites, different types of the underlying surfaces, and different latitudes.

4.4.3 Comparison with Saunders (1990)

Saunders (1990) directly measured or calculated all components of the radiation and energy budgets from November 1986 to July 1987, and from April to May 1988 for Scout Mountain (Canada). Scout Mountain, at 2350 m, is an alpine tundra, like Imingfjell. Hourly, daily and monthly radiation budgets were calculated by Saunders. However, we only had daily observations for several days in summer months. Therefore, we calculated monthly values using our existing data to make them comparable to Saunders's results. The radiation and energy budgets measured over August could not be compared, as Saunders did not make any observations this month. We also did not use the sensible and latent heat fluxes, since there were no observations from the STANDARD experiment, so only the soil heat flux was compared with Saunders. Table 4-3 showed the monthly radiation budgets and soil heat fluxes from the STANDARD experiment (lichens and shrubs) and Saunders (1990) for June and July.

Table 4-3 Components of the radiation budget in W m^{-2} from Saunders (1990) and the STANDARD experiment data calculated over June and July

Month	Location	Data	Years	K↓	K↑	K*	L↓	L↑	L*	Q_G	Q*
June	Scout Mountain, British Columbia 49°N 120°W	Sanders (1990)	1987	280,4	46,3	234,1	290,4	386,2	-95,8	-17,9	138,3
	Imingfjell, Norway 60°11'11.7"N 8°34'45.2"E	Lichen data	2019	261,8	80,1	181,7	304,6	377,6	-73,1	-15,4	108,6
		Shrub data	2019	262,5	41,4	221,2	304,8	372,4	-67,6	-7,8	153,5
July	Scout Mountain, British Columbia 49°N 120°W	Sanders (1990)	1987	239,1	37,5	201,6	299,0	375,2	-76,3	-12,0	125,3
	Imingfjell, Norway 60°11'11.7"N 8°34'45.2"E	Lichen data	2018, 2019	271,9	69,7	202,2	317,2	401,6	-84,4	-8,3	117,9
		Shrub data	2018, 2019	271,6	39,6	232,1	317,6	394,3	-76,7	-5,8	155,3

In June, shortwave radiation at Scout Mountain was more similar to the STANDARD experiment shrub data, whereas longwave radiation was more like lichen. In July, K↑, L↑ and L* from Sanders (1990) were closer to shrub data, while only K* was closer lichen K*. Both incoming shortwave and longwave radiation differed greatly between the STANDARD experiment and Sanders' data.

Net radiation was similar either to lichens or shrubs depending on the month. The Sanders's soil heat flux during both months was closer to lichen than shrub. Since the STANDARD experiment data were commensurate with Sanders's data, it can be concluded that our observations of the radiation and energy budgets components are typical for alpine tundra environments.

Additionally, Saunders (1990) modelled L↓ by calculating it through various equations and compared predicted values with those observed to assess the error between them. These equations, or Atmospheric Longwave Radiation Models, included: Swinbank (1963) and Idso-Jackson (1969), both of which are temperature-based; Brunt (1932), Brutsaert (1975) and ldso (1981), which uses vapour pressure; and Bolz's model, which was adjusted for Scout Mountain and uses cloud observations (Bolz 1949, Saunders 1990). Notwithstanding that these models were dated, all of them, with the exception of the Swinbank, worked reasonably well. The closest results to the observed ones were calculated using Brunt and Brutsaert equations (Saunders 1990).

Net radiation was also modelled in Saunders's research using the flux-by-flux (Saunders 1990) and empirical approaches of Bailey (1989), Isard (1989), Davies (1967), and Frischen (1967). The flux-by-flux method has been proven to produce excellent results for Q*. Analysing empirical methods, Bailey and Isard approaches gave fairly similar values of Q*, while Davies and Frischen methods performed poorly.

Further, the sensible heat flux was determined using 3 physically-based models: aerodynamic method (Thom 1975), Bowen ratio-energy budget (BREB) method and Ohm's Law (Saunders 1990). All three of them showed generally good predicted values, except that Ohm's Law overestimated the results at larger fluxes for Scout Mountain. Still, the results for Q_H slightly varied between methods with a mean difference of 50 W m^{-2}.

Saunders modelled the latent heat flux too. The same 3 methods as for the sensible heat flux (aerodynamic method, BREB method, Ohm's Law) were used, plus Q_E was modelled as residual in the energy budget, using eddy correlation ($Q_{E(RE1)}$). The best modelling results of the latent heat flux were obtained by BREB and $Q_{E(RE1)}$ methods. However, the aerodynamic equation seemed to underestimate the Q_E values, while Ohm's law gave poor results (Saunders 1990).

The equations Saunders used to model L↓, Q*, Q_H and Q_E required additional observations (temperature, pressure, clouds, wind speed, or shortwave radiation), but in the CLM4.5 model only the selection of a grid cell for studied object is needed, which greatly simplifies the modelling process and makes it possible for any territory. Moreover, models were only used for incoming longwave and net radiation, the sensible and latent heat fluxes, since observations and modelling of these at that time were sufficiently scarce for alpine tundra (Saunders 1990). In the CLM4.5 model, all components of radiation and energy budgets can be predicted.

Due to the technological advance of CLM4.5, more input parameters and equations were used to predict values, making our modelled values probably more accurate than Saunders's (1990). However, for that time (1990), the models used by Saunders gave mostly plausible results for the radiation and energy budgets.

4.4.4 Comparison with Saunders and Bailey (1994)

In contrast to the aforementioned studies, Saunders and Bailey (1994) did not conduct their own research, but were able to collect and compare results of other studies into a review paper. They summarised previous research on the radiation and energy budgets of alpine tundra environments as mean daily fluxes over summer. Observed radiation and the soil heat fluxes from the STANDARD experiment were calculated as the summer averages using 44 days of measurements so that they can be compared with Saunders and Bailey (1994). The combined results of STANDARD experiment and Saunders and Bailey data are presented in Table 4-4. Saunders's (1990) study was not included since it has already been analysed in detail with data from the STANDARD experiment in Section 4.4.3.

The observed radiation fluxes from the STANDARD experiment had values similar to those obtained for heights closer to ours in the studies of Halbsguth et al. (1984) and Aufdemberge (1974). The values of all fluxes in Kraus's (1971) research were also quite close to ours, although Imja Khola is at a much higher altitude than Imingfjell. However, all fluxes obtained by Terjung et al. (1969), with the exception of L*, differed significantly from ours. LeDrew's (1975) and Bailey's et al. (1989) values were only similar for shortwave fluxes. Staudinger's (1978) results seemed lower than ours, while the results of Gates and Jahnke (1966), on the contrary, were higher.

The comparison with older studies on the radiation and energy budgets in alpine areas showed that our data from the STANDARD experiment are plausible for the indicated in the model altitude of Imingfjell, however the values of fluxes are influenced by a huge number of factors.

Table 4-4 Radiation budget results and the soil heat flux in W m^{-2} from various researches and the STANDARD experiment. Adapted from Saunders and Bailey (1994)

Study	Location	Site and altitude	Measurement period	K↓	K↑	K*	L↓	L↑	L*	Q_G	Q*
STANDARD experiment (2020)	Imingfjell, Norway 60°11'11.7"N 8°34'45.2"E	Lichen and shrub alpine 1191 m	Jun.-Aug. (44 d)	245,3	51,2	194,1	317,3	387,6	-70,3	-6,0	123,8
Aufdemberge (1974)	Chitistone Pass, AK 61°N 139°W	Moss-lichen tundra 1770 m	Jul. (10 d)	224,5	42,8	181,7	278,9	344,9	-66,0	-24,3	115,7
Bailey et al. (1989)	Plateau Mtn, Alberta 50°N 114°W	Fellfield 2480 m	Jun.-Jul. (30 d)	298,6	50,9	247,7	241,9	348,4	-106,5	N/A	141,2
Gates and Janke (1966)	Niwot Ridge, CO 40°N 106°W	Tundra 3500 m	Jul. (1 d) Sept, (1 d)	355,3	65,4	289,9	332,2	398,1	-66,0	N/A	224,0
Halbsguth et al. (1984)	Dischma Valley, Switzerland 46°N 10°E	Subalpine grass meadow 1970 m	Aug. (10 d)	262,7	61,3	201,4	323,5	375,6	-52,1	-9,3	149,3
Kraus (1971)	Imja Khola, Nepal 30°N 106°W	Moraine 4570 m	Apr. (9 d)	291,7	47,5	244,2	247,7	329,9	-82,2	-5,8	162,0
LeDrew (1975)	Niwot Ridge, CO 40°N 106°W	Tundra 3500 m	Jun.-Aug, (62 d)	246,5	41,7	204,9	297,5	394,7	-97,2	-19,7	107,6
Staudinger (1978)	Otztal Alps, Austria 47°N 11°E	Tundra 2580 m	Aug. (31 d)	191,0	44,0	147,0	287,0	340,3	-53,2	N/A	93,7
Terjung et al. (1969)	White Mtns, CA 38°N 118°W	High desert mountain 4270 m	Jul. (1 d)	469,9	93,7	376,2	N/A	N/A	-97,2	N/A	278,9

4.5 Weaknesses/uncertainties of this work

Our study area was represented by only one grid cell in the CLM4.5 model. The simulated values were averaged over the large area (1x1 degree latitude-longitude or approximately 111.0 x 111.0 km), but our study subject was much smaller (2.5 x 0.2 km). This led to the underestimated simulated height, so the model values might not be entirely correct. Consequently, as the study area increases, for example, not only one mountain, but a ridge, more grid cells will be required, and modelled data may improve its accuracy.

Analysis of the simulated input data using the comparison with field data in most cases showed that the model gives plausible values, but the comparison itself had its drawbacks. Firstly, the nearest meteorological stations to our site were tens of kilometres away, so the initial datasets were different. Secondly, there was no single station that had data for each model input parameter, therefore two stations had to be used. Thirdly, no observed data on the total incident solar radiation was found, so we had to calculate potential radiation for Imingfjell, which does not take into account the variability of the atmosphere.

As for the output data, the main problem was the lack of observations for the sensible and latent heat fluxes, which did not allow obtaining a complete energy balance equation and analysing its modelled fluxes. Moreover, we had scattered observations (for individual days), so we had to average the parameters over the selected temperature regimes, which also introduced additional uncertainty in the data comparison.

4.6 Further research

As a follow-up to this research, we can try to minimize the shortcomings that were here, and possibly broaden the aims of the study. One of the way to achieve this is to improve the collection of observed data by:

1) Including in the fieldwork the observations of all modelled input parameters (temperature, specific humidity, wind speed, surface pressure, total precipitation, and total incident radiation), as well as the sensible or latent heat fluxes to complete the energy balance data;
2) Having a stable observation schedule. An ideal schedule would be to measure input parameters 4 times a day (the same frequency as in the model), and output data (components of the radiation and energy budgets) once a day for at least one calendar month.

Thus, we get a complete observed set of parameters for the one whole month, which can be directly compared with the model data for exactly the same time period.

In addition, several research objects located in different terrestrial ecosystems could be used to find if there is any differences in model performance depending on the type of environment. For example, one study area may be a site at Svalbard as a representative of a tundra environment, and the other may be same Imingfjell or another mountain in Southern Norway as a taiga type. Studies can also be carried out at different heights so that the dependences in the parameters on the height can be found.

Furthermore, we can try other models with a higher resolution than CLM4.5 or the latest version CLM5 to solve the “elevation” problem (one of the weaknesses in our research) and to simulate the radiation and energy budgets for comparisons to find out possible advantages and disadvantages in the models.

5 Conclusion

Our first research question was about the similarity extend of the CLM4.5 data to observations, and to answer that question, we compared simulated inputs and outputs to observed data.

In the input data, the simulated temperatures were on average 2.08°C higher than observed. Specific humidity was more or less the same between datasets with an average difference of 0.16 g kg^{-1}. Air pressure was 44 hPa higher in the simulated dataset. The modelled total precipitation was on average 12.5 mm lower than observed. Wind speed from the model was approximately 2 m s^{-1} higher and had seasonal fluctuations. The simulated total incident solar radiation was always lower than potential radiation by at least 90 W m^{-2}.

The model underestimated the Imingfjell height by almost 3 times, which initially affected the input data. Most input parameters (temperature, specific humidity, wind speed, precipitation), except air pressure, fell within the possible range of the observed values, meaning the model probably gave plausible values. However, CLM4.5 most likely modelled credible values for all input parameters, they were simply calculated for the underestimated elevation of Imingfjell.

As for the output, the modelled radiation budget and the soil heat flux (Q_G) were closer to the shrub data with 25% rejection of the null hypothesis (datasets are different) than the lichen data with 46%. Values of Q_G, K↓ and L↓ for both lichens and shrubs were proven similar to those modelled, with exception of L↓ in the "cold" period. The modelled K↑ differed from observed in almost all regimes. T-test results for net radiation (K*, L*, and Q*) and L↑ varied between the type of vegetation (lichens or shrubs) and temperature regimes, without a clear pattern of regularity.

The second research question was related to changes in the CLM4.5 radiation and energy budgets over time under the RCP4.5 scenario. Only half of the components from the radiation and energy budgets, such as Q_H, Q_E, K↑, L↓ and L*, have changed from pre-industrial times to the present day. Most of fluxes, with the exception of Q_E, Q_G, and L*, were predicted to change in the future according to the model. Values for Q_H and K↑ decreased from the "past" to the "present", but increased in the "future". Both Q_E and L* increased from the "past" to the "present", but remained unchanged in the "future". The soil heat flux (Q_G) has not changed over time. K↓, L↑, K* and Q* have not changed from the "past" to the "present", but increased in the "future". L↓ increased during all time periods.

We cannot say with certainty how accurate CLM4.5 models the data as further research is needed. However, despite that the modelled height of our object was underestimated, the model simulated fairly comparable radiation and energy budgets with the observed ones, especially with the data on shrubs. Therefore, the model can be used to facilitate the interpretation of field

observations and to fill data gaps. Still, it is recommended to check what the height of the study area is in the model, since an altitude calculated by CLM4.5 may differ greatly from the actual one, and also to choose the distribution and composition of vegetation that is closest to reality for the improvement of the results accuracy. CLM4.5 has also been useful in analysing climate change through the modelled radiation and energy budgets as shown in the RCP4.5 experiment. Our results confirmed that the climate will become warmer in the future, and these changes are happening at much faster pace in the future than in the past.

References

Aartsma, P., Asplund, J., Odland, A., Reinhardt, S., & Renssen, H. (2020). Surface albedo of alpine lichen heaths and shrub vegetation. *Arctic, Antarctic, and Alpine Research, 52*(1), 312-322. doi:10.1080/15230430.2020.1778890

Aufdemberge, T. P. (1974). Energy-balance studies over glacier and tundra surfaces, Chitistone Pass, Alaska, Summer 1969. *Icefield Ranges Research Project, Scientific Results, 4*, 63-79.

Bailey, W. G., Weick, E. J., & Bowers, J. D. (1989). The radiation balance of alpine tundra plateau mountain alberta canada. *Arctic & Alpine Research, 21*(2), 126-134. doi:10.2307/1551624

Baum, W. A. (1949). On the Relation between Mean Temperature and Height in the Layer of Air Near the Ground. *Ecology, 30*(1), 104-107. doi:10.2307/1932282

Bjordal, J. (2018). *Potential Implications of Lichen Cover for the Surface Energy Balance: Implementing Lichen as a new Plant Functional Type in the Community Land Model (CLM4.5).* (Master thesis). University of Oslo

Bolz, H. M. (1949). Die Abhängigkeit der infraroten Gegenstrahlung von der Bewölkung. *Zeitschrift für Meteorologic, 3*, 201-203.

Braunisch, V., Coppes, J., Arlettaz, R., Suchant, R., Zellweger, F., & Bollmann, K. (2014). Temperate mountain forest biodiversity under climate change: compensating negative effects by increasing structural complexity. *PLOS ONE, 9*(5), e97718. doi:10.1371/journal.pone.0097718

Brunt, D. (1932). Notes on radiation in the atmosphere. I. *Quarterly Journal of the Royal Meteorological Society, 58*(247), 389-420. doi:10.1002/qj.49705824704

Brutsaert, W. (1975). On a derivable formula for long-wave radiation from clear skies. *Water Resources Research, 11*(5), 742-744. doi:10.1029/WR011i005p00742

Burlando, P., Pellicciotti, F., & Strasser, U. (2002). Modelling mountainous water systems between learning and speculating looking for challenges: Selected paper from EGS General Assembly, Nice, April-2000 (Symposium OA36). *Hydrology Research, 33*(1), 47-74. doi:10.2166/nh.2002.0004

Davies, J. A. (1967). A note on the relationship between net radiation and solar radiation. *Quarterly Journal of the Royal Meteorological Society, 93*(395), 109-115. doi:10.1002/qj.49709339511

Du, E., Di Vittorio, A., & Collins, W. D. (2016). Evaluation of hydrologic components of community land model 4 and bias identification. *International Journal of Applied Earth Observation and Geoinformation, 48*, 5-16. doi:10.1016/j.jag.2015.03.013

Duarte, C. M., Lenton, T. M., Wadhams, P., & Wassmann, P. (2012). Abrupt climate change in the Arctic. *Nature Climate Change, 2*(2), 60-62. doi:10.1038/nclimate1386

eKlima. (2019). eKlima.met.no. Retrieved from http://sharki.oslo.dnmi.no/portal/page?_pageid=73,39035,73_39049&_dad=portal&_schema=PORTAL Accessed 19.08.2019

Elmendorf, S., Henry, G., Hollister, R., Björk, R., Bjorkman, A., Callaghan, T., . . . Wookey, P. (2012). Global assessment of experimental climate warming on tundra vegetation: Heterogeneity over space and time. *Ecology letters, 15*, 164-175. doi:10.1111/j.1461-0248.2011.01716.x

Farmer, G., & Cook, J. (2013). Earth's Energy Budget. In *Climate Change Science: A Modern Synthesis* (pp. 81-95).

Fritschen, L. J. (1967). Net and solar radiation relations over irrigated field crops. *Agricultural Meteorology, 4*(1), 55-62. doi:10.1016/0002-1571(67)90042-8

Füssel, H.-M., Jol, A., Hildén, M., Christiansen, T., Kurnik, B., Hemming, D., . . . Watkiss, P. (2012). *Climate change, impacts and vulnerability in Europe 2012*: EEA.

Gates, D. M., & Janke, R. (1966). The energy environment of the alpine tundra. *Oecologia Plantarum, 1*, 39-61.

Halbsguth, G., Kerschgens, M. J., Kraus, H., Meindl, G., & Schaller, E. (1984). Energy fluxes in an alipine valley. *Archives for meteorology, geophysics, and bioclimatology, Series A, 33*(1), 11-20. doi:10.1007/BF02265425

Hatzianastassiou, N., Matsoukas, C., Fotiadi, A., Pavlakis, K., Drakakis, E., Hatzidimitriou, D., & Vardavas, I. (2005). Global distribution of Earth's surface shortwave radiation budget. *Atmospheric Chemistry and Physics, 5*(10), 2847-2867. doi:10.5194/acpd-5-4545-2005

Herman, B., Brunke, M., Pielke Sr, R., Christy, J., & McNider, R. (2010). Satellite Global and Hemispheric Lower Tropospheric Temperature Annual Temperature Cycle. *Remote Sensing, 2*. doi:10.3390/rs2112561

Hirata, A., Kominami, Y., Matsui, T., & Hijioka, Y. (2020). Evaluation of the estimation of shortwave solar radiation in Japan using the Mountain Microclimate Simulation Model. *Journal of Agricultural Meteorology*. doi:10.2480/agrmet.D-19-00046

Hock, R., Rasul, G., Adler, C., Cáceres, B., Gruber, S., Hirabayashi, Y., . . . Steltzer, H. (2019). High Mountain Areas. In D. C. R. H.-O. Pörtner, V. Masson-Delmotte, P. Zhai, M. Tignor, E. Poloczanska, K. Mintenbeck, A. Alegría, M. Nicolai, A. Okem, J. Petzold, B. Rama, N.M. Weyer (Ed.), *IPCC Special Report on the Ocean and Cryosphere in a Changing Climate*.

Hu, Z., & Zhi-Peng, X. (2019). Origin and advances in implementing blowing-snow effects in the Community Land Model. *Sciences in Cold and Arid Regions, 11*(5), 335-339. doi:10.3724/SP.J.1226.2019.00335

Idso, S. B. (1981). A set of equations for full spectrum and 8- to 14-µm and 10.5- to 12.5-µm thermal radiation from cloudless skies. *Water Resources Research, 17*(2), 295-304. doi:10.1029/WR017i002p00295

Idso, S. B., & Jackson, R. D. (1969). Thermal radiation from the atmosphere. *Journal of Geophysical Research, 74*(23), 5397-5403. doi:10.1029/JC074i023p05397

IPCC. (2013). Summary for Policymakers. In T. F. Stocker, D. Qin, G.-K. Plattner, M. Tignor, S.K. Allen, J. Boschung, A. Nauels, Y. Xia, V. Bex, & P. M. Midgley (Eds.), *Climate Change 2013: The Physical Science Basis. Contribution of Working Group I to the Fifth Assessment Report of the Intergovernmental Panel on Climate Change*. United Kingdom and New York, NY, USA.: Cambridge University Press, Cambridge.

Isard, S. A. (1989). Topoclimatic controls in an alpine fellfield and their ecological significance. *Physical Geography, 10*(1), 13-31. doi:10.1080/02723646.1989.10642364

Ishaq, S., Khan, M. Z., Begum, F., Hussain, K., Amir, R., Hussain, A., & Ali, S. (2016). Climate change impact on mountain biodiversity: a special reference to Gilgit-Baltistan of Pakistan. *Journal of Mountain Area Research, 1*, 53-63. Retrieved from https://journal.kiu.edu.pk/index.php/JMAR/article/view/12

Jacob, D., Petersen, J., Eggert, B., Alias, A., Christensen, O., Bouwer, L., . . . Yiou, P. (2014). EURO-CORDEX: New high-resolution climate change projections for European impact research. *Regional Environmental Change, 14*. doi:10.1007/s10113-013-0499-2

Kapos, V., Rhind, J., Edwards, M., Price, M. F., & Ravilious, C. (2000). Developing a map of the world's mountain forests. In M. F. Price & N. Butt (Eds.), *Forests in sustainable mountain development: a state of knowledge report for 2000. Task Force on Forests in Sustainable Mountain Development.* (pp. 4-19). Wallingford: CABI Publishing.

Khalatov, V. Y., & Abdul'myanov, S. N. (2013). Geotopes of mountain territories: Definitions, approaches to the study, protection. *Geography and Natural Resources, 34*, 14-19. doi:10.1134/S1875372813010022

Kopáček, J., Bače, R., Hejzlar, J., Kaňa, J., Kucera, T., Matějka, K., . . . Turek, J. (2020). Changes in microclimate and hydrology in an unmanaged mountain forest catchment after insect-

induced tree dieback. *Science of The Total Environment, 720*, 137518. doi:10.1016/j.scitotenv.2020.137518

Körner, C. (2007). The use of 'altitude' in ecological research. *Trends in Ecology & Evolution, 22*(11), 569-574. doi:10.1016/j.tree.2007.09.006

Körner, C., Jetz, W., Paulsen, J., Payne, D., Rudmann-Maurer, K., & Spehn, E. (2017). A global inventory of mountains for bio-geographical applications. *Alpine Botany, 127*(1), 1-15. doi:10.1007/s00035-016-0182-6

Körner, C., Paulsen, J., & Spehn, E. M. (2011). A definition of mountains and their bioclimatic belts for global comparison of biodiversity data. *Alpine Botany, 121*, 73-78. doi:10.1007/s00035-011-0094-4

Kovats, R. S., Valentini, R., Bouwer, L. M., Georgopoulou, E., Jacob, D., Martin, E., . . . Soussana, J.-F. (2014). Europe. In V.R. Barros, C.B. Field, D.J. Dokken, M.D. Mastrandrea, K.J. Mach, T.E. Bilir, M. Chatterjee, K.L. Ebi, Y.O. Estrada, R.C. Genova, B. Girma, E.S. Kissel, A.N. Levy, S. MacCracken, P.R. Mastrandrea, & L.L.White (Eds.), *Climate Change 2014: Impacts, Adaptation, and Vulnerability. Part B: Regional Aspects. Contribution of Working Group II to the Fifth Assessment Report of the Intergovernmental Panel on Climate Change* (pp. 1267-1326). Cambridge, United Kingdom and New York, NY, USA Cambridge University Press

Kraus, H. (1971). Ein Beitrag zum Wärme- und Strahlungshaushalt im Himalaya-Gebirge [A Contribution to the Heat and Radiation Budget in the Himalayas]. *Archiv für Meteorologie, Geophysik und Bioklimatologie, Serie A, 20*(2), 175-182. doi:10.1007/BF02247992

Kumar, S., & Merwade, V. (2011). Evaluation of NARR and CLM3.5 outputs for surface water and energy budgets in the Mississippi River Basin. *Journal of Geophysical Research: Atmospheres, 116*(D08115). doi:10.1029/2010jd014909

Lang, P. R., & Lombargo, F. S. (2011). *Atmospheric turbulence, meteorological modeling and aerodynamics*: Nova Science.

Lawrence, D., Fisher, R., Koven, C., Oleson, K., Swenson, S., Bonan, G., . . . Zeng, X. (2019). The Community Land Model version 5: Description of new features, benchmarking, and impact of forcing uncertainty. *Journal of Advances in Modeling Earth Systems, 11*(12), 4245-4287. doi:10.1029/2018MS001583

LeDrew, E. F. (1975). The Energy balance of a mid-latitude alpine site during the growing season, 1973. *Arctic and Alpine Research, 7*(4), 301-314. doi:10.1080/00040851.1975.12003842

Lur'e, P. M., & Panov, V. D. (2011). Problems of exploration level of hydrometeorological regime of the Northern Caucasus territory. *Russian Meteorology and Hydrology, 36*, 273-278. doi:10.3103/S1068373911040091

Masson-Delmotte, V., Schulz, M., Abe-Ouchi, A., Beer, J., Ganopolski, A., González Rouco, J. F., . . . Timmermann, A. (2013). Information from Paleoclimate Archives. In T.F. Stocker, D. Qin, G.-K. Plattner, M. Tignor, S.K. Allen, J. Boschung, A. Nauels, Y. Xia, V. Bex, & P. M. Midgley (Eds.), *Climate Change 2013: The Physical Science Basis. Contribution of Working Group I to the Fifth Assessment Report of the Intergovernmental Panel on Climate Change*. Cambridge, United Kingdom and New York, NY, USA: Cambridge University Press.

Meybeck, M., Green, P., & Vörösmarty, C. (2001). A new typology for mountains and other relief casses. *Mountain Research and Development, 21*, 34-45. doi:10.1659/0276-4741(2001)021[0034:ANTFMA]2.0.CO;2

Müller, H. (1985). On the radiation budget in the Alps. *Journal of Climatology, 5*(4), 445-462. doi:10.1002/joc.3370050411

Myers, N., Mittermeier, R. A., Mittermeier, C. G., Fonseca, G. A. B., & Kent, J. (2000). Biodiversity hotspot for conservation priorities. *Nature, 403*, 853-858. doi:10.1038/35002501

Oke, T. R. (1987). Boundary Layer Climates - 2nd ed. In.

Oleson, K., Lawrence, D., Bonan, G., Drewniak, B., Huang, M., Koven, C., . . . Yang, Z.-L. (2013). *Technical description of version 4.5 of the Community Land Model (CLM)*.

Price, M., Arnesen, T., Gløersen, E., & Metzger, M. J. (2018). Mapping mountain areas: learning from Global, European and Norwegian perspectives. *Journal of Mountain Science*. doi:10.1007/s11629-018-4916-3

Rahbek, C., Borregaard, M., Colwell, R., Dalsgaard, B., Holt, B., Morueta-Holme, N., . . . Fjeldså, J. (2019). Humboldt's enigma: What causes global patterns of mountain biodiversity? *Science, 365*(6458), 1108-1113. doi:10.1126/science.aax0149

Rapp, J. M., & Silman, M. R. (2012). Diurnal, seasonal, and altitudinal trends in microclimate across a tropical montane cloud forest. *Climate Research, 55*(1), 17-32. doi:10.3354/cr01127

Rose, B. E. J. (2019). Lecture 11: Insolation. *ATM 623: Climate Modeling.* Retrieved from http://www.atmos.albany.edu/facstaff/brose/classes/ATM623_Spring2015/Notes/Lectures/Lecture11%20--%20Insolation.html Accessed 01.10.2019

Sauberer, F., & Dirmhirn, I. (1958). Das Strahlungsklima [The radiation climate]. *Klimatographie von Österreich (Steinhauser, F., Eckel, O., Lauscher, F., Hrsg.), 3*(1), 13-102.

Saunders, I. R. (1990). *Radiation and energy budgets of alpine tundra, Scout Mountain, southern British Columbia, Canada*.

Saunders, I. R., & Bailey, W. G. (1994). Radiation and energy budgets of alpine tundra environments of North America. *Progress in Physical Geography: Earth and Environment, 18*(4), 517-538. doi:10.1177/030913339401800403

Schluter, D., & Whitlock, M. (2015). *The analysis of biological data. 2nd edition*. Greenwood Village, CO, USA: Roberts and Company Publishers.

Shah, R. D. T., Sharma, S., Haase, P., Jähnig, S. C., & Pauls, S. U. (2015). The climate sensitive zone along an altitudinal gradient in central Himalayan rivers: a useful concept to monitor climate change impacts in mountain regions. *Climatic Change, 132*(2), 265-278. doi:10.1007/s10584-015-1417-z

Smagorinsky, J. (1974). Global atmospheric modeling and the numerical simulation of climate. *Weather and Climate Modification*, 633-686.

Staudinger, M. (1978). *Die Strahlungsbilanz zweier hochalpiner Stationen während der Vegetationsperiode [The radiation balance of two high alpine stations during the growing season]*. Paper presented at the 15th Int. Conference for Alpine Met., Switzerland.

Sturm, M., Douglas, T., Racine, C., & Liston, G. (2005). Changing snow and shrub conditions affect albedo with global implications. *Journal of Geophysical Research, 110*. doi:10.1029/2005JG000013

Sundstøl, S., & Odland, A. (2017). Responses of Alpine Vascular Plants and Lichens to Soil Temperatures. *Annales Botanici Fennici, 54*, 17-28. doi:10.5735/085.054.0304

SunEarthTools (2019). SunEarthTools.com. Retrieved from https://www.sunearthtools.com/dp/tools/pos_sun.php. Accessed 11.11.19

Svirin, A. (2019). Barometric Formula. Retrieved from https://www.math24.net/barometric-formula/ Accessed 23.10.2019

Swinbank, W. C. (1963). Long-wave radiation from clear skies. *Quarterly Journal of the Royal Meteorological Society, 89*(381), 339-348. doi:10.1002/qj.49708938105

Taylor, K., Ronald, S., & Meehl, G. (2011). A Summary of the CMIP5 experiment design. *PCDMI Rep., 4*.

Taylor, K., Ronald, S., & Meehl, G. (2012). An overview of CMIP5 and the Experiment Design. *Bulletin of the American Meteorological Society, 93*, 485-498. doi:10.1175/BAMS-D-11-00094.1

Terjung, W. H., Kickert, R. N., Potter, G. L., & Swarts, S. W. (1969). Terrestrial, atmospheric and solar radiation fluxes on a high desert mountain in mid-July: White Mountain Peak, California. *Solar Energy, 12*(3), 363-375. doi:10.1016/0038-092X(69)90050-4

Thom, A. S. (1975). *Momentum, mass and heat exchange of plant communities* (J. L. Monteith Ed. Vol. 1). London.

Tito, R., Vasconcelos, H., & Feeley, K. (2020). Mountain ecosystems as natural laboratories for climate change experiments. *Frontiers in Forests and Global Change, 3*(38). doi:10.3389/ffgc.2020.00038

USGS. (2019). Earth-Sun Distance in Astronomical Units for Days of the Year. Retrieved from https://www.usgs.gov/media/files/earth-sun-distance-astronomical-units-days-year Accessed 01.11.2019.

USGS. (2020). Digital elevation. Retrieved from https://earthexplorer.usgs.gov/ Accessed 20.01.2020.

Vasiakina, A., Renssen, H., Aartsma, P., & Kurovskaia, V. (2020). Microclimatological conditions at the Imingfjell mountain, Norway: comparison of model results with observed data. *E3S Web of Conferences, 163*, 01013. doi:10.1051/e3sconf/202016301013

Vowles, T., & Björk, R. (2019). Implications of evergreen shrub expansion in the Arctic. *Journal of Ecology, 107*, 650-655. doi:10.1111/1365-2745.13081

Wang, D., Xu, Y., Thornton, P., King, A., Steed, C., Gu, L., & Schuchart, J. (2014). A functional test platform for the Community Land Model. *Environmental Modelling & Software, 55*, 25–31. doi:10.1016/j.envsoft.2014.01.015

Zhang, L., Lei, H., Shen, H., Cong, Z., Yang, D., & Liu, T. (2019). Evaluating the representation of vegetation phenology in the Community Land Model 4.5 in a temperate grassland. *Journal of Geophysical Research: Biogeosciences, 124*(2). doi:10.1029/2018JG004866

Annexes

Annex 1: Statistics calculated over 2002-2016 for monthly temperature (°C) at Imingfjell (modelled data) and 'Dagali Lufthavn' station (observed data) with a number of years used for its calculations

Data	Statistics	Month												All mean
		Jan	Feb	Mar	Apr	May	Jun	Jul	Aug	Sep	Oct	Nov	Dec	
Imingfjell	Mean	-7,59	-6,75	-2,66	2,51	7,06	11,25	13,78	12,81	9,08	2,87	-1,27	-4,18	3,08
	Number of years	15	15	15	15	15	15	15	15	15	15	15	15	15
Dagali Lufthavn	Mean	-9,28	-7,88	-4,32	0,33	4,88	9,52	12,14	10,35	6,76	0,91	-3,65	-7,80	1,00
	Max	3,10	5,10	7,80	7,30	15,50	17,50	19,50	16,90	13,60	10,50	7,20	4,90	10,74
	Min	-36,90	-27,40	-22,50	-11,50	-2,70	1,40	7,00	3,50	-1,20	-15,20	-24,30	-30,90	-13,39
	Number of years	14	14	14	14	14	14	14	13	13	15	14	15	14
ΔI-D		-1,69	-1,12	-1,67	-2,18	-2,17	-1,74	-1,65	-2,46	-2,32	-1,96	-2,38	-3,62	-2,08

Annex 2: Statistics calculated over 2002-2016 for specific humidity (g kg^{-1}) at Imingfjell (modelled data) and 'Dagali Lufthavn' station (observed data) with a number of years used for its calculations

Data	Statistics	Month												All mean
		Jan	Feb	Mar	Apr	May	Jun	Jul	Aug	Sep	Oct	Nov	Dec	
Imingfjell	Mean	1,92	2,01	2,21	3,13	4,12	5,28	6,99	6,79	5,18	3,69	3,07	2,36	3,90
	Number of years	15	15	15	15	15	15	15	15	15	15	15	15	15
Dagali Lufthavn	Mean	1,96	2,02	2,38	3,06	4,02	5,09	6,80	6,44	5,24	3,81	2,94	2,27	3,83
	Max	4,20	4,40	4,30	5,70	7,80	9,40	10,30	10,10	8,80	7,00	6,10	4,70	6,90
	Min	0,10	0,30	0,50	1,00	1,70	2,30	4,00	3,40	2,60	1,10	0,50	0,30	1,48
	Number of years	10	10	11	10	10	9	10	11	12	10	12	11	10,5
Δm-o		0,04	0,01	0,16	-0,06	-0,10	-0,19	-0,19	-0,36	0,07	0,12	-0,13	-0,09	-0,06

Annex 3: Statistics calculated over 2002-2016 for wind speed (m s^{-1}) at Imingfjell (modelled data) and 'Dagali Lufthavn' station (observed data) with a number of years used for its calculations

Data	Statistics	Month												All mean
		Jan	Feb	Mar	Apr	May	Jun	Jul	Aug	Sep	Oct	Nov	Dec	
Imingfjell	Mean	5,67	5,07	4,73	3,98	3,70	3,46	3,28	3,49	4,58	4,77	5,27	5,58	4,46
	Number of years	15	15	15	15	15	15	15	15	15	15	15	15	15
Dagali Lufthavn	Mean	2,25	2,36	2,86	2,79	2,78	2,67	2,29	2,09	2,54	1,97	2,05	2,18	2,40
	Max	11,50	9,50	10,00	9,20	10,50	8,70	6,60	8,60	8,60	6,00	11,20	12,30	9,39
	Min	0,00	0,00	0,00	0,20	0,20	0,00	0,50	0,30	0,30	0,00	0,00	0,00	0,13
	Number of years	14	14	14	14	14	14	14	14	14	14	14	15	14,08
Δm-o		-3,42	-2,71	-1,87	-1,20	-0,92	-0,79	-0,98	-1,39	-2,03	-2,79	-3,22	-3,40	-2,06

Annex 4: Statistics calculated over 2002-2016 for air pressure (hPa) at Imingfjell (modelled data) and 'Dagali Lufthavn' station (observed data) with a number of years used for its calculations

Data	Statistics	Month												All mean
		Jan	Feb	Mar	Apr	May	Jun	Jul	Aug	Sep	Oct	Nov	Dec	
Imingfjell	Mean	958,8	960,9	963,5	965,1	965,3	965,7	964,6	964,4	965,6	964,3	959,5	959,7	963
	Number of years	15	15	15	15	15	15	15	15	15	15	15	15	15
Dagali Lufthavn	Mean	913,3	916,4	918,1	919,3	920,0	920,5	920,2	920,0	920,9	919,3	914,7	914,5	918
	Max	947,2	945,7	947,2	945,2	943,2	938,9	938,8	934,4	941,0	942,2	948,5	950,0	944
	Min	881,2	878,9	873,8	894,8	899,5	899,7	902,9	896,2	892,6	887,8	882,9	880,8	889
	Number of years	14	14	14	14	14	14	14	15	15	15	15	15	14
ΔI-D		-46	-45	-45	-46	-45	-45	-44	-44	-45	-45	-45	-45	-45

Annex 5: Statistics calculated over 2002-2016 for monthly total precipitation (mm) at Imingfjell (modelled data) and 'Tunhovd' station (observed data) with a number of years used for its calculations

Dataset	Statistics	**Month**												All mean
		Jan	Feb	Mar	Apr	May	Jun	Jul	Aug	Sep	Oct	Nov	Dec	
Imingfjell	Mean	31,6	21,9	21,2	24,3	45,9	49,3	63,9	60,4	42,8	46,4	40,8	24,6	39,4
	Number of years	15	15	15	15	15	14	15	15	15	15	15	14	14,8
Tunhovd	Mean	44,4	27,5	28,5	31,0	49,9	72,3	99,8	91,9	51,9	44,5	43,9	37,6	51,9
	Max	84,0	61,4	60,0	70,9	129,0	169,5	200,1	150,7	138,1	128,7	83,4	62,9	111,6
	Min	19,7	1,5	8,7	6,2	25,1	21,3	17,2	36,8	15,0	5,5	18,3	17,7	16,1
	Number of years	15	15	15	15	15	15	15	15	15	15	15	15	15
ΔI-T		12,8	5,6	7,3	6,6	4,0	23,1	35,9	31,5	9,1	-1,9	3,1	12,9	12,5

Annex 6: Mean, maximum and minimum values of the soil heat flux for the observed (lichen and shrub) and modelled data in the “extremely warm”, the “normal” and the “cold” regimes (these tabular data were used to plot Annex 7)

Dataset	Value	Extremely warm	Normal	Cold
Model	mean	9,14	6,52	3,40
	max	13,08	15,18	8,10
	min	3,78	-2,83	-3,44
Lichen	mean	12,25	6,69	2,36
	max	19,58	20,70	13,68
	min	3,88	-5,78	-9,40
Shrub	mean	7,14	5,05	2,22
	max	11,65	9,32	6,91
	min	2,76	0,13	-6,33

Annex 7: Mean values of the soil heat flux and their range from minimum to maximum

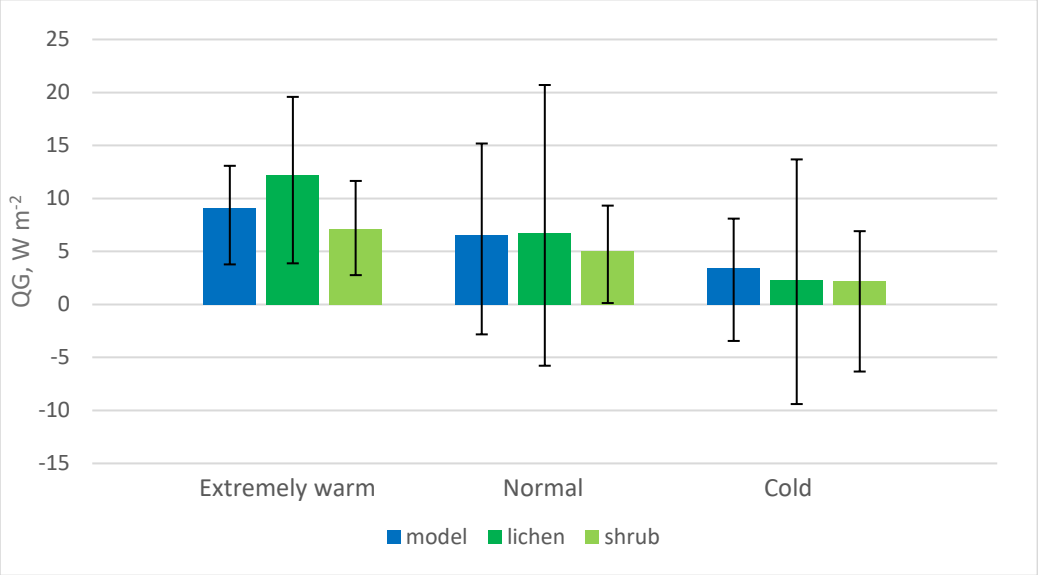

Annex 8: Mean, maximum and minimum values of the latent heat flux for the modelled data in the “extremely warm”, the “normal” and the “cold” regimes (these tabular data were used to plot Annex 9)

Dataset	Value	Extremely warm	Normal	Cold
Model	mean	110,84	97,02	81,31
	max	135,44	124,43	100,84
	min	89,78	66,90	67,79

Annex 9: Mean values of the latent heat flux and their range from minimum to maximum

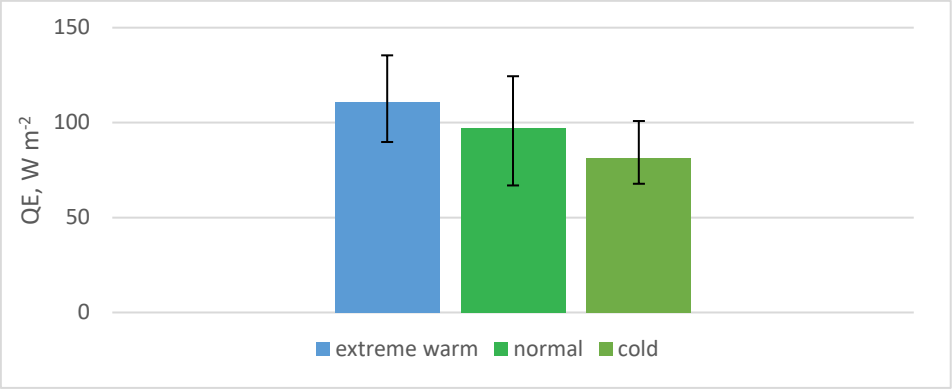

Annex 10: Mean, maximum and minimum values of the sensible heat flux for the modelled data in the “extremely warm”, the “normal” and the “cold” regimes (these tabular data were used to plot Annex 11)

Dataset	Value	Extremely warm	Normal	Cold
Model	mean	40,17	30,81	37,65
	max	62,51	85,86	79,11
	min	0,53	-24,60	9,92

Annex 11: Mean values of the sensible heat flux and their range from minimum to maximum

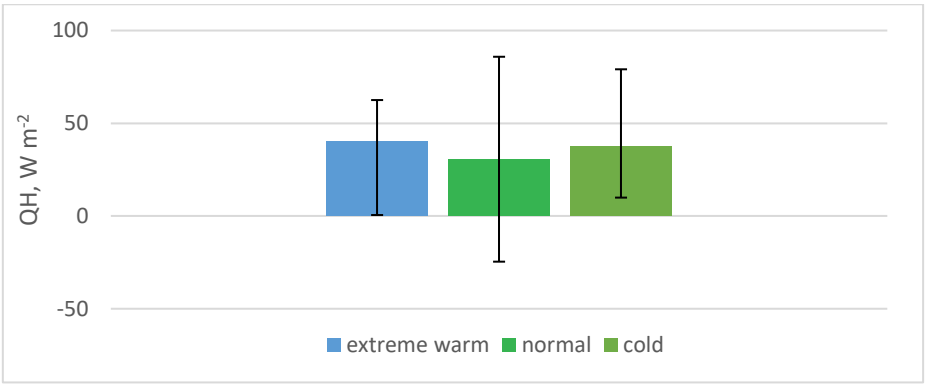

Annex 12: Mean, maximum and minimum values of incoming longwave radiation for the observed (lichen and shrub) and modelled data in the “extremely warm”, the “normal” and the “cold” regimes (these tabular data were used to plot Annex 13)

Dataset	Value	Extremely warm	Normal	Cold
Model	mean	327,34	309,61	295,19
	max	350,50	328,24	306,88
	min	296,30	284,29	283,90
Lichen	mean	323,19	315,70	312,93
	max	361,28	356,10	356,21
	min	298,51	282,74	268,51
Shrub	mean	323,46	315,99	313,23
	max	362,99	356,23	356,19
	min	298,99	284,51	269,68

Annex 13: Mean values of incoming longwave radiation and their range from minimum to maximum

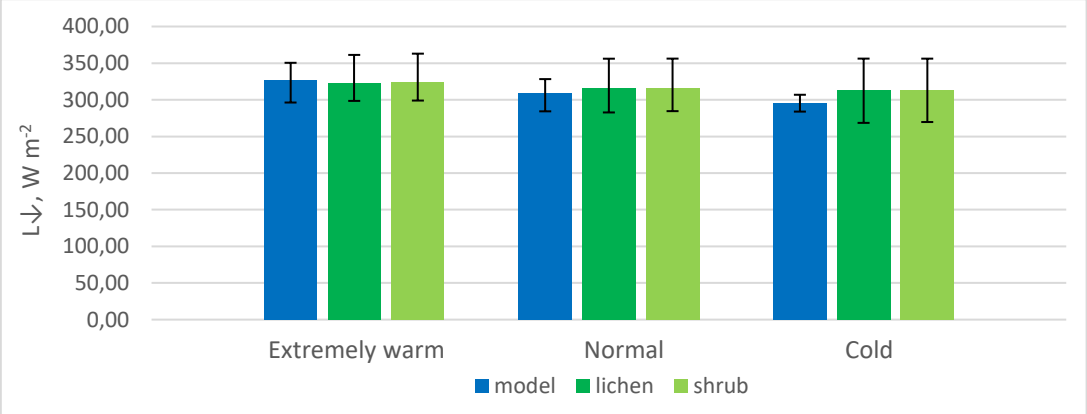

Annex 14: Mean, maximum and minimum values of outgoing longwave radiation for the observed (lichen and shrub) and modelled data in the “extremely warm”, the “normal” and the “cold” regimes (these tabular data were used to plot Annex 15)

Dataset	Value	Extremely warm	Normal	Cold
Model	mean	395,38	376,75	365,92
	max	405,19	390,62	373,62
	min	369,45	356,47	352,72
Lichen	mean	407,82	395,13	365,62
	max	422,81	416,21	380,51
	min	394,03	370,89	352,88
Shrub	mean	401,35	387,55	361,24
	max	415,88	404,52	372,72
	min	389,61	370,20	348,59

Annex 15: Mean values of outgoing longwave radiation and their range from minimum to maximum

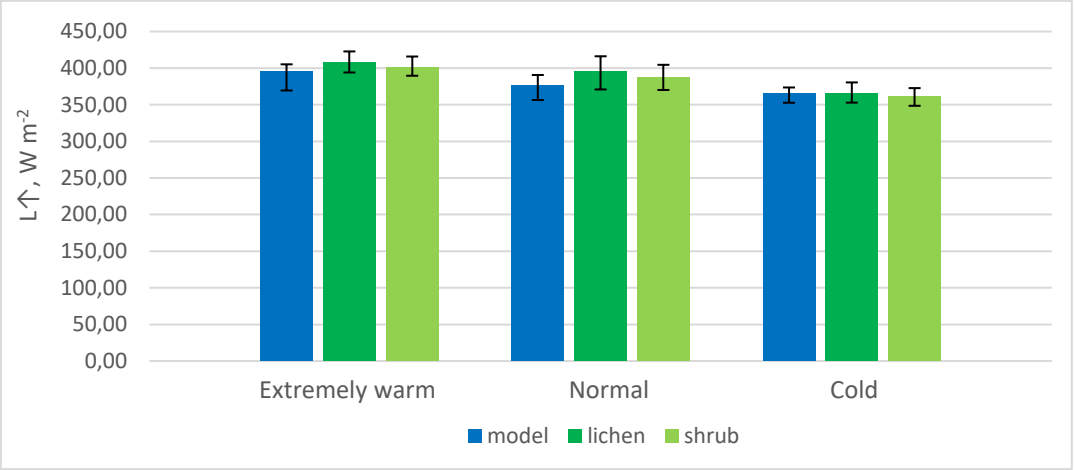

Annex 16: Mean, maximum and minimum values of net longwave radiation for the observed (lichen and shrub) and modelled data in the "extremely warm", the "normal" and the "cold" regimes (these tabular data were used to plot Annex 17)

Dataset	Value	Extremely warm	Normal	Cold
Model	mean	-68,05	-67,14	-70,73
	max	-54,28	-58,79	-64,82
	min	-77,00	-78,60	-79,64
Lichen	mean	-84,63	-79,43	-52,69
	max	-32,76	-14,79	-6,35
	min	-117,07	-131,13	-112,00
Shrub	mean	-77,89	-71,56	-48,01
	max	-26,62	-13,97	-5,54
	min	-109,75	-116,39	-100,53

Annex 17: Mean values of net longwave radiation and their range from minimum to maximum

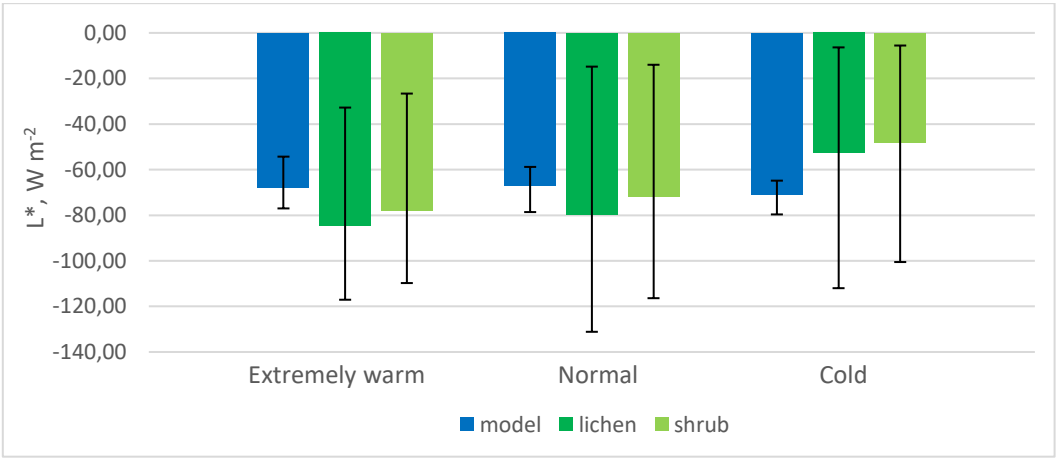

Annex 18: Mean, maximum and minimum values of incoming shortwave radiation for the observed (lichen and shrub) and modelled data in the “extremely warm”, the “normal” and the “cold” regimes (these tabular data were used to plot Annex 19)

Dataset	Value	Extremely warm	Normal	Cold
Model	mean	281,27	249,08	238,01
	max	336,71	331,40	294,85
	min	217,83	188,86	199,45
Lichen	mean	277,46	258,74	190,45
	max	350,89	361,58	344,95
	min	204,75	53,28	45,71
Shrub	mean	276,72	258,76	188,88
	max	351,78	363,08	347,82
	min	204,57	53,19	45,02

Annex 19: Mean values of shortwave incoming radiation and their range from minimum to maximum

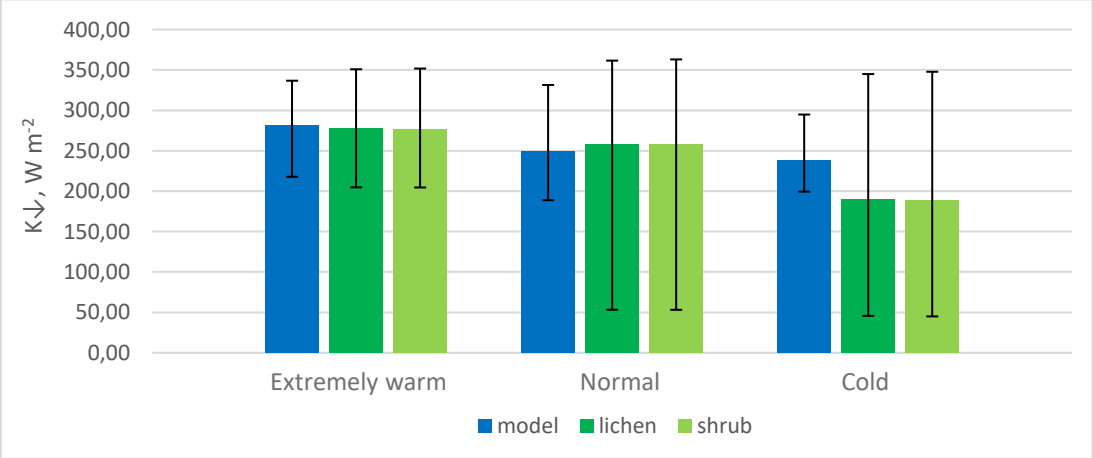

Annex 20: Mean, maximum and minimum values of outgoing shortwave radiation for the observed (lichen and shrub) and modelled data in the “extremely warm”, the “normal” and the “cold” regimes (these tabular data were used to plot Annex 21)

Dataset	Value	Extremely warm	Normal	Cold
Model	mean	53,08	47,58	44,93
	max	63,21	63,08	56,04
	min	40,96	36,10	36,21
Lichen	mean	69,96	70,17	55,88
	max	99,04	109,69	106,37
	min	46,31	14,52	12,86
Shrub	mean	41,97	37,05	28,76
	max	50,86	57,88	55,00
	min	30,69	7,32	5,59

Annex 21: Mean values of outgoing shortwave radiation and their range from minimum to maximum

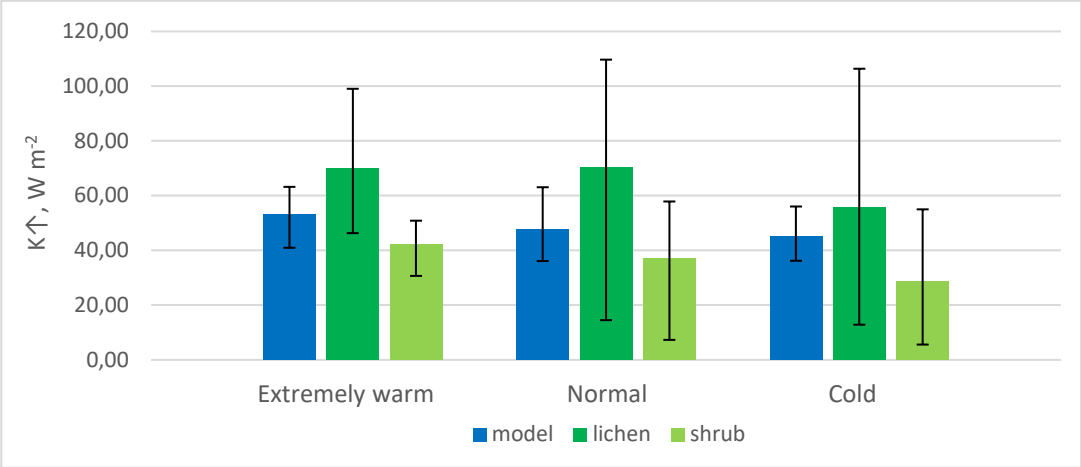

Annex 22: Mean, maximum and minimum values of net shortwave radiation for the observed (lichen and shrub) and modelled data in the “extremely warm”, the “normal” and the “cold” regimes (these tabular data were used to plot Annex 23)

Dataset	Value	Extremely warm	Normal	Cold
Model	mean	228,19	201,49	193,09
	max	273,49	268,32	241,31
	min	176,87	152,76	158,23
Lichen	mean	207,50	188,57	134,58
	max	266,33	269,17	238,58
	min	145,48	38,75	32,85
Shrub	mean	234,75	221,70	160,12
	max	303,24	308,16	292,81
	min	173,54	45,87	39,43

Annex 23: Mean values of net shortwave radiation and their range from minimum to maximum

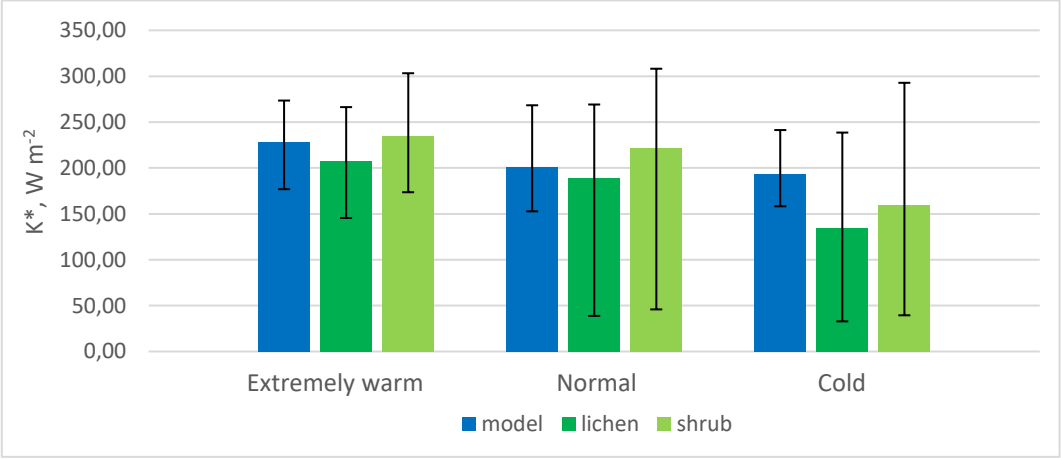

Annex 24: Mean, maximum and minimum values of net all-wave radiation for the observed (lichen and shrub) and modelled data in the “extremely warm”, the “normal” and the “cold” regimes (these tabular data were used to plot Annex 25)

Dataset	Value	Extremely warm	Normal	Cold
Model	mean	160,14	134,35	122,36
	max	196,49	189,72	162,48
	min	122,59	91,76	91,34
Lichen	mean	122,87	109,13	81,89
	max	149,27	141,57	126,58
	min	79,12	23,96	26,50
Shrub	mean	156,85	150,14	112,11
	max	194,12	205,67	192,29
	min	112,54	31,90	33,89

Annex 25: Mean values of net all-wave radiation and their range from minimum to maximum

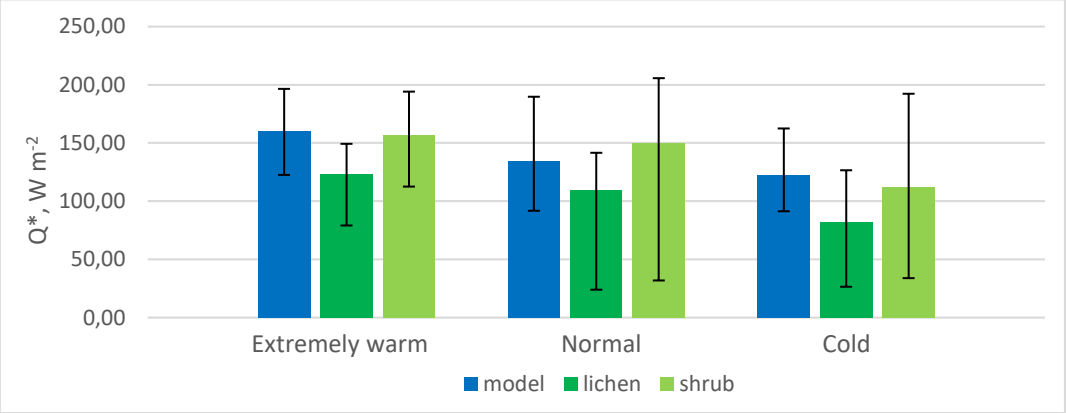

Annex 26: Energy balance for the model data during “extremely warm” regime

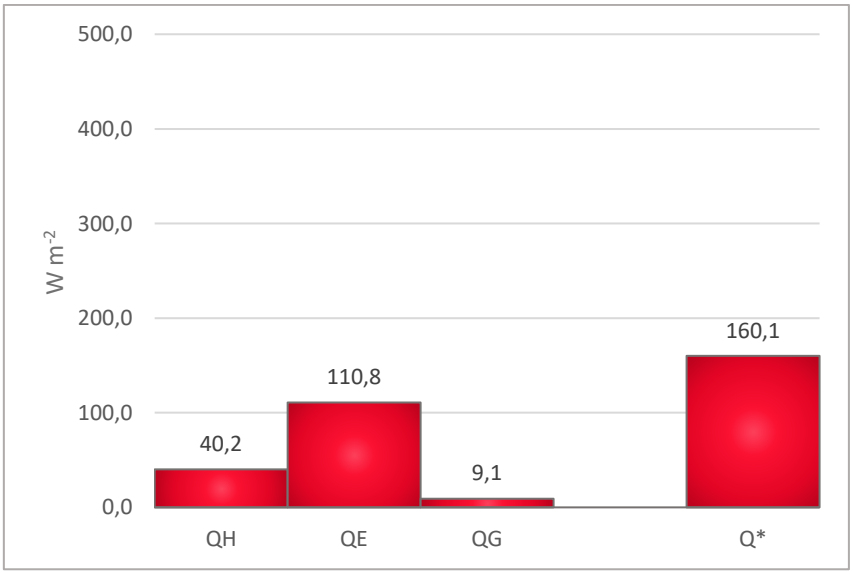

Annex 27: Energy balance for the model data during “normal” regime

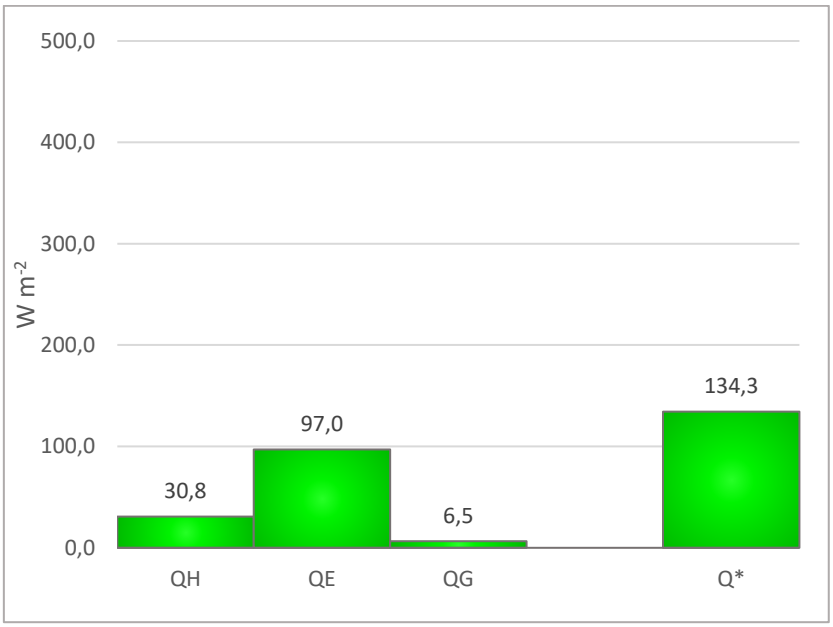

Annex 28: Energy balance for the model data during “cold” regime

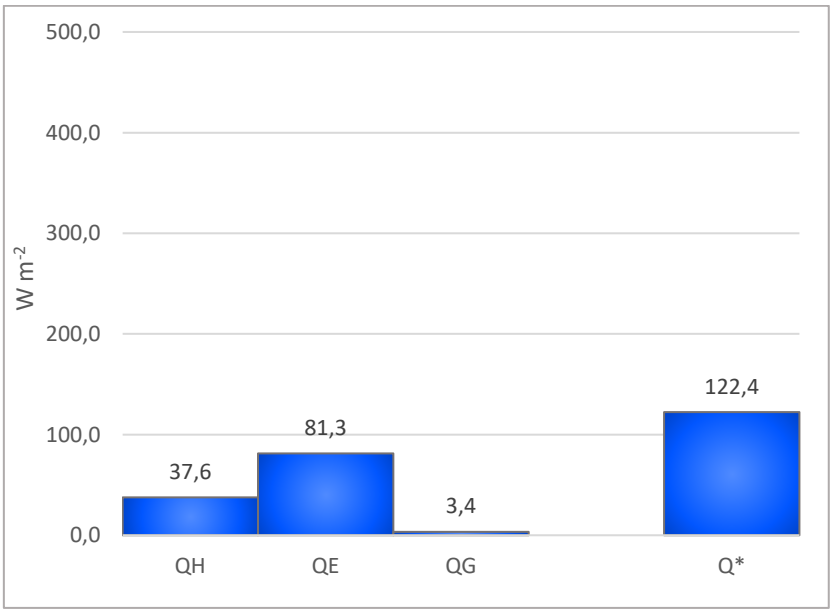

Annex 29: Values of radiation budget components for “extremely warm” regime and their statistics

"Extremely warm" regime						
Flux	Statistic	Data			Δ	
		Model	Lichen	Shrub	Model/Lichen	Model/Shrub
K↓	Mean	281,3	277,5	276,7	3,8	4,5
	SD[1]	30,1	49,8	49,4	-19,7	-19,2
	CV[2]	0,11	0,18	0,18	-0,07	-0,07
K↑	Mean	53,1	70,0	42,0	-16,9	11,1
	SD	5,7	15,1	7,9	-9,4	-2,3
	CV	0,11	0,22	0,19	-0,11	-0,08
K*	Mean	228,2	207,5	234,7	20,7	-6,6
	SD	24,6	37,8	42,4	-13,3	-17,8
	CV	0,11	0,18	0,18	-0,07	-0,07
L↓	Mean	327,3	323,2	323,5	4,1	3,9
	SD	16,6	16,8	16,6	-0,2	0,1
	CV	0,05	0,05	0,05	0,00	0,00
L↑	Mean	395,4	407,8	401,4	-12,4	-6,0
	SD	11,7	9,4	8,2	2,3	3,5
	CV	0,03	0,02	0,02	0,0	0,0
L*	Mean	-68,0	-84,6	-77,9	16,6	9,8
	SD	6,3	22,8	22,3	-16,5	-16,0
	CV	-0,09	-0,27	-0,29	0,2	0,2
Q*	Mean	160,1	122,9	156,9	37,3	3,3
	SD	19,7	23,7	25,8	-4,0	-6,1
	CV	0,12	0,19	0,16	-0,1	0,0

[1]SD - Standard deviation; [2]CV - Coefficient of variation

Annex 30: Values of radiation budget components for “normal” regime and their statistics

"Normal" regime						
Flux	Statistic	Data			Δ	
		Model	Lichen	Shrub	Model/Lichen	Model/Shrub
K↓	Mean	249,1	258,7	258,8	-9,7	-9,7
	SD	34,7	83,4	84,1	-48,7	-49,4
	CV	0,14	0,32	0,32	-0,2	-0,2
K↑	Mean	47,6	70,2	37,1	-22,6	10,5
	SD	6,4	22,5	12,7	-16,1	-6,2
	CV	0,14	0,32	0,34	-0,2	-0,2
K*	Mean	201,5	188,6	221,7	12,9	-20,2
	SD	28,3	62,4	71,7	-34,1	-43,5
	CV	0,14	0,33	0,32	-0,2	-0,2
L↓	Mean	309,6	315,7	316,0	-6,1	-6,4
	SD	13,0	22,0	21,6	-9,0	-8,6
	CV	0,04	0,07	0,07	0,0	0,0
L↑	Mean	376,7	395,1	387,5	-18,4	-10,8
	SD	9,5	14,4	11,4	-4,9	-1,9
	CV	0,03	0,04	0,03	0,0	0,0
L*	Mean	-67,1	-79,4	-71,6	12,3	4,4
	SD	4,6	32,9	29,8	-28,3	-25,2
	CV	-0,07	-0,41	-0,42	0,3	0,3
Q*	Mean	134,3	109,1	150,1	25,2	-15,8
	SD	25,5	31,5	43,4	-6,0	-17,8
	CV	0,19	0,29	0,29	-0,1	-0,1

Annex 31: Values of radiation budget components for “cold” regime and their statistics

"Cold" regime						
Flux	Statistic	Data			Δ	
		Model	Lichen	Shrub	Model/Lichen	Model/Shrub
K↓	Mean	238,0	190,5	188,9	47,6	49,1
	SD	33,3	80,3	80,7	-47,0	-6,6
	CV	0,14	0,42	0,43	-0,3	-0,3
K↑	Mean	44,9	55,9	28,8	-11,0	16,2
	SD	6,2	24,1	12,9	-17,9	-6,6
	CV	0,14	0,43	0,45	-0,3	-0,3
K*	Mean	193,1	134,6	160,1	58,5	33,0
	SD	27,4	56,4	68,0	-29,0	-40,6
	CV	0,14	0,42	0,42	-0,3	-0,3
L↓	Mean	295,2	312,9	313,2	-17,7	-18,0
	SD	8,2	25,7	26,9	-17,4	-18,6
	CV	0,03	0,08	0,09	-0,1	-0,1
L↑	Mean	365,9	365,6	361,2	0,3	4,7
	SD	6,3	9,1	7,6	-2,8	-1,2
	CV	0,02	0,02	0,02	0,0	0,0
L*	Mean	-70,7	-52,7	-48,0	-18,0	-22,7
	SD	6,2	29,2	27,2	-23,0	-21,0
	CV	-0,09	-0,55	-0,57	0,5	0,5
Q*	Mean	122,4	81,9	112,1	40,5	10,3
	SD	22,5	32,6	45,9	-10,1	-23,4
	CV	0,18	0,40	0,41	-0,2	-0,2

Annex 32: Values of radiation and energy budgets components calculated over the summer for the "past" (1850-1869), the "present" (2006-2025) and the "future" (2081-2100), and their statistics

Flux	Statistic	Data			Δ	
		Past	Present	Future	Past/present	Present/Future
K↓	Mean	212,1	205,0	217,9	7,2	-13,0
	SD	14,5	18,9	15,6	-4,4	3,3
	CV	0,07	0,09	0,07	-0,02	0,02
K↑	Mean	22,6	21,1	22,6	1,5	-1,5
	SD	1,9	2,2	1,8	-0,2	0,4
	CV	0,09	0,10	0,08	-0,02	0,02
K*	Mean	189,6	183,9	195,4	5,7	-11,5
	SD	12,6	16,7	13,9	-4,1	2,9
	CV	0,07	0,09	0,07	-0,02	0,02
L↓	Mean	309,8	319,7	326,9	-9,9	-7,2
	SD	3,6	4,8	4,8	-1,2	0,0
	CV	0,01	0,02	0,01	0,00	0,00
L↑	Mean	383,6	386,4	397,0	-2,8	-10,6
	SD	5,6	6,6	7,9	-1,1	-1,3
	CV	0,01	0,02	0,02	0,00	0,00
L*	Mean	-73,8	-66,7	-70,1	-7,1	3,4
	SD	5,5	6,8	5,7	-1,3	1,1
	CV	-0,08	-0,10	-0,08	0,03	-0,02
Q_H	Mean	68,8	62,4	68,8	6,4	-6,5
	SD	7,8	8,6	6,9	-0,9	1,8
	CV	0,11	0,14	0,10	-0,03	0,04
Q_E	Mean	42,1	49,9	51,4	-7,7	-1,6
	SD	3,3	3,2	3,4	0,1	-0,2
	CV	0,08	0,06	0,07	0,01	0,00
Q_G	Mean	4,8	4,9	5,0	-0,1	-0,1
	SD	0,5	0,5	0,6	0,1	-0,1
	CV	0,11	0,10	0,11	0,01	-0,02
Q*	Mean	115,8	117,2	125,2	-1,4	-8,1
	SD	7,4	10,2	8,4	-2,8	1,8
	CV	0,06	0,09	0,07	-0,02	0,02
β		1,63	1,25	1,34	0,38	-0,09